Targeting Glycogen Phosphorylase as a Potential Therapeutic Strategy for Glioblastoma

By

NIAH SCHRAM

A thesis submitted in partial fulfilment for the requirements for the degree of MSc (by Research), at the University of Central Lancashire

August 2024

RESEARCH STUDENT DECLARATION FORM

Type of Award School

MSc by Research

Pharmacy and Biomedical Science

Sections marked * delete as appropriate

1. Concurrent registration for two or more academic awards

*I declare that while registered as a candidate for the research degree, I have not been a registered candidate or enrolled student for another award of the University or other academic or professional institution

2. Material submitted for another award

> *I declare that no material contained in the thesis has been used in any other submission for an academic award and is solely my own work.

3. Collaboration

> Where a candidate's research programme is part of a collaborative project, the thesis must indicate in addition clearly the candidate's individual contribution and the extent of the collaboration. Please state below:

The candidate carried out all experimental work, data analysis, and writing for the thesis.

4. Use of a Proof-reader

*No proof-reading service was used in the compilation of this thesis.

Signature of Candidate

Print name: NIAH SCHRAM

Targeting Glycogen Phosphorylase as a Potential Therapeutic Strategy for Glioblastoma

Niah Schram, Dr. Izabela Stasik, and Dr. Joeseph Hayes

Master of Science (by Research)

School of Pharmacy and Biomedical Sciences, University of Central Lancashire

Abstract

Glioblastoma (GB) is one of the most aggressive malignancies of the brain and spinal cord. The current standard of care has remained surgical resection of the tumour, followed by radiotherapy and/or chemotherapy. Crucial challenges in the effective treatment of GB include resistance to the main chemotherapeutic, temozolomide. Prognosis is poor with median survival remaining at 14.6 months. A now established hallmark of cancer is the ability of malignant cells to "modify, or reprogram, cellular metabolism", such as glycogenolysis upregulation. This hallmark could suggest the potential of targeting a specific metabolic component within glycolysis, thus reducing energy production, resulting in possible apoptosis or suppressed proliferation. Studies suggest that glycogen phosphorylase (GP), an enzyme in glycogenolysis, could be inhibited for a therapeutic effect in GB. In this project, GP levels across the three different isoforms (PYGB, PYGL, and PYGM) and the effect of the GP inhibitor CP-91149 was investigated across three different GB cell lines. Cell viability of T98G, U251, and U87 glioblastoma cell lines and SVGp12 human foetal glial cell line was measured after administration of CP-91149 for 24, 48, and 72 hours. Migration of T98G and U251 cells following treatment with CP-91149 was measured in a wound healing assay. Visualisation of the three GP isoforms was achieved through western blotting and confirmed by immunocytochemistry. Flow cytometry was utilised to expand analysis on GP inhibition by assessing the cell cycle before and after treatments. Results showed that CP-91149 had a significant dose- and time-dependent effect in vitro on all GB cell lines. Inhibition of GP caused a reduction in cell viability and cell migration. Western blot and immunocytochemistry analysis showed that PYGL is the most predominant isoform of GP. There was no clear effect on the cell cycle following treatment with CP-91149. Inhibition of glycogenolysis by targeting GP shows potential as a novel therapeutic approach in the treatment of glioblastoma.

Table of Contents

Α	Abstract	3
Α	acknowledgements	7
Α	Abbreviations	8
1	. Introduction	10
	1.1 Glioblastoma	
	1.2 Treatment of Glioblastoma and Challenges	
	1.3 Temozolomide	
	1.4 Hallmarks of Glioblastoma	
	1.5 Glycogenolysis and Glycogen Phosphorylase	17
	1.6 Glycogen Phosphorylase Inhibitor (CP-91149)	20
	1.7 Aims and Hypothesis	22
2	. Materials and Methods	23
_	2.1 Materials	
	2.2 Cell Culture Conditions	25
	2.3 Western Blotting	25
	2.4 Immunofluorescence	28
	2.5 Viability Assays with CP-91149	29
	2.6 Combination Treatment of Temozolomide with CP-91149	30
	2.7 Wound Healing Assay	30
	2.8 Cell Cycle Analysis	31
	2.9 Apoptosis Assay	32
	2.10 Statistical Analysis	32
3	. Results	33
	3.1 Western Blotting	34
	3.2 Immunofluorescence	38

3.3 The Effect of CP-91149 on Cell Viability				
3.4 Clonogenic Assay	42			
3.5 Combination Treatment	43			
3.6 Wound Healing Assay				
3.7 Cell Cycle Analysis	53			
3.8 Apoptosis Assay	58			
4. Discussion	59			
4.1 Levels of GP as Found in Western Blot and Fluorescence	60			
4.2 Effects on Cell Viability	62			
4.5 Inhibitor Effect on Colony Formation	65			
4.3 Combination Treatment Effect on Cell Viability	67			
4.4 Inhibitor Effect on Migration	69			
4.6 Inhibitor Effect on Cell Cycle	70			
4.7 Conclusion	73			
4.8 Limitations	73			
4.9 Future Work	77			
5. References	80			
Annendices	97			

Table of Figures

Figure 1.1: Diagram of glycogenolysis	18
Figure 1.2: The structure of the three isoforms of glycogen phosphorylase	20
Figure 3.1: Western blot images of glycogen phosphorylase expression	35
Figure 3.2: Raw ratio of expression of glycogen phosphorylase	36
Figure 3.3: Relative expression of glycogen phosphorylase	.37
Figure 3.4: Immunofluorescence of glycogen phosphorylase	.39
Figure 3.5: Cell viability following treatment with CP-91149	41
Figure 3.6: Colony formation following treatment with CP-91149	42
Figure 3.7: Cell viability following 24h combination treatment	44
Figure 3.8: Cell viability following 48h combination treatment	46
Figure 3.9: Cell viability following 72h combination treatment	49
Figure 3.10: Wound healing of T98G following treatment with CP-91149	51
Figure 3.11: Wound healing of U251 following treatment with CP-911495	2
Figure 3.12: Representative graphs for cell cycle analysis	53
Figure 3.13: Cell cycle distribution following treatment with CP-91149	57
Figure 3.14: Immunofluorescence with DAPI staining following treatment with CP-91149	58
List of Tables	
Table 2.1: Antibody details	27
Table 3.1: Mean distribution of cell cycle phases	54

Acknowledgements

Firstly, I would like to thank my Director of Studies Dr. Izabela Stasik for guiding me throughout this entire project. Without her words of wisdom and endless support this MSc would not have been possible. In addition, I would like to thank my supervisor, Dr. Joseph Hayes, for his support and advice during this project.

I would also like to thank the Cell Culture Laboratory manager Dr. Julie Burrow for always being there to help and all the laboratory technicians who always kindly offered their support.

A special thank you to fellow laboratory users, office sharers, and friends Rebecca Chandler and Ellie Taylor-Chilton for being there during difficult times and providing encouragement that I am forever grateful for. We have shared many fun times and without them, my experience during my project would not have been the same.

Finally, my deepest gratitude to my partner and family for their unconditional love and support. Their help made this degree much more manageable and without them I wouldn't have gotten this far.

Abbreviations

ADP Adenosine diphosphate

AMP Adenosine monophosphate

AMPK AMP-activated protein kinase

ANOVA Analysis of Variance

ATCC American Type Culture Collection

ATP Adenosine triphosphate

BBB Blood Brain Barrier

CP-91149 [R-(R*,S*)]-5-chloro-*N*-[3-(dimethylamino)-2-hydroxy-3-oxo-

1-(phenylmethyl)propyl]-1H-indole-2-carboxamide

CNS Central Nervous System

DNA Deoxyribonucleic acid

EDTA Ethylenediaminetetraacetic acid

FBS Foetal Bovine Serum

GDE Glycogen debranching enzyme

NEAA Non-Essential Amino Acids

NOS Not otherwise specified

GB Glioblastoma

HCl Hydrogen Chloride

IDH Isocitrate Dehydrogenase

MGMT O⁶-methylguanine-DNA methyltransferase

PBS Phosphate Buffered Saline

PD Patient derived

PhK Phosphorylase kinase

PI Propidium Iodide

PLP pyridoxal phosphate

RT Radiotherapy

SD Standard Deviation

siRNA Small interfering RNA

TMZ Temozolomide

WHO World Health Organisation

1. Introduction

1.1 Glioblastoma

Glioblastoma (GB) is the most aggressive form of cancer originating from the brain and spinal cord. It is classified by the World Health Organisation (WHO) as a grade 4 adult-type diffuse astrocytic glioma that derives from glial cells, more specifically astrocytes (Louis *et al.*, 2021; WHO, 2021). The signs and symptoms of GB can vary and may include headaches, memory loss, visual impairments, seizures, and personality changes (Mckinnon *et al.*, 2021; Posti *et al.*, 2015). Symptoms tend to progress over time and are relatively non-specific, meaning it can be difficult to identify GB early, linking to the poor prognosis of the disease. Diagnosis often involves imaging of the brain initially, using magnetic resonance imaging (MRI), to identify the presence of tumours (Shukla *et al.*, 2017). Then, a molecular diagnosis can be done using a biopsy of the tumour tissue, either before or during surgical resection, to classify and grade the tumour by identifying histopathological markers, such as isocitrate dehydrogenase (IDH) status (Gilard *et al.*, 2021).

Previously, GBs were separated into three categories based on the molecular classification of their IDH status: IDH-wildtype; IDH-mutant; and NOS (not otherwise specified) (Louis *et al.*, 2016). GB IDH-wildtype, a glioma lacking IDH mutation, would account for 90% of cases, predominantly in patients over 55 (Yang *et al.*, 2015). In contrast, GB IDH-mutant would account for approximately 10% of cases, involving predominantly younger patients. The NOS category was utilised for undetermined specimens. As of 2021, the WHO classification guidelines were changed to reflect evidence that suggested IDH-wildtype and IDH-mutant GB were distinct entities of their own, resulting in the elimination of the "IDH-mutant GB" and this was reclassified and replaced as astrocytoma IDH-mutant CNS WHO grade 4 (Louis *et al.*, 2020). Therefore, the current diagnostic criteria for an adult grade 4 diffuse astrocytic glioma (glioblastoma) includes IDH-wildtype and *H3*-wildtype and one or more of the following: +7/-10 chromosome copy number change; *TERT* promoter mutation; *EGFR* gene amplification; necrosis; microvascular proliferation.

While GB is uncommon, with an incidence of 0.59-5 per 100,000 people, it is the most common malignancy of the brain and central nervous system (CNS) as it accounts for almost half of the cancers diagnosed within this category (Miller *et al.*, 2021). Additionally, it has been reported that the incidence of GB is rising, with an incidence of 2.4 to 5.0 per 100,000 from 1995 to 2015 in England (Philips *et al.*, 2018). This has also been observed in other countries, with an incidence of 0.73 per 100,000 in 2008 to an incidence of 4.49 per 100,000 in 2017 in Malta (Grech *et al.*, 2020). This could be for several reasons, including the improvement of neuroimaging techniques leading to overdiagnosis (Rao *et al.*, 2001).

1.2 Treatment of Glioblastoma and Challenges

Treatment of GB has proven challenging due to how inaccessible the tumour is. Surgical removal of as much of the tumour as possible is the first line of treatment for GB, with many studies supporting a positive correlation between maximal surgical resection and overall survival in GB patients post-surgery (Molinaro *et al.*, 2020; Brown *et al.*, 2016; Grabowski *et al.*, 2014). However, due to the 'finger-like' projections of the tumour, it is almost impossible to fully remove it (Wu *et al.*, 2021). Therefore, the current standard of care for GB requires radiotherapy (RT) and/or chemotherapy, most commonly temozolomide (TMZ), following surgical removal with the aim of targeting the remaining GB cells (Weller *et al.*, 2021). This method was developed in 2005 by Stupp *et al.*, (2005) and is often referred to as the Stupp protocol. Regular monitoring using brain MRIs is required indefinitely due to the high rate of recurrence in GB (Zikou *et al.*, 2018).

One of the main complications for drug-based therapeutic approaches is the blood-brain barrier (BBB), a protective barrier between circulating blood and the central nervous system that is comprised of vasculature, glial, and neuronal cells which form tight junctions, physically and

chemically blocking influx of certain molecules in a selective manner (Sweeney *et al.*, 2019; Jena *et al.*, 2020). These cells are tightly packed, making the BBB semi-permeable to prevent the entry of potential pathogens and toxins, while allowing essential nutrients in. However, this means GB is sheltered from many potential treatments as the BBB limits sufficient drug concentrations from entering the brain (Noch *et al.*, 2018). Therefore, many therapeutics fail to target GB successfully if they cannot enter the CNS to reach the site of malignancy. For example, a common chemotherapeutic used in the treatment of a variety of different cancers is Cisplatin, however, it has a BBB penetration rate of 3.7%, meaning it is not suitable for GB treatment (Jacobs *et al.*, 2005).

These complications restrict the progression of successful treatments, which is vital due to the poor survival rates of those with GB and the common reoccurrence following treatment. After treatment following current guidelines, the 5-year survival rate is only 6.7% (Noch *et al.*, 2018), and the average survival of patients with GB is 15 months (Thakkar *et al.*, 2014). Additionally, treatment following the recommended 'Stupp protocol' is not often well tolerated by patients, with side effects that cause a low quality of life for the patients, further demonstrating the importance of new treatment options (Rick *et al.*, 2018; Niewald *et al.*, 2011).

1.3 Temozolomide

The most common chemotherapeutic administered to those with GB is TMZ, a small and lipophilic alkylating agent that can penetrate the BBB (Lee, 2016; Strobel *et al.*, 2019). This is a crucial feature of TMZ that sets it apart from many other chemotherapeutical molecules that are hydrophilic, protein-bound and/or too large (>150 kDa), preventing BBB penetration (Inno *et al.*, 2016).

TMZ is a monofunctional DNA alkylating agent that works at the DNA level by inducing DNA damage indirectly (Arora & Somasundaram, 2019; Singh *et al.*, 2021). At physiological pH, TMZ is converted into MTIC (5-(3-methyltriazol-1-yl)imidazole-4-carboxamide), then hydrolysed to AIC (5-amino-imidazole-4-methyl Amide) and a methyl diazonium ion. This ion donates a methyl group to guanine at position O⁶, forming the adduct O⁶ methylguanine (O⁶-MeG), which consists of approximately 5% of adducts formed by TMZ, with other adducts such as N7 methyl guanine and N3 adenine being in higher abundance. The O⁶-MeG adduct forms a mismatch as, instead of pairing with cytosine, O⁶-MeG is paired with thymine during DNA replication, which is then detected as a mismatch by the mismatch repair machinery, whereas other adducts don't result in a mismatch. Instead of returning O⁶-MeG to guanine, the mismatch machinery can only remove the thymine to be replaced with another thymine. As a result, cell cycle arrest is induced at the G2 phase, followed by apoptosis (Abe *et al.*, 2018) This is the mechanism of the cytotoxic effect of TMZ.

While TMZ remains the most effective chemotherapeutic for GB available, "at least 50% of TMZ-treated patients do not respond to TMZ" due to either acquired or intrinsic TMZ resistance (Lee, 2016; Arora & Somasundaram, 2019). This resistance is linked to the overexpression of O⁶-methylguanine-DNA methyltransferase (MGMT) within GB cells.

MGMT is normally present in cells as a DNA repair enzyme that specifically removes the methyl group from O⁶-MeG, restoring guanine to its natural form, and mismatch repair machinery then fixes the guanine-thymine mismatch. Each MGMT molecule can only remove one methyl group before it is degraded, thus sufficient amounts of MGMT are required to fully repair all mismatches caused by TMZ. In half of GB tumours MGMT expression is lost due to methylation of the *MGMT* promotor (Abe *et al.*, 2018), allowing TMZ to successfully alkylate DNA and induce cell apoptosis. However, the other 50% have been found to display MGMT overexpression. With an overexpression of MGMT, mismatch repair machinery is able to fix the guanine-thymine mismatch, meaning the GB cell passes

the G2 and M phases of the cell cycle and can follow through with DNA replication, thus the neoplastic cells escape apoptosis. This resistance to TMZ is a limitation of the chemotherapeutic that affects half of GB patients (Arora & Somasundaram, 2019).

Despite the significance of this theory, thorough analysis of this mechanism proves difficult, and evidence is inconclusive. There is some evidence that suggests no correlation between MGMT and TMZ resistance, suggesting it could be a non-functional p53 response to DNA damage responsible for resistance (Lee, 2016). However, most studies show increased levels of MGMT protein in TMZ resistant tumours when compared to TMZ sensitive tumours.

A five-year study found that overall, there was a greater survival in GB patients that had combined therapy of TMZ and radiotherapy vs radiotherapy alone (combined: 27.2% at 2 years, 9.8% at 5 years; versus radiotherapy alone: 10.9% at 2 years, 1.9% at 5 years) (Stupp *et al.*, 2009). While this study shows that TMZ is an effective radiosensitiser, it also shows that 5-year survival rates are still very low. This could be due to the resistance within some GB cell lines to TMZ, as discussed above, suggesting the importance of finding alternative options for patients that are resistant. Resistance of TMZ in certain GB cells can be altered by a combination treatment. These TMZ resistant cells can potentially be sensitised by using other therapies alongside TMZ in order to boost its effectiveness (Lee, 2016).

Overall, the outcome of this therapeutic method for GB is not ideal. Therefore, alternative treatments are required to overcome TMZ resistant variants of GB to provide effective treatments for all GB patients. One of the main methods of developing novel cancer therapeutic is by delving into the origins of the cancer of interest to find potential molecular targets that support the proliferation or survival of the malignant cells. This can be explored by looking at the hallmarks of cancer.

1.4 Hallmarks of Glioblastoma

As discussed by Hanahan and Weinberg (2011), one of the now established hallmarks of cancer is the ability of malignant cells to "modify, or reprogram, cellular metabolism", such as glycolysis upregulation. Normally, cells will process free glucose to produce adenosine triphosphate (ATP) under aerobic conditions via glycolysis in the cytosol before the Krebs cycle and the electron transport chain (oxidative phosphorylation) in the mitochondria. When in anaerobic conditions, normal cells will instead rely on glycolysis to produce ATP since the Krebs cycle and oxidative phosphorylation aren't useable in hypoxia. However, many malignant cells, such as GB cells, will use aerobic glycolysis, an unusual occurrence caused by reprogramming of malignant cells to favour glycolysis for their energy production even in an oxygen sufficient environment, thus termed aerobic glycolysis (Naifeh *et al.*, 2023). This seems inefficient for the cancer cell as they need to upregulate glucose transporters to acquire more glucose in the cell to compensate for ~ 18-fold lower efficiency of ATP production when favouring aerobic glycolysis.

Despite this, the glycolic switch, also known as the Warburg effect, is believed to be utilised to support the proliferation of cancerous cells as it might in turn support the production of nucleosides, amino acids, and other components that will be required later in cell division (Hanahan & Weinberg, 2011). More specifically, with glycolysis upregulated it can further support the pentose phosphate pathway, which acts in parallel to glycolysis, generating these components such as nucleosides and reducing agents that promote cell proliferation and DNA repair (Mathieu *et al.*, 2017).

This hypothesis can be further supported through observations of the Warburg effect occurring in rapidly dividing embryonic tissues, further suggesting the possibility of glycolysis upregulation having a functional role in supporting increased cellular proliferation. This hallmark could suggest the potential of targeting a specific metabolic component to block or reduce glycolysis and thus

reduce energy production, resulting in possible apoptosis or suppressed proliferation of cancerous cells.

Additionally, hypoxia is a hallmark of GB (Park & Lee, 2022). Through further proliferation of GB cells, the extracellular conditions are stripped from essential components, such as glucose and oxygen, as they are vastly taken by GB cells to support the uncontrolled and rapid divisions. When the environment reaches a hypoxic/hypoglycaemic level due to malignant proliferation, the GB cells can continue their proliferation by utilising alternative sources of energy. Most commonly, this energy source comes from glycogen, the stored form of glucose, in the cytosol (Mathieu *et al.*, 2017; Migocka-Patrzałek & Elias, 2021). Utilising glycogen can generate a greater overall net amount of ATP in GB cells as it generates three ATP molecules whereas free glucose creates two ATP molecules (Zois & Harris, 2016).

Glycogen can be initially broken down in a process known as glycogenolysis. Considering the hallmarks mentioned above, investigating glycogenolysis could be beneficial to identify a specific component within the pathway that could be targeted, aiming to prevent glycogen breakdown and thus starve GB cells of energy.

1.5 Glycogenolysis and Glycogen Phosphorylase

Glycogenolysis is a process by which stored glycogen is broken down into its subunits, glucose (Paredes-Flores *et al.*, 2024). The formation of glucose from reserves, i.e. glycogen, is an integral part of many metabolic processes as it serves as a key source of energy. The initial degradation of glycogen (Figure 1.1) requires the involvement of three enzymes: phosphorylase kinase (PhK); glycogen phosphorylase (GP); and glycogen debranching enzyme (GDE) (Nadeau *et al.*, 2018). The first enzyme, PhK, is activated through phosphorylation and then activates GP by phosphorylation

(Lane *et al.*, 2012). When GP is phosphorylated, it is in its active form, allowing it to carry out its enzymatic function to phosphorylase the α -1,4-glycosidic bonds (Yang *et al.*, 2024). Additionally, GDE hydrolyses the α -1,6-glycosidic bonds. Both GP and GDE work together to release glucose-1-phosphate from glycogen (Nadeau *et al.*, 2018).

The mechanism of GDE is not well understood, but it has a dual enzymatic property meaning it has two catalytic sites that act separately as a glucosyltransferase and a glucosidase (Zhai *et al.*, 2016). Additionally, it has been suggested that GDE can associate with other proteins, such as AMP-activated protein kinase (AMPK), and thus potentially play a role in other metabolic pathways (Sakoda *et al.*, 2005).

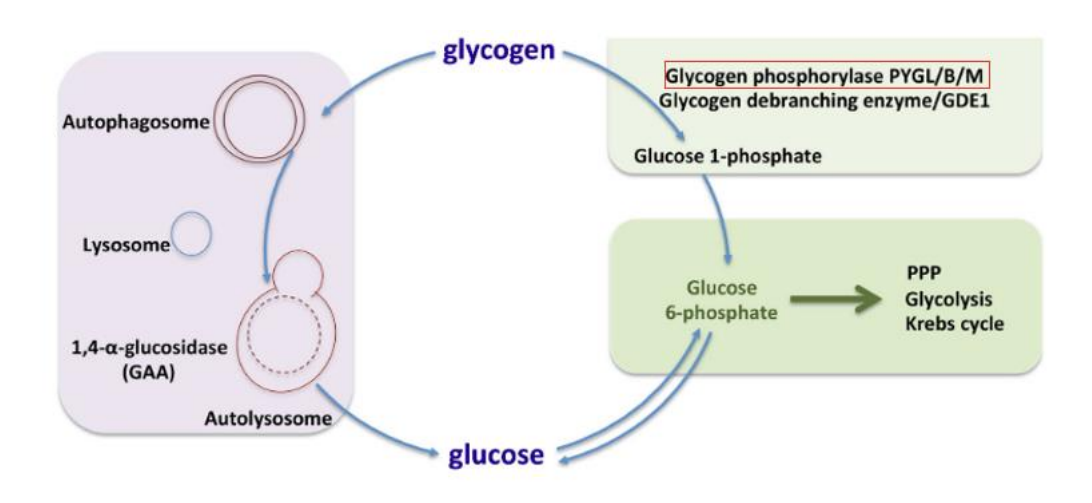


Figure 1.1: A simple diagram demonstrating the process of glycogenolysis, and the key enzymes involved.

Cytosolic glycogen is usable in metabolic pathways via the degradation of glycogen into glucose 1-phosphate by the enzymes GP and glycogen debranching enzyme (Zois & Harris, 2016).

GP is a highly specialised and genetically conserved enzyme, heavily involved specifically in the glycogenolysis pathway, that is activated via allosteric effectors such as adenosine monophosphate (AMP) and/or phosphorylation of Ser14 by phosphorylase kinase (Mathieu *et al.*, 2017; Migocka-Patrzałek & Elias, 2021). When in its phosphorylated form, it breaks down glycogen into glucose 1-phosphate. Present in all cell types are three different isoforms: brain GP (PYGB), muscle GP (PYGM), and liver GP (PYGL). While the three isoforms are relatively similar in structure there are some variations in function, believed to relate to the requirements of the organ in which it has been named, and sensitivity to AMP.

The liver isoform, PYGL, is the most widely studied and is responsible for regulating glycaemic levels and it therefore the least sensitive as it is controlled more strictly by phosphorylation. On the other hand, PYGM and PYGB are both altered allosterically by AMP in order to release sufficient glucose for muscle contraction and in response to hypoglycaemia and hypoxia in glial cells, respectively (Mathieu *et al.*, 2017). All cell types will express these isoforms at different levels, and, despite its name, PYGB is only expressed at a relatively low level in glial cells (Jakobs *et al.*, 2006).

While they are the most similar, there are subtle differences between PYGB and PYGM structure and their properties suggest a different biological role for each isoform (Figure 1.2). For example, PYGB is most predominantly expressed in foetal tissue rather than adult tissue, and it is less sensitive to AMP when levels are low (Sato *et al.*, 1976; Migocka-Patrzałek & Elias, 2021). It is responsible for providing an emergency source of energy in conditions such as hypoglycaemia and hypoxia (Lillpopp *et al.*, 2012). Conversely, PYGM is more sensitive to allosteric activation by AMP in response to external signals, supporting muscle contraction (Crerar *et al.*, 1995).

As discussed in the hallmarks of GB, GP could be a potential molecular target for GB. This suggests that GP inhibition could reduce GB cell proliferation by inhibiting glycogen degradation.

While research related to GP inhibition in GB cells is limited, there is evidence from Zois *et al.*, (2022)

that supports the potential of GP inhibition as a novel treatment option for GB. This study found that liver GP (PYGL) is upregulated in human GB cells and that a high expression of PYGL correlated with poor survival in GB patients. Additionally, they found that survival of GB cell lines was reduced by the knockdown of PYGL and both knockdown and inhibition of PYGL sensitised U87 GB cells to ionising radiation. Therefore, GP inhibition has promising potential against GB.

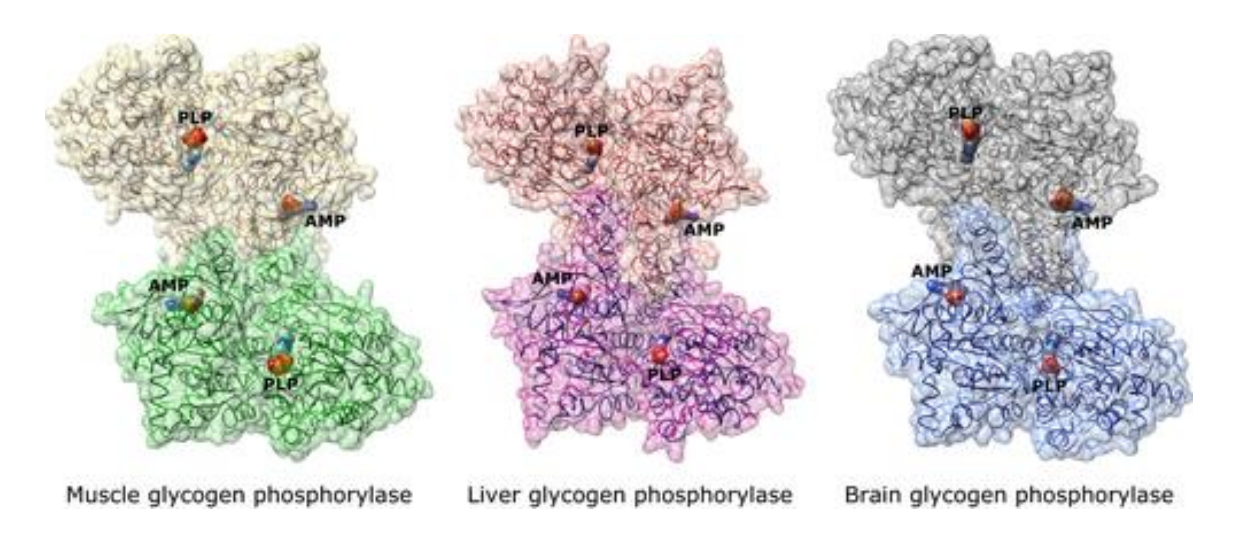


Figure 1.2: The structure of the three isoforms of GP: muscle GP (PYGM); liver GP (PYGL); brain GP (PYGB). The binding site is labelled AMP (adenosine monophosphate). The catalytic site is where the PLP (pyridoxal phosphate) cofactor is labelled (Mathieu, Dupret & Rodrigues Lima, 2017).

1.6 Glycogen Phosphorylase Inhibitor (CP-91149)

Martin *et al.*, (1998) established a selective human liver GP (PYGL) inhibitor, called CP-91149 ([R-(R*,S*)]-5-chloro-*N*-[3-(dimethylamino)-2-hydroxy-3-oxo-1-(phenylmethyl)propyl]-1H-indole-2-carboxamide), that is effective both *in vitro* and *in vivo*. The study found administration of CP-91149 to diabetic *ob/ob* mice rapidly lowered glucose levels without inducing hypoglycaemia. Conversely, when administered to nondiabetic and normoglycemic mice glucose levels were not affected. While this suggests that PYGL inhibition could aid the treatment of type 2 diabetes, it also shows that PYGL inhibition is effective in limiting glycogen degradation both *in vitro* and *in vivo*.

The inhibition site among the three isoforms of GP is relatively similar, suggesting that an inhibitor of GP would most likely inhibit all isoforms (Jakobs *et al.*, 2006). While it is known that CP-91149 can inhibit PYGL, it can also inhibit brain GP (PYGB), of which this isoform is often overexpressed in many transformed cell lines including T98G human GB cell lines (Schnier *et al.*, 2003). This supports the ability of CP-91149 to be non-selective towards one isoform of GP, acting as an effective inhibitor when targeting GP in diseases such as malignant neoplasms.

GP is a plausible molecular target for the potential treatment of cancer that has been considered, but not widely tested. Inhibition of glycogenolysis by the inhibition of GP has previously been studied as an anti-diabetic therapeutic approach, however, it has rarely been investigated in cancer models (Khan *et al.*, 2020). There are findings of cell cycle arrest and apoptosis in pancreatic tumour cells and hepatocellular carcinoma cells following GP inhibition which disrupted glycogenolysis (Lee *et al.*, 2004; Barot *et al.*, 2019). More specifically, the GP inhibitor CP-91149 has demonstrated growth inhibition in pancreatic and prostate cancers as well as hepatocellular carcinoma (Schnier *et al.*, 2003; Schnier *et al.*, 2005; Barot *et al.*, 2019).

In the context of GB, research regarding GP inhibition is limited. Zois *et al.*, (2022) found that inhibition of PYGL via PYGL knockdown was effective in sensitising GB cells to ionising radiation. This was observed through a reduction in cell growth and further confirmed by the induction of mitotic catastrophe as GB cells displayed DNA fragmentation. Additionally, inhibition of PYGB expression in U87 GB cells has been reported to elicit cell cycle arrest in the G2 phase and inhibit proliferation (Ferraro *et al.*, 2022). Mathomes *et al.*, (2023) studied the GP inhibitor Baicalein, another effective glycogenolysis inhibitor. Results following the administration of Baicalein to GB cell lines U251, T98G, and U87 revealed a dose-dependent and time-dependent decrease in cell viability, supporting the promise of the cytotoxic capability of GP inhibition on GB.

1.7 Aims and Hypothesis

Overall, the rate of survival of GB remains low, with limited treatment options that are suitable for all patients. This demonstrates the importance of novel therapeutics for GB. Therefore, this project aimed to investigate the effects of GP inhibition, using CP-91149, in human GB cell lines (U251, T98G, and U87) *in vitro*. This involved measuring several parameters, including cell viability, migration, and effects on the cell cycle following treatment. Combination treatment was also used to determine the ability of CP-91149 to sensitise GB cells to TMZ. Additionally, levels of GP were studied across these GB cell lines to investigate any possible correlation.

It is hypothesised that CP-91149 will negatively affect cell viability, migration, and cell cycle within GB cell lines and enhance the cytotoxic effect of TMZ when used in combination treatment. Additionally, GP is expected to be overexpressed in GB cell lines compared to a normal control cell line (SVGp12).

Main Aim: To investigate CP-91149 as a novel therapeutic option for GB and measure levels of GP within GB cell lines, *in vitro*.

Objectives:

- To determine the effect of CP-91149 independently on cell viability, migration, cell cycle arrest, and colony formation of GB cells.
- To establish and compare the effects of CP-91149 in combination with temozolomide on cell viability of GB cells.
- To observe the levels of each isoform of GP (PYGB, PYGL, PYGM) within GB cell lines using
 western blot and immunofluorescence analysis and compare to propose a potential
 connection of GP levels with viability.

2. Materials and Methods

2.1 Materials

The consumables used in this project were purchased from the following suppliers: SVGp12, U87, and T98G cell lines (American Type Culture Collection, ATCC); U251 cell line (University of Wolverhampton); Gibco[™] minimum essential medium (MEM) with L-glutamine; 10% fetal bovine serum (FBS, Life Science Production), 1% non-essential amino acids (NEAA, Sigma), 1% sodium pyruvate (Sigma), 100 units of Penicillin-Streptomycin/mL (PenStrep, Sigma); Trypsin (Sigma); CP-91149 (Selleck, S2717); Temozolomide (Biorbyt, orb1101303); dimethyl sulfoxide (DMSO, Sigma); resazurin sodium salt (APExBio, B6098); bovine serum albumin (BSA) powder (Sigma, BSAV-RO); crystal violet powder (Sigma, C0775-25G); methanol (Thermo Scientific); protease inhibitors (Thermo Scientific[™] Pierce Protease Inhibitor and Phosphatase Inhibitor Mini Tablets, A32953 & A32957); Pierce[™] BCA Protein Assay Kit (Thermo Scientific[™]); precast gel (Bio-Rad Mini-PROTEAN[®]TGX[™] precast gels, 4-20%, Cat. #456-1094); protein ladder (PageRuler™ prestained protein ladder, 10 to 180 kDa, Thermo ScientificTM); nitrocellulose membrane (AmershamTM ProtranTM, 0.2μM); 5% skimmed milk powder (Marvel); ECL substrate (Thermo Scientific[™] Pierce[™] ECL western blotting substrate, 32106); poly-L-lysine solution (0.01%, Sigma, A-005-M); rabbit polyclonal anti-PYGB (Sigma-Aldrich, HPA031067); rabbit polyclonal anti-PYGL (Abcam, ab198268); rabbit polyclonal anti-PYGM (Abcam, ab231963); rabbit polyclonal β-actin antibody (Bioss, bs-0061R); HRP-conjugated Affinipure goat anti-rabbit IgG (Protein Tech, SA00001-2); fluoromount-G with DAPI (Invitrogen, 00-4959); goat anti-rabbit IgG Alexa Fluor[™] 568 (1:250, Invitrogen, A-11011); plates (Thermo Fisher Scientific, NuncTM).

Reconstitutions:

CP-91149 and TMZ were dissolved in DMSO to form a stock solution, which was then diluted into concentrations required using MEM. The final DMSO concentration administered to cells never

exceeded 0.1% and, therefore, had no cytotoxic effect on the cell lines. Appropriate vehicle controls were tested and had no significant effect compared to untreated controls.

Resazurin sodium salt was dissolved in sterile PBS. Bovine serum albumin (BSA) powder was dissolved in PBS. Crystal violet powder was dissolved in 25% methanol to achieve a 0.5% crystal violet solution.

2.2 Cell Culture Conditions

Non-cancerous human fetal glial cell line, SVG p12, was used as a control glial cell line, and U87, T98G, and U251 GB cell lines were utilised. Cells were cultured in MEM with L-glutamine supplemented with 10% fetal bovine serum (FBS), 1% non-essential amino acids (NEAA), 1% sodium pyruvate, and 100 units of Penicillin-Streptomycin/mL (PenStrep) in T75 flasks at 37°C with 5% CO₂ in a humidified atmosphere. When 70-80% confluency was achieved, cells were washed with 1X phosphate-buffered saline (PBS) before coating the cell surface in 1X trypsin and placing the flask in the incubator for cells to detach. Detachment was observed microscopically, then MEM was included to neutralise the trypsin. Cell suspension was used for passaging and/or seeding.

2.3 Western Blotting

Cells (SVGp12, U251, T98G, and U87) were plated in T75 flasks and grown to reach 70-80% confluency. The cell surface was washed with cold phosphate-buffered saline (PBS) and harvested from flasks by adding radioimmunoprecipitation assay (RIPA) buffer (Appendix 1) containing protease inhibitors and manually scraping before transferring to Eppendorf tubes. Cells were subsequently lysed for 30 minutes with occasional agitation before being centrifuged at 16,000 g at 4°C for 20 min. The total protein concentration was measured using the PierceTM BCA Protein Assay Kit.

Protein separation was achieved through sodium dodecyl-sulfate polyacrylamide gel electrophoresis (SDS-PAGE) by loading 30µg of protein in 4X loading buffer (Appendix 1) per well in a precast gel. A protein ladder was used on each gel to identify the protein of interest. The SDS-PAGE tank was filled appropriately for the number of gels with 1X running buffer (Appendix 1), and SDS-PAGE ran for 10 mins at 80V before increasing to 150V until the loading dye reached the bottom of the gel. Next, the gel containing separated protein was removed from the cast and assembled in a cassette between two sponges and two pieces of filter paper with a nitrocellulose membrane directly contacting the gel, ensuring the gel was on the cathode side and the membrane was on the anode side of the cassette. All components were briefly soaked in transfer buffer (Appendix 1) and the cassette was placed into a transfer tank filled with cold transfer buffer. Proteins were transferred onto the nitrocellulose membrane for 60 minutes at 100 V, 4°C.

To reduce non-specific binding, membranes were incubated for 1 h at room temperature (RT) in blocking buffer, containing 5% skimmed milk in tris-buffered saline (TBS, Appendix 1) with 0.1% tween-20 (TBS-T, Appendix 1). Then, the membranes were cut in half, below the 70kDa marker, so that the upper half could be incubated overnight at 4°C with primary GP antibodies, and the lower half with primary β -actin antibody at room temperature (RT) for 1h (Table 2.1). Following primary antibody incubation, the membranes were rinsed with TBS-T four times, then incubated with secondary antibody (Table 2.1) for 1 h at RT. Then, membranes were washed five times with TBS-T. ECL substrate was used for 3 minutes before imaging using the ChemiDocTM XRS+ system (BioRad).

Table 2.1: Antibody details

	ANTIBODY	DILUTION	DILUTANT
PRIMARY	Rabbit polyclonal anti-PYGB	1:1000	5% milk in TBS-T
ANTIBODY	Rabbit polyclonal anti-PYGL	1:1000	5% milk in TBS-T
	Rabbit polyclonal anti-PYGM	1:500	5% milk in TBS-T
	Rabbit polyclonal β-actin	1:2000	5% milk in TBS-T
	antibody		
SECONDARY	HRP-conjugated Affinipure	1:5000	5% milk in TBS-T
ANTIBODY	goat anti-rabbit IgG		

Three independent experiments were conducted, using lysates of different passage number. Images were quantified using ImageJ by measuring the mean grey area of the bands for PYGB, PYGL, PYGM, and β -actin for each cell line. Mean grey area of the background was measured for each band by selecting an area directly above or below the band. Initial protein expression was calculated as follows (MGA is the mean grey area):

Inverted Protein – Inverted Respective Background
Inverted β-actin – Inverted Respective Background

Inverted protein/background = 255-MGA

2.4 Immunofluorescence

A 6-well plate was prepared with coverslips that were coated with a 0.01% poly-L-lysine solution and left for at least 15 minutes. Coverslips were washed with PBS three times, then GB cell lines (U251, T98G, and U87) were seeded onto coverslips at a density of 75,000 cells per well and left to attach overnight to achieve 60-70% confluency. The next day, cells were fixed with 100% ice-cold methanol for 10 minutes at -20°C. Coverslips fixed with cells were blocked in 1% BSA in PBS for 45 minutes. Primary antibodies used to detect the three isoforms of GB were the same as for WB, all in 1:50 dilution. in 1% BSA in PBS. The primary antibody solution was placed on the coverslip's surface, cells facing upwards, and left overnight at 4°C in a humidified chamber. Coverslips were washed gently four times with PBS, then incubated with the secondary antibody, goat anti-rabbit IgG Alexa Fluor 568 (1:250), diluted in 1% BSA in PBS, for 1h. Coverslips were washed four times in PBS, then dipped in distilled water twice. Finally, coverslips were mounted onto a slide using fluoromount-G with DAPI before sealing the edges with nail polish. All images were acquired with Zeiss Axio Observer microscope using an oil immersion 63x objective. All images for each experiment were taken using the same settings for comparison. Two independent experiments were conducted for each primary antibody, with 10 images taken on different areas of the slide for each experiment.

Fluorescent intensity was measured using a manual method outlined by Shihan *et al.*, (2021) by firstly converting images into greyscale, then using ImageJ software to manually draw around a single cell and calculate the mean grey value. The background was calculated by measuring the mean grey area of 3 areas around the cell of interest. The final fluorescent intensity for each cell repeat was calculated as follows:

Mean grey value of cell – mean grey value of background = Final mean fluorescent intensity

Means were calculated for each isoform appropriately, using 10 repeats per experiment.

2.5 Viability Assays with CP-91149

All cell lines were plated in 96-well plates at a density of 1000 cells/well and left overnight at 37°C with 5% CO₂. Cells were treated the following day with 0, 5, 10, 20, 50 and 100 μM CP-91149 for 24, 48, and 72 h. CP-91149 powder was dissolved in DMSO to form a stock solution, which was then diluted into the concentrations required using MEM. After the treatment period, a Resazurin solution (made using resazurin sodium salt was dissolved in sterile PBS) was added to each well containing cells in a 1:10 ratio of the total volume. Plates were incubated at 37°C with 5% CO₂ for 4 hours before measuring fluorescence at Ex 535 nm/Em 612 nm on Tecan Spark® Multimode Microplate Reader. Three independent experiments, each with three repeats, were conducted and means were calculated. The final DMSO concentration administered to cells never exceeded 0.1% and, therefore, had no cytotoxic effect on the cell lines. Appropriate vehicle controls were tested and had no significant effect compared to untreated controls. Cell viability was calculated using the following equation:

% Cell Viability =
$$\frac{A_{treatment} - A_{blank}}{A_{control} - A_{blank}} X 100$$

Where A is absorbance. Means were calculated for each triplicate within each experiment and used to calculate cell viability.

A clonogenic assay was performed using U87 and U251 cell lines. These were seeded in 6-well plates at a density of 500 cells per well and left overnight at 37°C with 5% CO₂. Following attachment, media was replaced and cells were treated with 0, 10, and 50 μ M CP-91149 and then incubated at 37°C with 5% CO₂ for a total treatment period of 2 weeks. After this time, the medium was removed, cells were washed with PBS, fixed with 100% methanol for 10 minutes on ice and

stained with a 0.5% crystal violet solution to visualise colonies (crystal violet powder was dissolved in 25% methanol to achieve a 0.5% crystal violet solution).

2.6 Combination Treatment of Temozolomide with CP-91149

As with the resazurin assay previously, all cell lines were seeded in 96-well plates at a density of 1000 cells/well and left overnight at 37°C with 5% CO₂. Cells were treated the following day with one of 9 treatments: 0, 20, and 50 μM CP-91149; 50 and 100 μM TMZ; 20μM CP-91149 + 50μM TMZ; 20μM CP-91149 + 100μM TMZ; 50μM CP-91149 + 100μM TMZ. CP-91149 and TMZ were dissolved in DMSO to form a stock solution, which was then diluted into concentrations required using MEM. Cells were incubated for 24, 48, or 72 h, then a Resazurin solution was added to each well containing cells in a 1:10 ratio of the total volume. Plates were incubated at 37°C with 5% CO₂ for 4 hours before measuring fluorescence at Ex 535 nm/Em 612 nm on Tecan Spark® Multimode Microplate Reader. Three independent experiments, with three repeats, were conducted and means were calculated. The final DMSO concentration administered to cells never exceeded 0.1% and, therefore, had no cytotoxic effect on the cell lines. Appropriate vehicle controls were tested and had no significant effect compared to untreated controls. Cell viability was calculated using the formula in section 2.5.

2.7 Wound Healing Assay

A monolayer of cells was created in 24-well plates by seeding cells at a density of 200,000 cells per well. The cell lines used for this were U251 and T98G. The day following seeding, a single vertical 'scratch' in the monolayer was created manually using a p20 pipette tip in each well containing cells. Immediately following the scratch, wells were washed twice with PBS to remove debris, then media was re-introduced with a low serum MEM (0.5% FBS). Wells were then treated with CP-91149 (0, 10, & 50µM) in duplicate. The scratches were imaged at 0h, 4h, 8h, and 24h to observe the migration of

cells across the gap, aiming to image the same area across time points by comparison to the previous image. In order to properly image the gap at 24h, due to debris that affected the image, media was removed and replaced before imaging. Imaging was conducted using Zeiss Axiovert 5 to image the gap, including the borders, at 10X objective, phase-contrast. Three independent experiments were completed, each with two repeats, and means were calculated appropriately.

The area of the gap was measured utilising ImageJ software. Firstly, the scale was set using the scale bar, then the edge of the gap was manually outlined, and the area was calculated via the software (μ M²). These values could then be used to calculate the migration rate over the time points:

%
$$Migration = \frac{(A_{t=0} - A_{t=n})}{A_{t=0}} \times 100\%$$

Where $A_{t=0}$ is the initial wound area at 0h, $A_{t=n}$ is the wound area after n hours of the initial scratch (i.e., 4h, 8h, 24h), both μ m².

2.8 Cell Cycle Analysis

6-well plates were seeded with U251, T98G, and U87 GB cell lines at a density of 200,000 cells per well. Then, cells were treated with CP-91149 (0, 10, 50, and 100μM) for 48h. Following treatment, cells were washed twice with PBS, collecting the spent media and PBS. Cells were harvested using trypsin (1X) and added to the collected cells from media/washes. Once collected, cells were washed twice with PBS (Ca²⁺ and Mg²⁺ free) by centrifuging at 1000 rpm for 5 min, before fixing cells using 100% ice-cold methanol at 4°C for at least 30 minutes. Cells were then washed twice by centrifuging at 2000 rpm for 10 min in PBS containing 2% FBS to minimize loss of cells. The supernatant was removed, and the cells were resuspended in 0.25ml of a stain solution per sample

made in a 4:1 ratio containing PI (50μg/ml) and RNase (100μg/ml) before incubating at 37°C for 30 min. Analysis of the cell cycle was done using the Agilent NovoSampler® Pro flow cytometer producing a fluorescent signal excitation 488 nm and detection 572/28 nm.

2.9 Apoptosis Assay

A 6-well plate was prepared with coverslips that were coated with a 0.01% poly-L-lysine solution and left for at least 15 minutes. Coverslips were washed with PBS three times, then GB cell lines (U251, T98G, and U87) were seeded onto coverslips at a density of 75,000 cells per well and left to attach overnight to achieve 60-70% confluency. The next day, cells were treated with 100μM CP-91149 and the control cells were given an equal volume of MEM, then incubated at 37°C with 5% CO₂. After 72h of treatment, cells were fixed with 100% ice-cold methanol for 10 minutes at -20°C. Coverslips were washed four times in PBS, then dipped in distilled water twice. Finally, coverslips were mounted onto a slide using fluoromount-G with DAPI before sealing the edges with nail polish. Images were acquired with Zeiss Axio Observer microscope using an oil immersion 63x objective. This experiment was done once with no repeats, and a total of 3 images were taken per slide.

2.10 Statistical Analysis

Statistical analysis was performed in IBM SPSS Statistics (version 29.0.1). An ANOVA (analysis of variance) with Bonferroni's post-hoc test was performed to confirm the significance of data with a value of p<0.05 to identify significant differences. Significance indicated via * in comparison to the control (* p<0.05, ** p<0.01, *** p<0.001). All data presented represent the average of 3 independent repeats, unless otherwise specified, and error bars are ± SD (standard deviation).

3. Results

3.1 Western Blotting

Visualisation of the expression of the GP isoforms (PYGB, PYGL, and PYGM) amongst untreated SVGp12, U251, T98G, and U87 cell lines was achieved through western blotting (Figure 3.1). Bands were quantified via densitometry following imaging to calculate relative protein expression (Figure 3.3).

Initial observation of the blots themselves revealed that the liver isoform, PYGL, was the most prominent across all GB cell lines and SVGp12 cells (B in Figure 3.1 and 3.2), whereas the muscle isoform was the least expressed (C in Figure 3.1 and 3.2). Additionally, U251 cells showed the highest protein expression consistently across all three isoforms.

After densitometry analysis to calculate the relative expression of each isoform in the GB cell lines relative to the control, SVG p12 cells, it appeared that U251 cells overexpress all isoforms of GP consistently (Figure 3.3). However, the overexpression of PYGL (B in figure 3.3) is lower than that of PYGB (A in figure 3.3) and PYGM (C in figure 3.3) in U251 cells compared to SVG p12 cells.

Additionally, T98G cells overexpress the PYGB isoform (A in figure 3.3). No other overexpression relative to the control was observed. Instead, there was underexpression of all three isoforms in U87 cells, as well as underexpression of PYGL and PYGM in T98G cells.

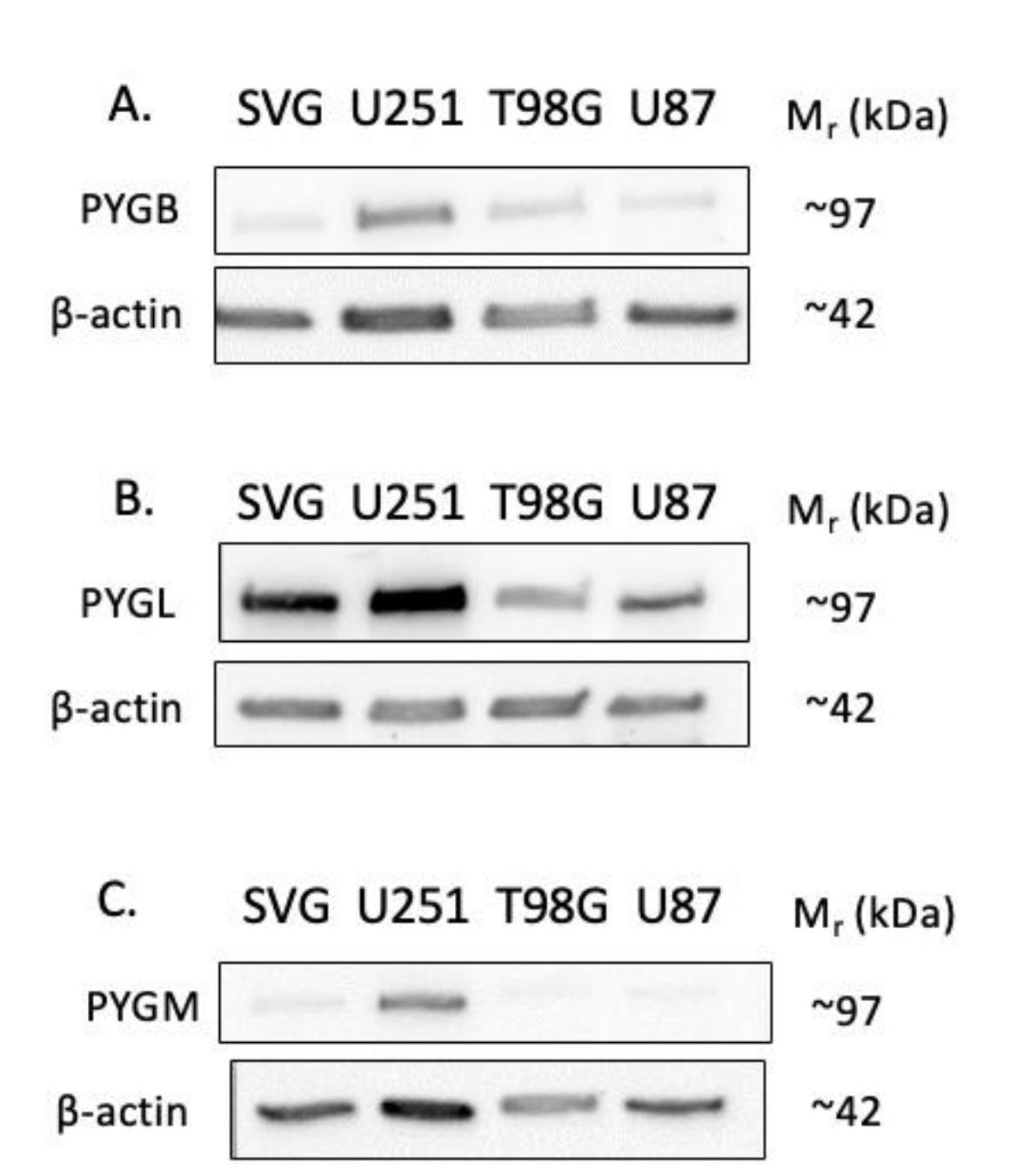
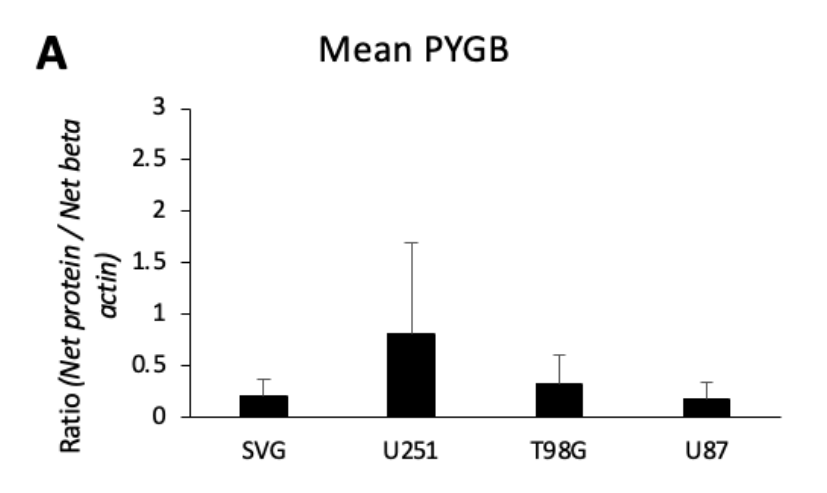
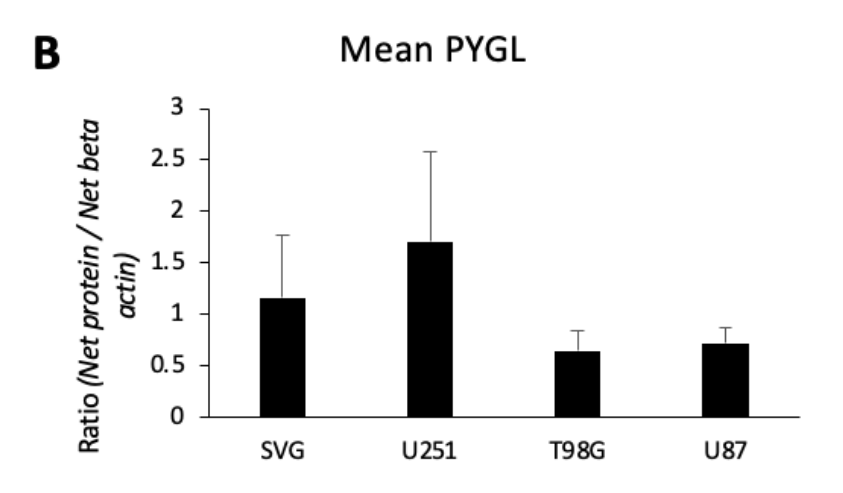


Figure 3.1: Representative images of western blot showing PYGB (A), PYGL (B), and PYGM (C) expression in SVGp12, U251, T98G, and U87 cell lines.





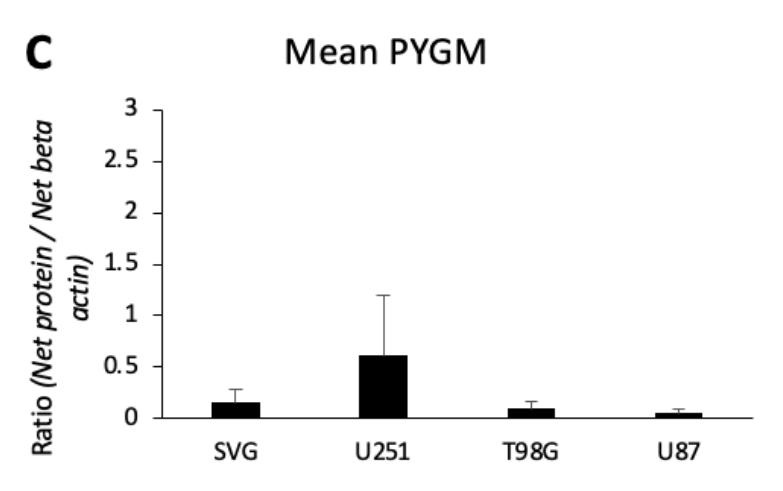
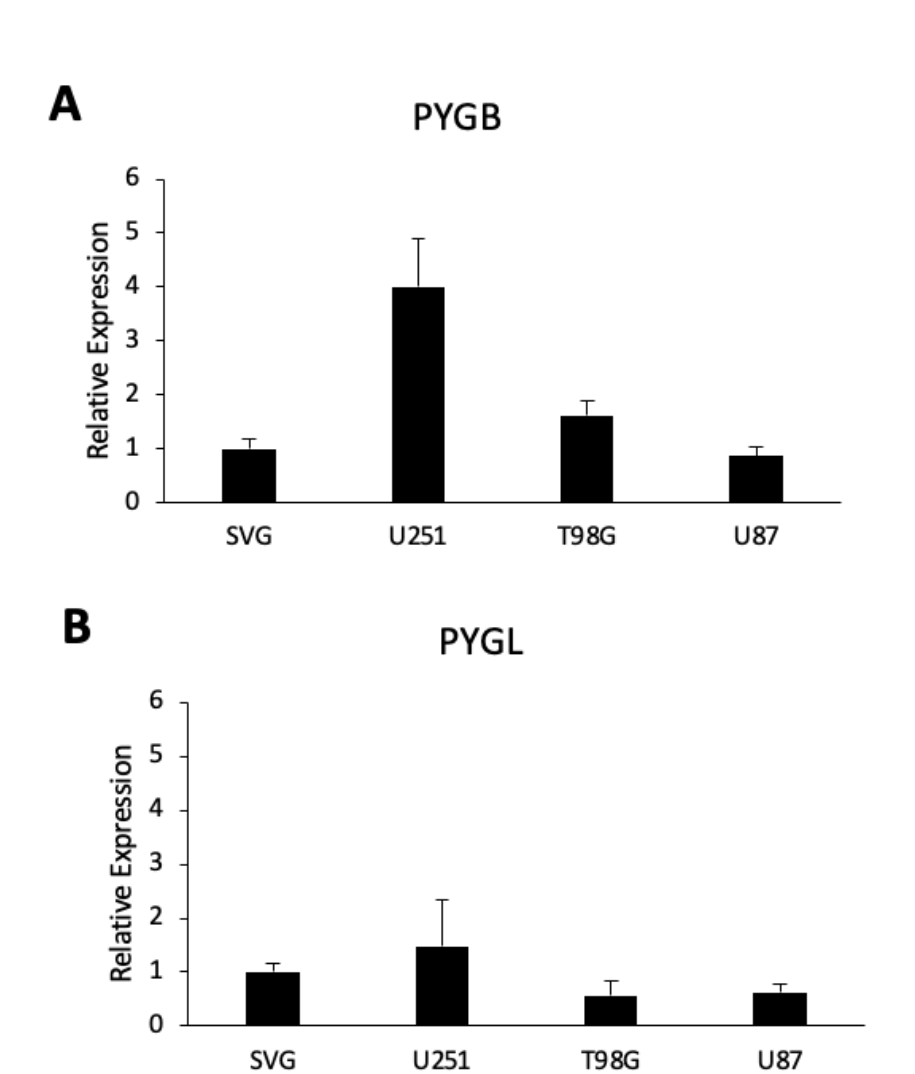


Figure 3.2: Western blot data showing expression of GP. Graphs depicting the raw calculated ratio of PYGB (A), PYGL (B), and PYGM (C) proteins from β -actin loading control following densitometry analysis using ImageJ software. Data is presented as the average and was collected from three independent experiments; error bars are \pm SD.



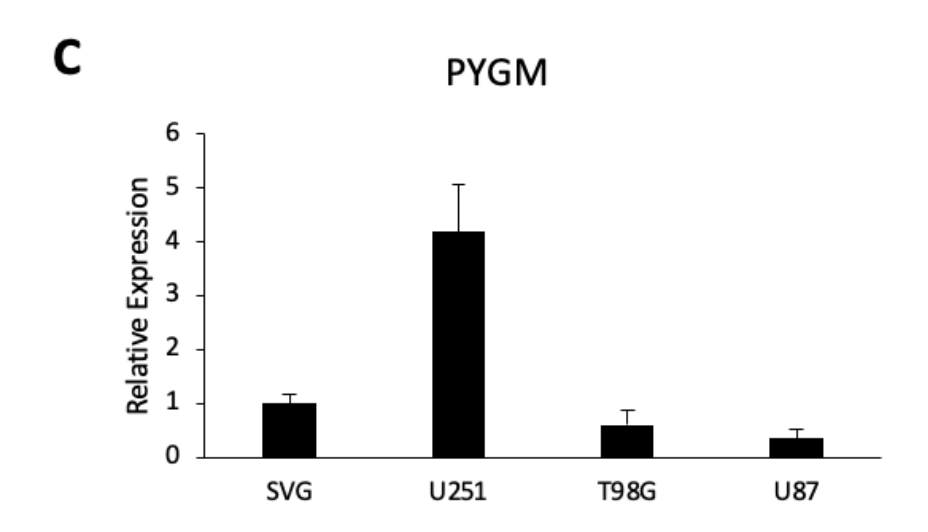


Figure 3.3: Western blot data showing expression of GP. Graphs showing PYGB (A), PYGL (B), and PYGM (C) protein expression in U251, T98G, and U87 cells relative to the expression in SVGp12 control cells. Data is presented as the average and was collected from three independent experiments; error bars are ± SD.

3.2 Immunofluorescence

To confirm western blot analysis results, the expression of GP was assessed by fluorescence microscopy. untreated U251, T98G, and U87 cells were fixed and stained for the three isoforms of GP and then imaged using a fluorescent microscope (Figure 3.4). Initial observation confirmed western blot results as the PYGL isoform (B and E in figure 3.4) was the most predominant while PYGM (C and F in figure 3.4) was the least. Slight differences in intensity were hard to distinguish visually, so ImageJ software was used to quantify fluorescent intensity. These results corresponded with initial western blot quantification (D-F in figure 3.4) as U251 displayed greater intensity when probed for all three isoforms of GP. It also confirmed the same results for levels of GP within T98G and U87 cells, where T98G showed the least PYGL levels and U87 had the least PYGB and PYGM levels. Microscopical analysis also revealed the presence of all isoforms of GP within both the cytosol and nucleus of all GB cell lines.

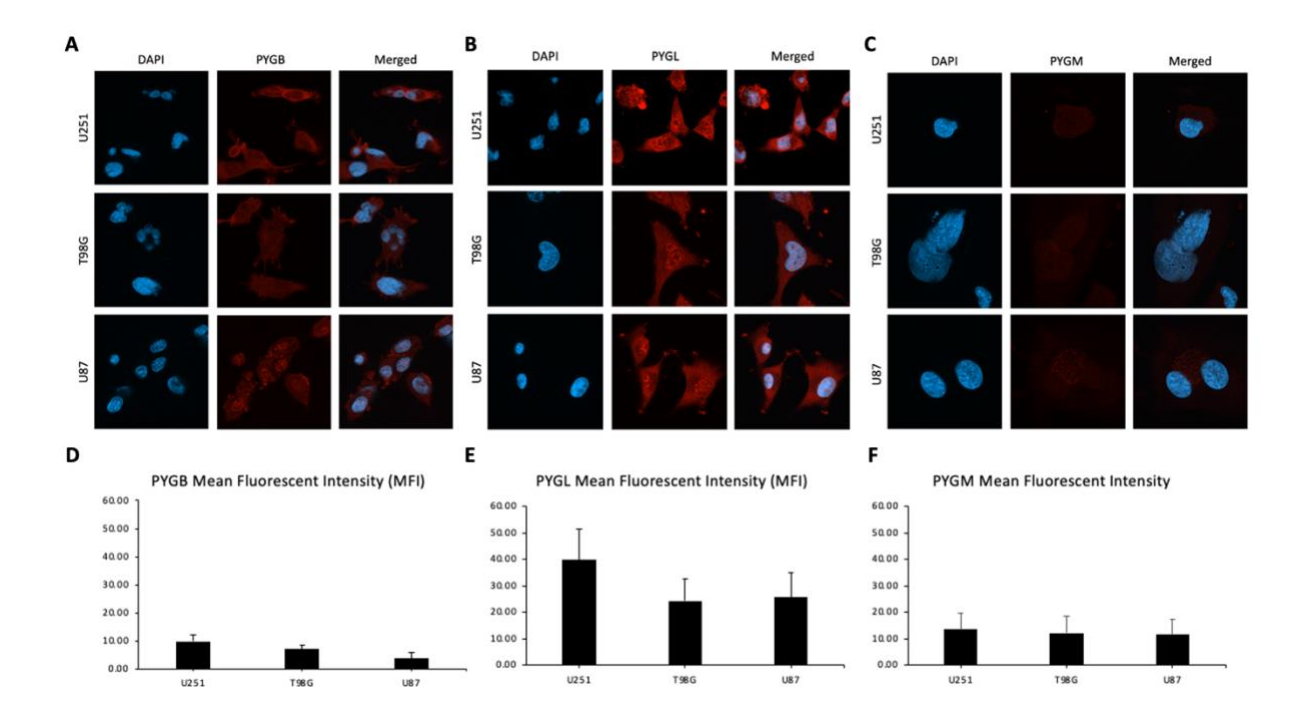


Figure 3.4: Immunofluorescence data showing expression of GP. Representative images of immunofluorescence showing PYGB, PYGL, and PYGM expression in U251, T98G, and U87 cell lines (A-C). Graphs depicting the calculated mean fluorescent intensity using ImageJ software (D-F). Data is presented as the average and was collected from two independent experiments, each with ten repeats; error bars are ± SD. Images were taken at 63x with oil immersion.

3.3 The Effect of CP-91149 on Cell Viability

The effect of CP-91149 (0, 5, 10, 20, 50, and 100μM) on SVG p12, U251, T98G, and U87 cell viability was investigated *in vitro using resazurin assay*. CP-91149 produced a clear dose-dependent decrease in cell viability across all four cell lines (Figure 3.5).

Following treatment of SVG p12 cells with CP-91149 at a concentration of $100\mu M$, a significant decrease was observed across all time points (p<0.001): $11\pm12\%$ at 24h; $6.7\pm11.6\%$ at 48h; $0\pm0\%$ at 72h (graph A in figure 3.5). However, statistical significance was not consistent across all concentrations of CP-91149. 72h treatment showed a greater reduction of viability when compared to 24h and 48h in the lower concentrations, but, at the highest concentration, this effect was less obvious.

Within U251 cells, there was a significant reduction in cell viability observed at the concentration $100\mu\text{M}$ (graph B in figure 3.5) after 24h (45±10%, p<0.05) and 72h (19±7%, p<0.001). No significant differences in cell viability were observed at 48h or across other concentrations. Again. There was a clear dose-dependent reduction in cell viability, however, longer treatment time didn't show as much of a difference, specifically when observing 48h compared to 72h at the higher concentrations. Additionally, this cell line shows less of a reduction in cell viability than the others.

Similarly, CP-91149 showed significant reductions in cell viability at 100μ M in T98G (graph C in figure 3.5) at 24h (14±8.4%, p<0.05), 48h (3.9±7.3%, p<0.001), and 72h (3.5±6%, p<0.01). There was also a significant decrease demonstrated at 50μ M for 48h (55±29%, p<0.05), however, no other statistically significant differences were observed within the treatment of this cell line. There was a sharp decrease in cell proliferation when the concentration of CP-9114 exceeded 10μ M.

Comparisons between different concentrations of CP-91149 in U87 cells showed significant decreases in cell viability at 100μ M (graph D in figure 3.5) at 24h (47±8%, p<0.05), as well as at 48h

 $(32\pm4\%, p<0.001)$ and 72h $(16\pm9\%, p<0.001)$. Additionally, a statistically significant reduction was observed at 50 μ M after 72h $(77\pm7\%, p<0.01)$, but no other statistically significant differences were identified. Like U251, U87 displayed less reduction in cell viability in lower doses. Furthermore, a time-dependent effect was not apparent until the highest concentration of 100μ M.

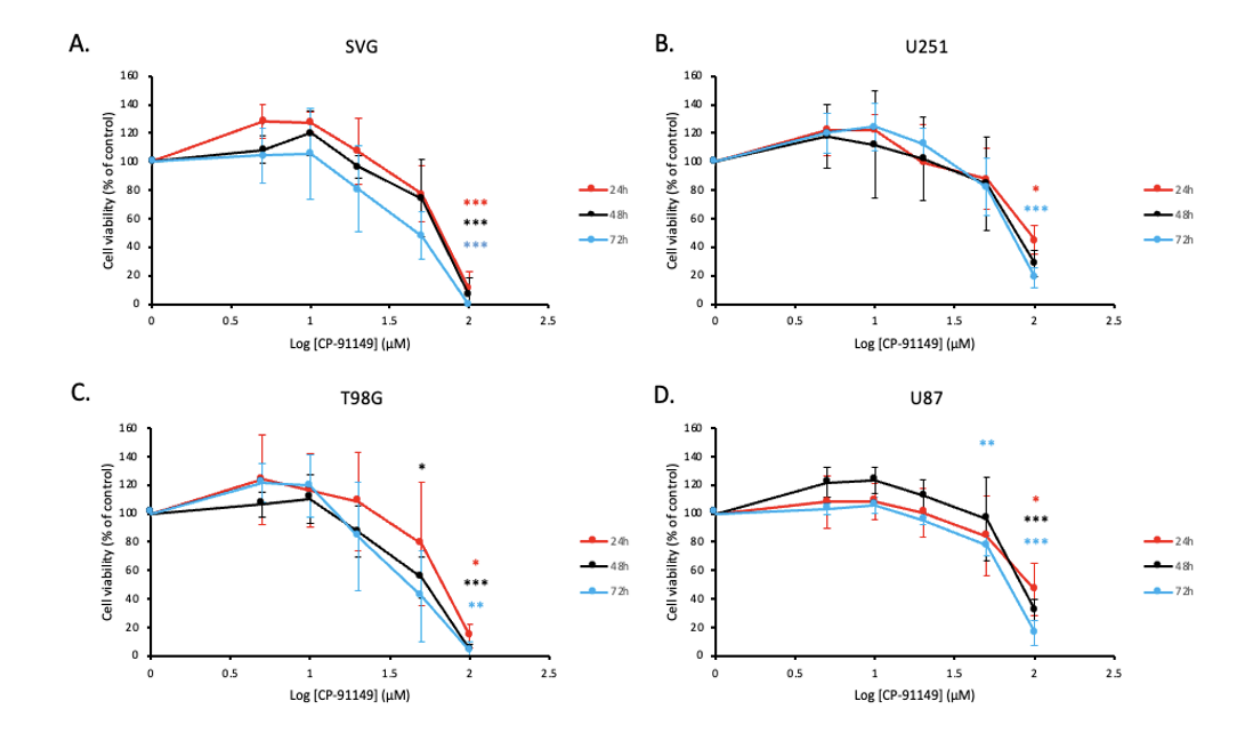


Figure 3.5: The effect of CP-91149 (0, 5, 10, 20, 50, and 100 μ M) on cell viability of SVG p12 (A), U251 (B), T98G (C), and U87 (D) cell lines at three different time points (24, 48, 72 h). Data presented as the average obtained from three independent repeats, error bars are \pm SD. Significant differences compared to the control are shown by * (*p < 0.05, **p < 0.01, ***p < 0.001). Statistical analysis results in appendix 2-5.

At lower concentrations, cell viability increased above 100% across all three time points in all cell lines. This increase lessened as the time point increased, with average cell viability following $5\mu M$ and $10\mu M$ of CP-91149 at 24h being 129% and 128% respectively, at 48h cell viability was 109% and 120% respectively, and at 72h it was 105% and 106% respectively.

3.4 Clonogenic Assay

Long-term effects on cell viability were assessed using a clonogenic assay. Results following 14 days of treatment with low density of cells presented similar results in both U87 and U251 cell lines (Figure 3.6). Treatment with $10\mu M$ of CP-91149 shows a similar level of colony growth in both cells. Following treatment with $50\mu M$ yielded greater changes in colony formation, with U25 having smaller colonies and U87 appearing sparser.

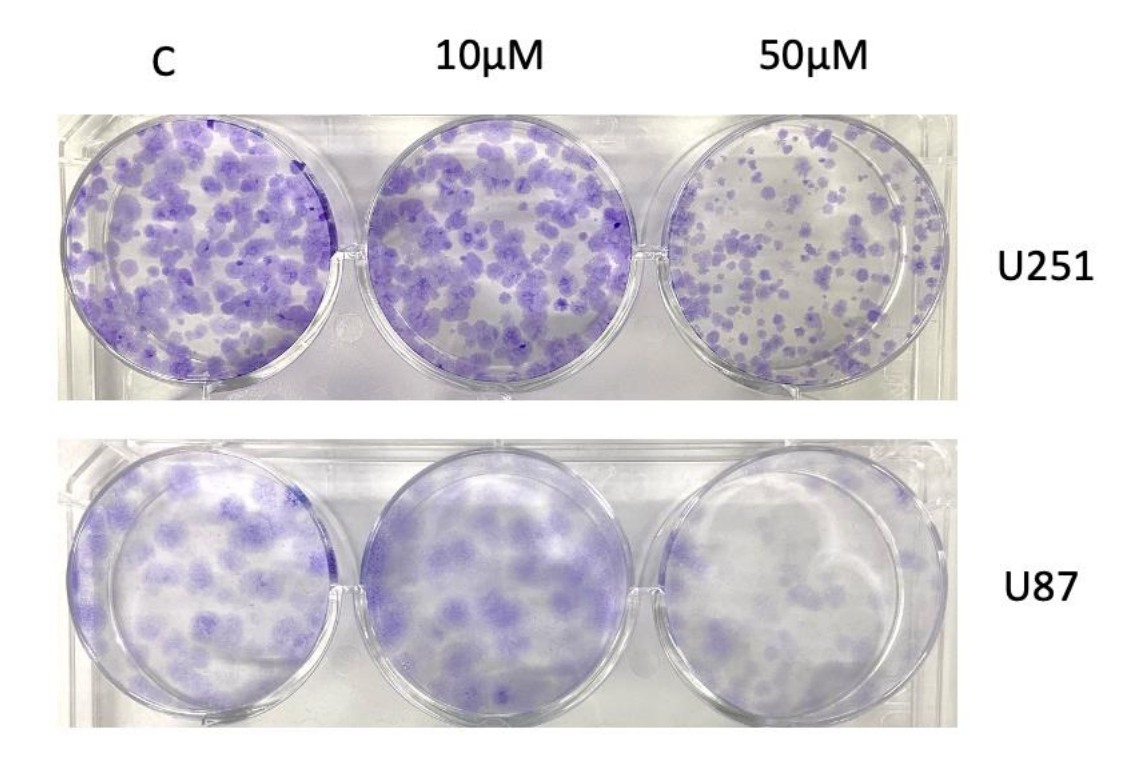


Figure 3.6 The effect of CP-91149 on colony formation of U251 (A) and U87 (B) cell lines after treatment with CP-91149 (0 μ M, 10 μ M, and 50 μ M) following 2 weeks of incubation.

3.5 Combination Treatment

The effect of CP-91149 in combination with TMZ was investigated *in vitro* on SVG p12, U251, T98G, and U87 cell viability. This was done across three time points: 24h, 48h, and 72h (Figures 3.7-3.9) and consisted of three independent experiments. Concentrations of CP-91149 ($20\mu M$ and $50\mu M$) were chosen from prior cell viability results to achieve a slight, not maximal, reduction in cell viability. Concentrations of TMZ ($50\mu M$ and $100\mu M$) were selected with the same premise.

24h Treatment

TMZ alone after 24h showed little reduction in cell viability in all cell lines, with the lowest cell viability being 75±26% in SVG p12 (A in figure 3.7) with 50μM TMZ. Also, in all cell lines treated with TMZ alone, cell viability was greater in cells treated with 100μM TMZ (99±48% in SVG p12, 117±7% in U251, 97±10% in T98G, 103±12% in U87) than cells treated with 50μM TMZ (75±26% in SVG p12, 113±28% in U251, 87±12% in T98G, 87±7% in U87). When all cell lines were treated with CP-91149 alone for 24h, results aligned with those outlined in section 3.3. Combination treatment after 24h resulted in minimal differences in cell viability when compared to independent treatments. When comparing the combination treatment to independent treatments involving the same concentration of TMZ or CP-91149, cell viability appears the same or higher in combination treatment across all four cell lines. In all cell lines cell viability was greater in cells treated in combination with CP-91149 and 100µM TMZ than in cells treated in combination with CP-91149 and 50µM TMZ regardless of CP-91149 concentration. Cell viability was consistently reduced in all cell lines treated with the same concentration of TMZ but with 50µM of CP-91149. For instance, mean cell viability results for U251 following 24h combination treatment (B in figure 3.7) were as follows: 117±15% in 20μM CP-91149 + 50μ M TMZ, $104\pm11\%$ in 20μ M CP- $91149 + 100\mu$ M TMZ, $111\pm26\%$ in 50μ M CP- $91149 + 50\mu$ M TMZ, $117\pm34\%$ in 50μ M CP- $91149 + 100\mu$ M TMZ.

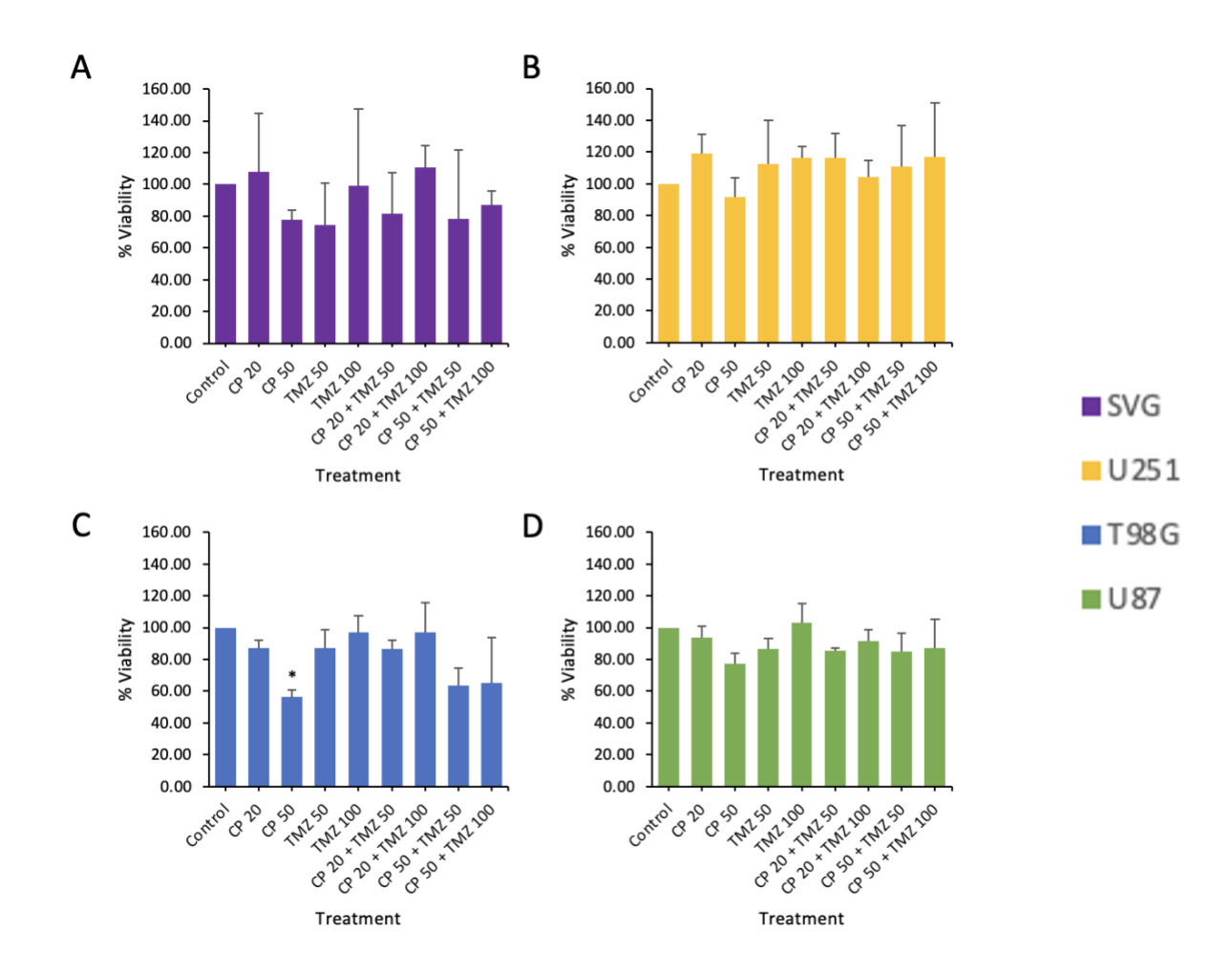


Figure 3.7. Combination treatment of CP-91149 and temozolomide on SVG p12 (A), U251 (B), T98G (C), and U87 (D) cell lines after 24h. Data presented as the average obtained from three independent repeats, error bars are \pm SD. Significant differences compared to the control are shown by * (*p < 0.05). Statistical analysis results in appendix 8.

48h Treatment

TMZ alone after 48h again showed little reduction in cell viability in all cell lines, with the lowest cell viability being 72±16% in SVG p12 with 50µM TMZ (A in figure 3.8). Also, in all cell lines treated for 48h with TMZ alone, cell viability was also greater in cells treated with 100μM TMZ (100±5% in SVG p12, 89±7% in U251, 100±10% in T98G, 112±11% in U87) than cells treated with 50μM TMZ (72±16% in SVG p12, 75±10% in U251, 81±8% in T98G, 108±17% in U87). When all cell lines were treated with CP-91149 alone for 48h, results were similar to those outlined in section 3.3. Combination treatment after 48h resulted in minimal effect on cell viability when compared to independent treatments (Figure 3.8). When comparing the combination treatment to independent treatments involving the same concentration of TMZ or CP-91149, cell viability after 48h also appears the same or higher in combination treatment across all four cell lines. As with 24h treatment, cell viability in all cell lines was greater in cells treated in combination with CP-91149 and 100μM TMZ than cells treated in combination with CP-91149 and 50μM TMZ regardless of CP-91149 concentration. Cell viability was reduced in all cell lines, except U251 (B in figure 3.8), treated with the same concentration of TMZ but with 50µM of CP-91149. Mean cell viability results for U251 following 48h combination treatment weren't very different with different doses but did appear slightly less in combination containing 100μM TMZ despite TMZ 100μM alone yielding higher viability than TMZ 50µM alone, results for combination treatment of U251 were as follows: 86±23% in 20μM CP-91149 + 50μM TMZ, 81±19% in 20μM CP-91149 + 100μM TMZ, 82±32% in 50μM CP- $91149 + 50\mu$ M TMZ, $73\pm31\%$ in 50μ M CP- $91149 + 100\mu$ M TMZ.

In T98G cells a greater reduction in cell viability was observed after 48h in the combination treatments (C in figure 3.8) when compared to 24h (C in figure 3.7). Both combination treatments including 50μ M CP-91149 (with 50μ M or 100μ M TMZ) had similar results of $35\pm30\%$ and $32\pm28\%$ respectively. The same was observed in SVG p12 ($77\pm11\%$ in 20μ M CP-91149 + 50μ M TMZ, $98\pm19\%$

in 20μ M CP- $91149 + 100\mu$ M TMZ, $70\pm33\%$ in 50μ M CP- $91149 + 50\mu$ M TMZ, $78\pm9\%$ in 50μ M CP- $91149 + 100\mu$ M TMZ) and U87 ($101\pm7\%$ in 20μ M CP- $91149 + 50\mu$ M TMZ, $106\pm17\%$ in 20μ M CP- $91149 + 100\mu$ M TMZ, $95\pm15\%$ in 50μ M CP- $91149 + 50\mu$ M TMZ, $106\pm6\%$ in 50μ M CP- $91149 + 100\mu$ M TMZ) but differences were not as obvious. Statistically significant decreases in cell viability were only observed in T98G cells at this timepoint between treatment with 50μ M CP-91149 and the combination treatment of 50μ M CP-91149 with 100μ M temozolomide ($32\pm28\%$, p<0.05) when compared to the control and when compared to cells treated with 100μ M temozolomide alone within T98G.

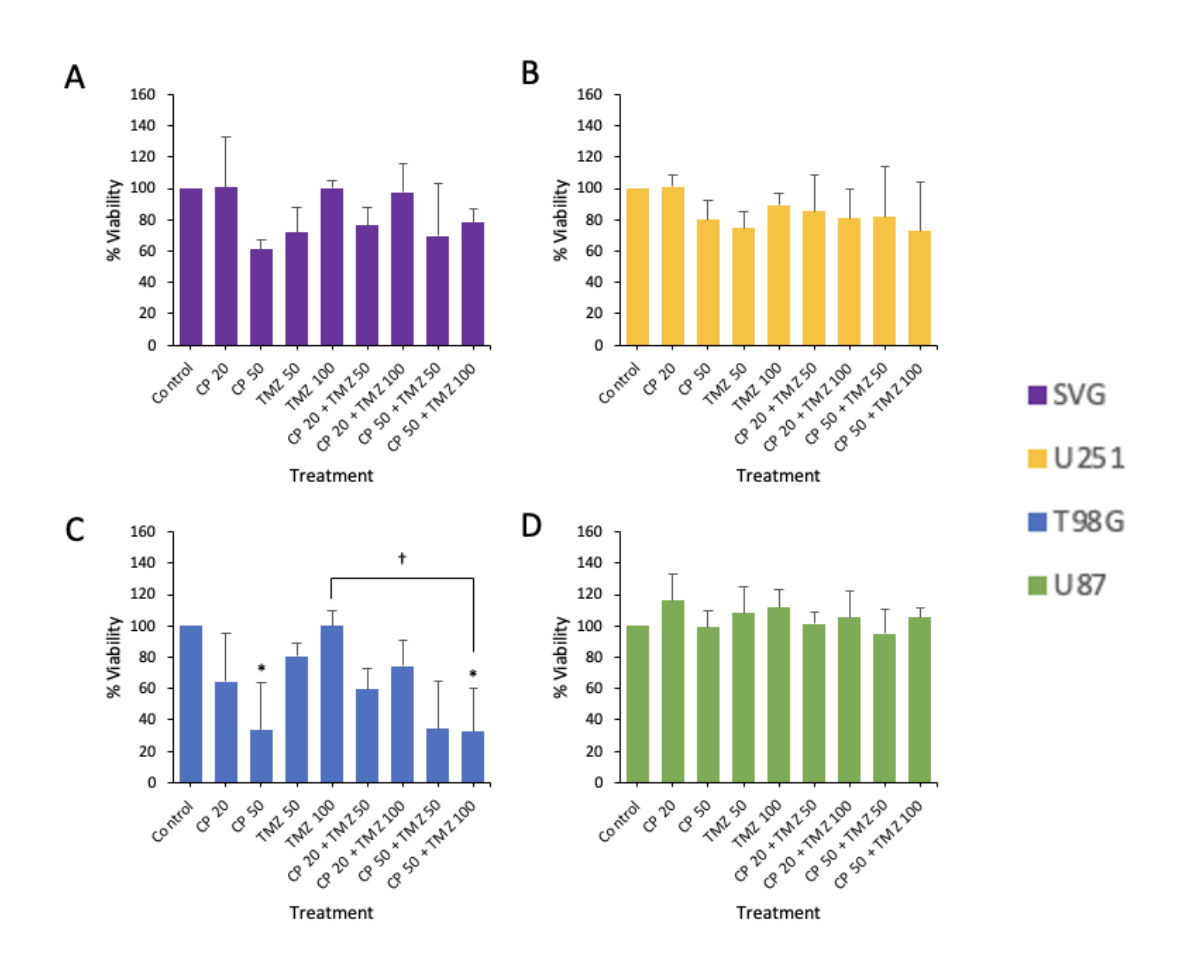


Figure 3.8. Combination treatment of CP-91149 and temozolomide on SVG p12 (A), U251 (B), T98G (C), and U87 (D) cell lines after 48h. Data presented as the average obtained from three independent repeats, error bars are \pm SD. Significant differences compared to the control are shown by * (*p < 0.05). Statistical analysis results in appendix 8.

72h Treatment

After 72h treatment with TMZ alone, there was slightly more of a reduction in cell viability in all cell lines, with the lowest cell viability being 55±5% in U251 with 50µM TMZ (B in figure 3.9). In all cell lines treated with TMZ alone for 72h, cell viability was greater in cells treated with 100μM TMZ (73±24% in SVG p12, 66±14% in U251, 116±30% in T98G, 117±11% in U87) than cells treated with 50μM TMZ (70±18% in SVG p12, 56±5% in U251, 104±30% in T98G, 99±6% in U87). When all cell lines were treated for 72h with CP-91149 alone, results were similar to those outlined in section 3.3. Combination treatment after 72h showed minimal differences in cell viability when compared to independent treatments (Figure 3.9). When comparing the combination treatment to independent treatments involving the same concentration of TMZ or CP-91149 within cell lines, cell viability after 72h shows more variation where some combinations resulted in lower cell viability whereas some showed higher cell viability than the comparative single treatment. In T98G cells (C in figure 3.9) the cell viability in combination treatment was similar to the CP-91149 only results that used the same concentration of CP-91149, but it was not similar to the respective TMZ alone treatment. Within T98G cells statistical significance compared to the control and 100µM TMZ alone was observed in 50μM CP-91149 and the combination treatment of 50μM CP-91149 with 100μM temozolomide $(34\pm27\% p<0.05 \text{ and } p<0.01 \text{ respectively})$. Both combination treatments including $50\mu\text{M}$ CP-91149 (with 50µM or 100µM TMZ) had similar results of 35±30% and 32±28% respectively. The same was observed in SVG p12 (77±11% in 20μM CP-91149 + 50μM TMZ, 98±19% in 20μM CP-91149 + 100μM TMZ, $70\pm33\%$ in 50μ M CP- $91149\pm50\mu$ M TMZ, $78\pm9\%$ in 50μ M CP- $91149\pm100\mu$ M TMZ) and U87 $(101\pm7\% \text{ in } 20\mu\text{M CP-}91149 + 50\mu\text{M TMZ}, 106\pm17\% \text{ in } 20\mu\text{M CP-}91149 + 100\mu\text{M TMZ}, 95\pm15\% \text{ in } 20\mu\text{M CP-}91149 + 100\mu\text{M TMZ}, 95\pm15\% \text{ in } 20\mu\text{M CP-}91149 + 100\mu\text{M TMZ}, 95\pm15\% \text{ in } 20\mu\text{M CP-}91149 + 100\mu\text{M TMZ}, 95\pm15\% \text{ in } 20\mu\text{M CP-}91149 + 100\mu\text{M TMZ}, 95\pm15\% \text{ in } 20\mu\text{M CP-}91149 + 100\mu\text{M TMZ}, 95\pm15\% \text{ in } 20\mu\text{M CP-}91149 + 100\mu\text{M TMZ}, 95\pm15\% \text{ in } 20\mu\text{M CP-}91149 + 100\mu\text{M TMZ}, 95\pm15\% \text{ in } 20\mu\text{M CP-}91149 + 100\mu\text{M TMZ}, 95\pm15\% \text{ in } 20\mu\text{M CP-}91149 + 100\mu\text{M TMZ}, 95\pm15\% \text{ in } 20\mu\text{M CP-}91149 + 100\mu\text{M TMZ}, 95\pm15\% \text{ in } 20\mu\text{M CP-}91149 + 100\mu\text{M TMZ}, 95\pm15\% \text{ in } 20\mu\text{M CP-}91149 + 100\mu\text{M TMZ}, 95\pm15\% \text{ in } 20\mu\text{M CP-}91149 + 100\mu\text{M TMZ}, 95\pm15\% \text{ in } 20\mu\text{M CP-}91149 + 100\mu\text{M TMZ}, 95\pm15\% \text{ in } 20\mu\text{M CP-}91149 + 100\mu\text{M TMZ}, 95\pm15\% \text{ in } 20\mu\text{M CP-}91149 + 100\mu\text{M TMZ}, 95\pm15\% \text{ in } 20\mu\text{M CP-}91149 + 100\mu\text{M TMZ}, 95\pm15\% \text{ in } 20\mu\text{M CP-}91149 + 100\mu\text{M TMZ}, 95\pm15\% \text{ in } 20\mu\text{M CP-}91149 + 100\mu\text{M TMZ}, 95\pm15\% \text{ in } 20\mu\text{M CP-}91149 + 100\mu\text{M TMZ}, 95\pm15\% \text{ in } 20\mu\text{M CP-}91149 + 100\mu\text{M TMZ}, 95\pm15\% \text{ in } 20\mu\text{M CP-}91149 + 100\mu\text{M TMZ}, 95\pm15\% \text{ in } 20\mu\text{M CP-}91149 + 100\mu\text{M TMZ}, 95\pm15\% \text{ in } 20\mu\text{M CP-}91149 + 100\mu\text{M TMZ}, 95\pm15\% \text{ in } 20\mu\text{M CP-}91149 + 100\mu\text{M TMZ}, 95\pm15\% \text{ in } 20\mu\text{M CP-}91149 + 100\mu\text{M TMZ}, 95\pm15\% \text{ in } 20\mu\text{M CP-}91149 + 100\mu\text{M TMZ}, 95\pm15\% \text{ in } 20\mu\text{M CP-}91149 + 100\mu\text{M CP-}91149$ 50μM CP-91149 + 50μM TMZ, 106±6% in 50μM CP-91149 + 100μM TMZ) but differences were less obvious.

Significant differences at 72h were measured in U251 between the treatment with 50 μ M CP-91149 and the combination treatment of 50 μ M CP-91149 with 100 μ M temozolomide (56±11%, p<0.05) when compared to the control. Additionally, there was a significant difference between the combination treatments of 20 μ M CP-91149 with 50 μ M temozolomide as well as 20 μ M CP-91149 with 100 μ M temozolomide (65±10% and 68±15% respectively, p<0.05) compared to U251 cells treated with 20 μ M CP-91149 only. However, viability was similar to TMZ alone. Results for SVG p12 at 72h were statistically insignificant, although there was a downward trend for combinations with 50 μ M CP-91149 (53±18% with 50 μ M TMZ and 51±16% with 100 μ M TMZ).

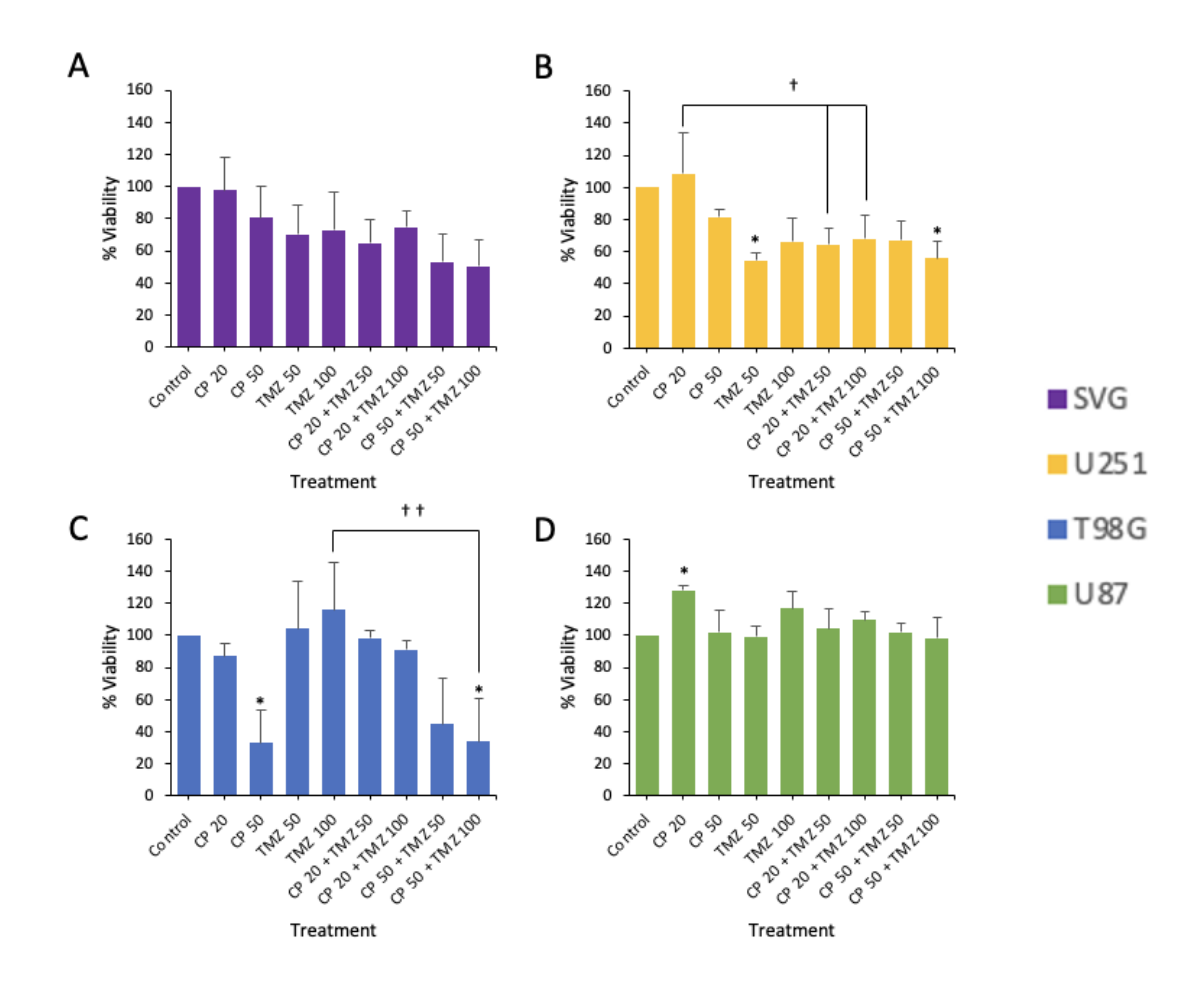


Figure 3.9: Combination treatment of CP-91149 and temozolomide on SVG p12 (A), U251 (B), T98G (C), and U87 (D) cell lines after 72h. Data presented as the average obtained from three independent repeats, error bars are \pm SD. Significant differences compared to the control are shown by * (*p < 0.05). Statistical analysis results in appendix 8.

Across all time points, TMZ had no dose-dependent effect and cell viability appeared to increase in the higher concentrations of TMZ in most cases, with the exception of U251 at 48h and 72h, which is observed both independently and in the combination treatments with TMZ. Overall, the results do not indicate that CP-91149 can increase the sensitivity of GB cells to temozolomide.

3.6 Wound Healing Assay

The effects of CP on the migratory potential of GB cells were assessed by a wound healing assay. Treatment of T98G and U251 cells following a scratch made in the monolayer showed that CP-91149 inhibited cell migration (Figures 3.10 and 3.11). In T98G cells after 24h the average percentage (%) of wound healing of the control was 75.2% (B in figure 3.10). When treated with 10μ M and 50μ M CP-91149 the average % closure was 52% and 43.6% respectively, with 50μ M treatment showing statistical significance compared to the control (p<0.05). Similarly, U251 average % closure after 24h was 73.8%, whereas cells treated with 10μ M or 50μ M CP-91149 resulted in 62.5% and 43.8% respectively (B in figure 3.11). In both cell lines, there was a reduction in migration by almost half following 24h treatment with CP-91149 when compared to the control.

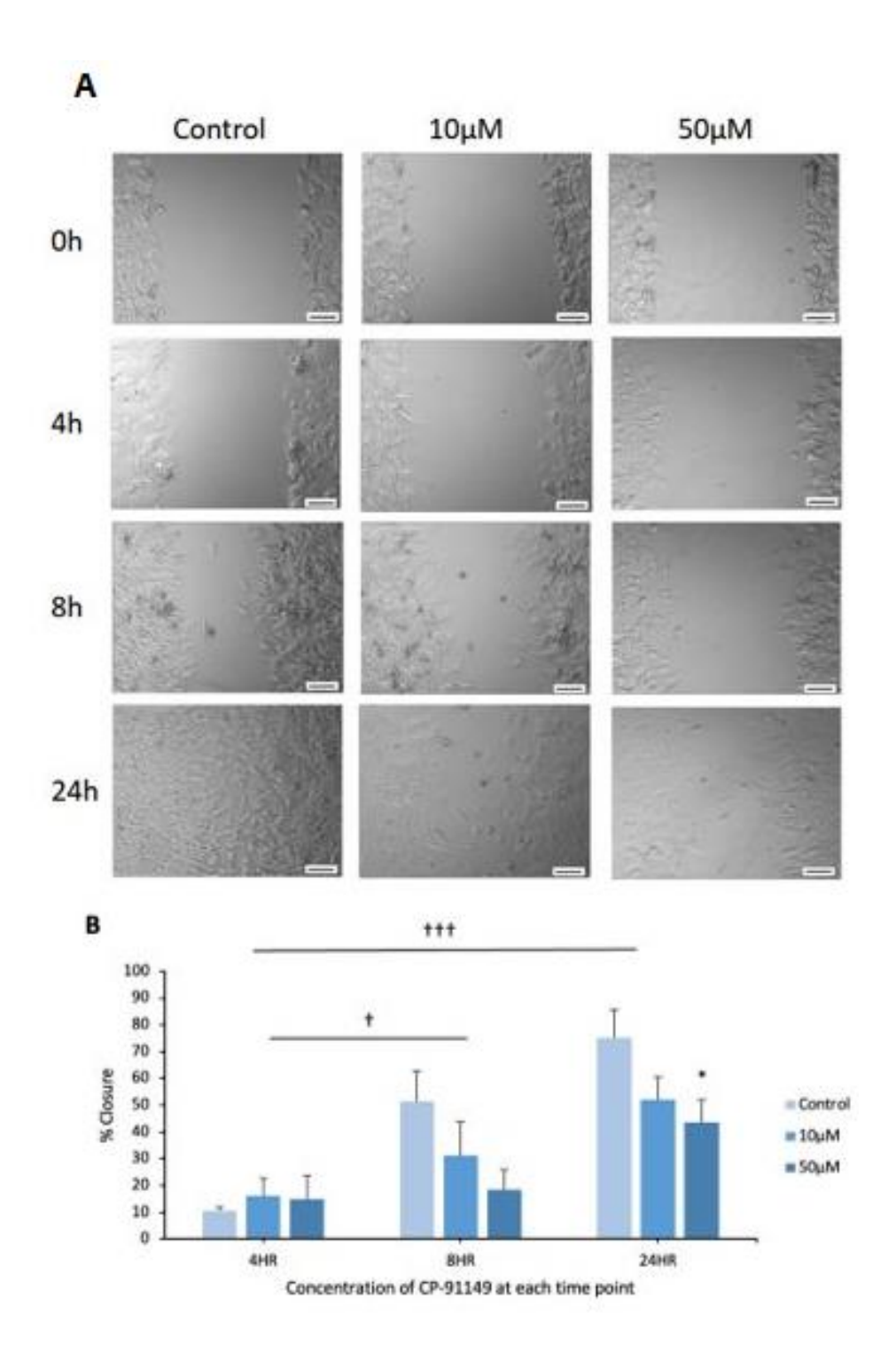


Figure 3.10 The effect of CP-91149 on the migration of T98G cells. Cell migration in response to CP-91149 at $10\mu M$ and $50\mu M$ compared to control. A), Representative images of the distance CP-91149 treated T98G cells travelled at 4, 8, and 24h compared to control (n=3). C), Graph demonstrating the average percentage (%) migration of T98G cells as a % of the area of the gap at 0h (n=3, error bars are \pm SD). Scale bars 100 μM . Images were taken at 10x magnification. Statistical analysis results in appendix 6.

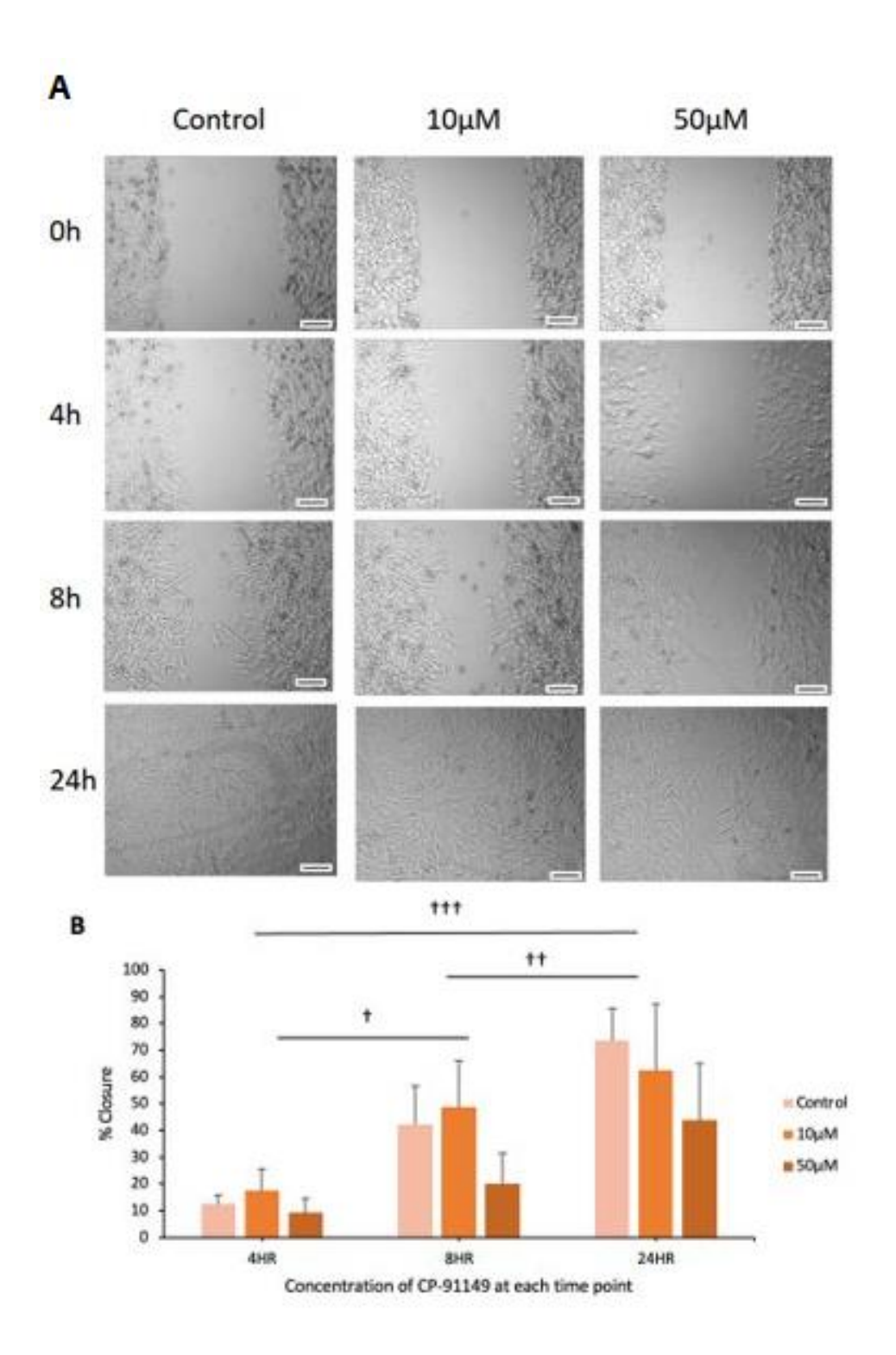


Figure 3.11 The effect of CP-91149 on the migration of U251 cells. Cell migration in response to CP-91149 at 10μ M and 50μ M compared to control. A), Representative images of the distance CP-91149 treated U251 cells travelled at 4, 8, and 24h compared to control (n=3). B), Graph demonstrating the average percentage (%) migration of U251 cells as a % of the area of the gap at 0h (n=3, error bars are \pm SD). Scale bars 100 μ m. Images were taken at 10x magnification. Statistical analysis results in appendix 7.

3.7 Cell Cycle Analysis

Based on previous cell viability assay results, three concentrations of CP-91149 ($10\mu M$, $50\mu M$, and $100\mu M$) were selected to investigate the effect of GP inhibition *in vitro on the cell cycle*, following 48h treatment, using PI staining and flow cytometry analysis.

Although minimal statistically significant differences were observed, there were differences between concentrations and between the GB cell lines, as seen in the representative images of cell cycle distribution (Figure 3.12).

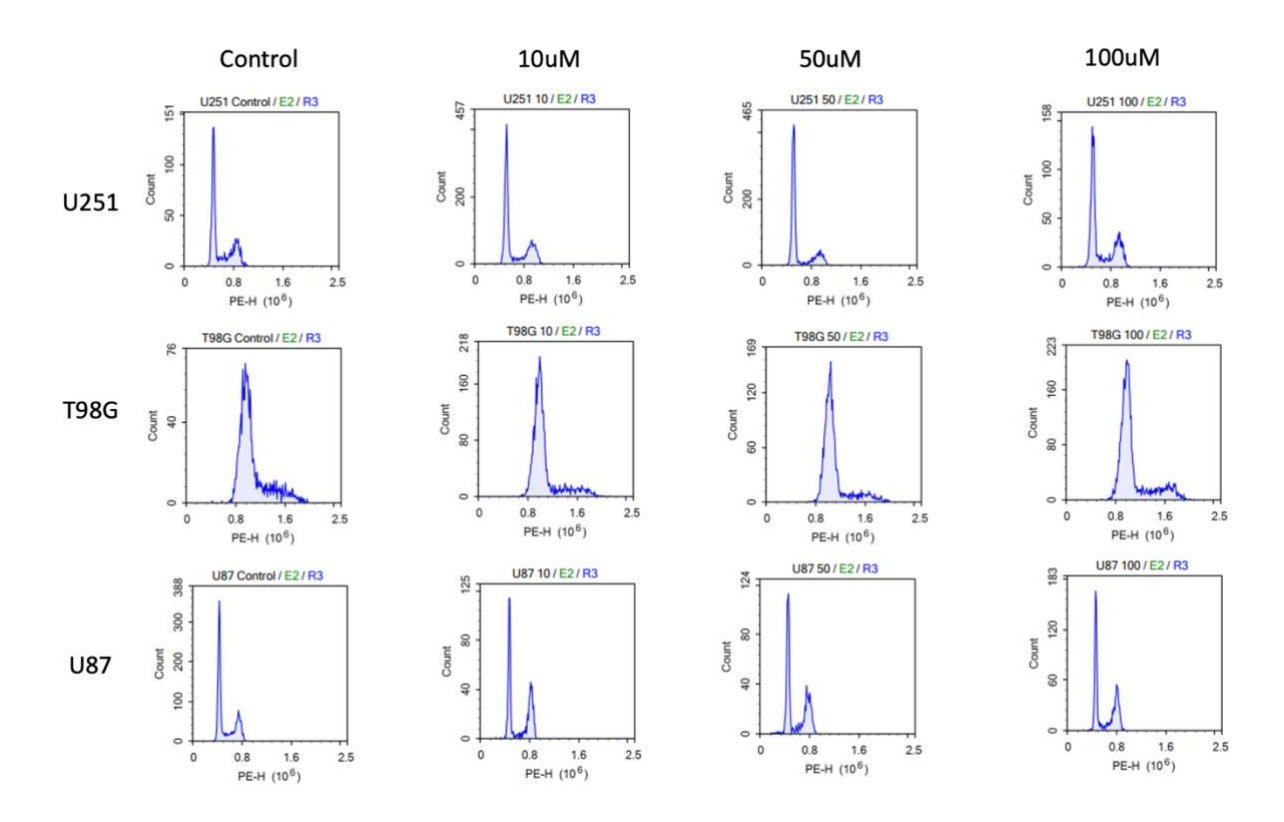


Figure 3.12: Representative graphs showing the cell cycle distribution of GB cell lines. U251, T98G, and U87 cells following 48h treatment with varying concentrations of CP-91149 (0μM, 10μM, 50μM, and 100μM), measured after PI staining using flow cytometry. Graphs reflect three independent experiments.

		[CP-91149] (μM)			
Cell Line	Phase	0	10	50	100
U251	G1	59.36	69.30	70.75	66.53
	S	14.27	8.30	7.90	15.97
	G2	25.30	21.76	21.04	17.29
	Sub G1	1.07	0.64	0.31	0.21
T98G	G1	71.87	80.87	81.02	75.88
	S	20.95	11.54	11.41	12.19
	G2	3.88	6.06	5.79	8.90
	Sub G1	3.29	1.54	1.78	3.02
U87	G1	58.95	55.74	53.44	62.92
	S	12.06	6.96	9.18	9.05
	G2	28.61	36.92	36.65	26.88
	Sub G1	0.38	0.38	0.73	1.15

Table 3.1: Mean values of the % of cells in each phase of the cell cycle following 48h treatment with CP-91149. % is of the population of the parent (i.e. of the gate selected to remove outliers such as doublets and debris).

In treated U251 cells there was an increase in the population of cells in the G1 phase (A in figure 3.13), with 10μ M (69±9%), 50μ M (71±5%), and 100μ M (67±7%) all having similar results, compared to untreated cells (59±1%). A decrease in the proportion of U251 cells in the S phase was observed when treated with 10μ M (8±2%) and 50μ M (8±1%) of CP-91149 compared to the control (14±5%), whereas cells treated with 100μ M had a similar number of cells in the S phase (16±10). The percentage of cells in the G2/M phase changed with treatment as untreated cells yielded the most cells in the G2/M phase (25±5%) and cells treated with CP-91149 at 10μ M (22±7%), 50μ M (21±6%), and 100μ M (17±12%) showed reduction in a dose-dependent manner (Figure 3.13). While the proportion of U251 cells in the sub-G1 phase decreased as CP-91149 concentration increased, the values were all extremely low and variances were minimal. These differences observed in U251 cells were not statistically significant.

The percentage of T98G cells in the G1 phase increased slightly following 48h treatment (B in figure 3.13) with $10\mu\text{M}$ (81±1%), $50\mu\text{M}$ (81±5%), and $100\mu\text{M}$ (76±2%) of CP-91149 when compared to untreated cells (72±4%). Within the S phase of the cell cycle, the population of cells in the control (21±6%) was greater than what was measured in the treatments of $10\mu\text{M}$ (12±2%), $50\mu\text{M}$ (11±4%), and $100\mu\text{M}$ (12±2%). On the other hand, the proportion of T98G cells in the G2/M phase increased slightly with GP inhibition, with $10\mu\text{M}$ (6±3%), $50\mu\text{M}$ (6±4%), and $100\mu\text{M}$ (9±2%), in comparison to untreated T98G cells (4±2%). The proportion of cells in the sub-G1 phase appears to decrease but the values are again very low (Fig.3.13). All differences in the cell cycle measured in T98G cells displayed no statistical significance.

In U87 cells, a slight decrease in the average population of cells in the G1 phase of the cell cycle was observed (C in figure 3.13) following drug treatment with CP-91149 at 10μ M (56±5%) and 50μ M (53±2%) compared to the control (59±5%), whereas there was a slight increase following treatment at 100μ M (63±17%). The proportion of cells in the S phase U87 cells treated with 10μ M CP-91149

was significantly reduced by almost half (7±2%) (p<0.05) of that of the control (12±2%), however, this proportion raised slightly in higher concentrations of 50 μ M (9±2%) and 100 μ M (9±1%). An increase was measured in the percentage of U87 cells in the G2/M phase when treated with 10 μ M (37±3%) and 50 μ M (37±1%) of CP-91149 when compared to untreated cells (29±7%), although the 100 μ M treatment (27±17) showed a similar average to the control. Differences in the number of cells in the sub-G1 phase were not comparable due to very low percentages (Figure 3.13).

Overall, when compared to the control there were some minor changes in the cell cycle following treatment with CP-91149 and there was high variability observed. There were no notable cell numbers in the sub-G1 phase, which would indicate apoptosis induction. Another common trend was a decrease in S-phase cells with an increase in either G1 or G2/M phase following treatment with 10uM and 50uM (Figure 3.13).

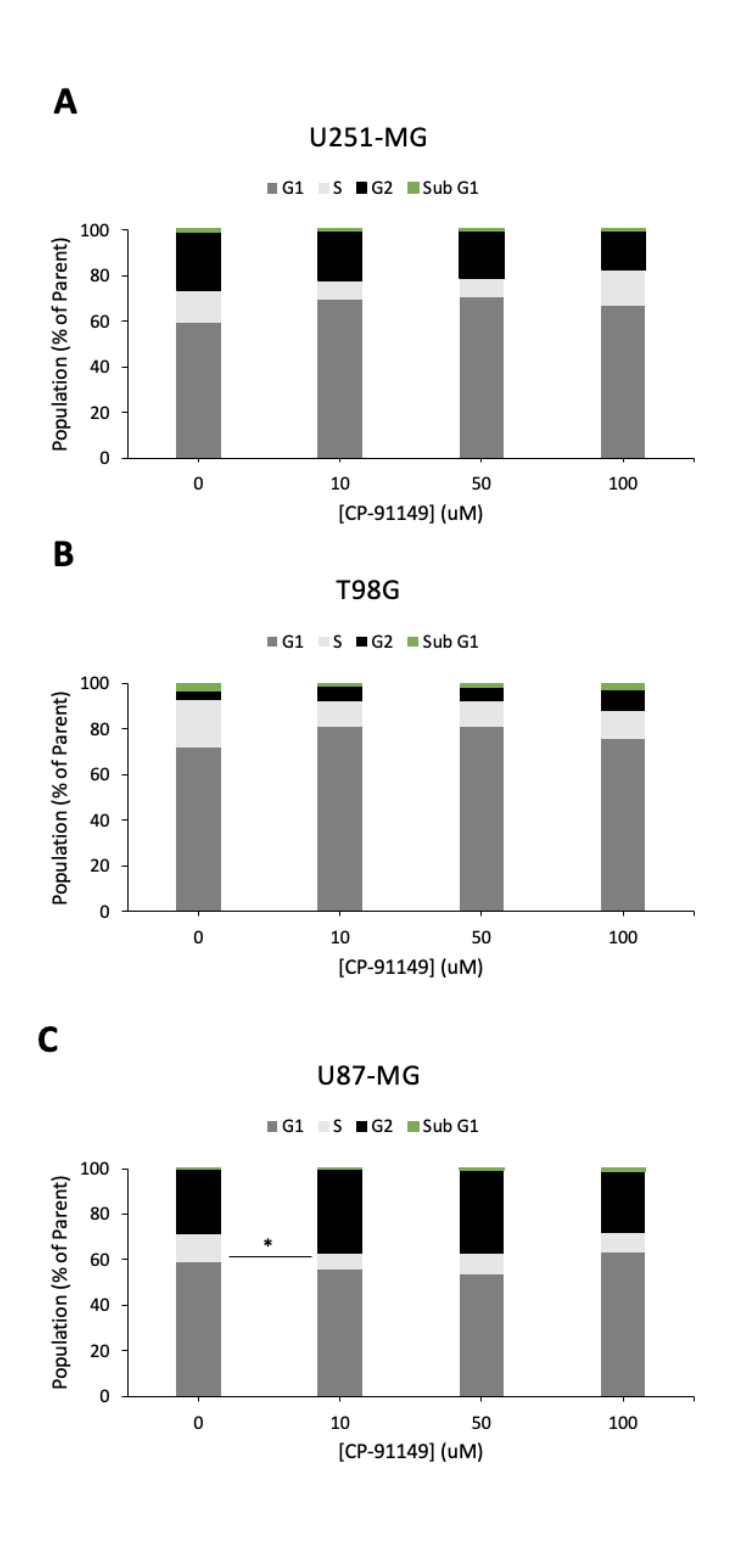


Figure 3.13: Average cell cycle distribution of GB cell lines following GP inhibition. Cell cycle analysis results from PI staining of U251 (A), T98G (B), and U87 (C) cell lines following 48h treatment with varying concentrations of CP-91149 (0 μ M, 10 μ M, 50 μ M, and 100 μ M). Data is presented as a percentage of the parent (total within a gated area to remove debris/doublets) and represents the average of three independent experiments. Significant differences compared to the control are shown by * (*p < 0.05). Statistical analysis results in appendix 9.

3.8 Apoptosis Assay

Previous viability assays showed a reduction in viability following CP-91149 in all cell lines. However, flow cytometry didn't show noticeable apoptosis after 48h treatment, as assessed by the sub-G1 phase. To validate the results from cell cycle analysis, apoptosis induction was examined with fluorescence microscopy. GB cells treated with the maximum concentration of CP-91149 (100 μ M) and for a maximal period of 72h were fixed and stained with DAPI to visualise any nuclear changes, such as condensation or fragmentation. No clear abnormalities were observed in the nuclei of individual treated GB cell lines following 72h treatment with 100 μ M CP-91149 when compared to the control. Instead, there was an obvious reduction in cell density when observing treated cells compared to untreated cells (Figure 3.14). These results again suggest that CP-91149 exerts its effects on cell viability not by induction of apoptosis, but rather by inhibition of proliferation.

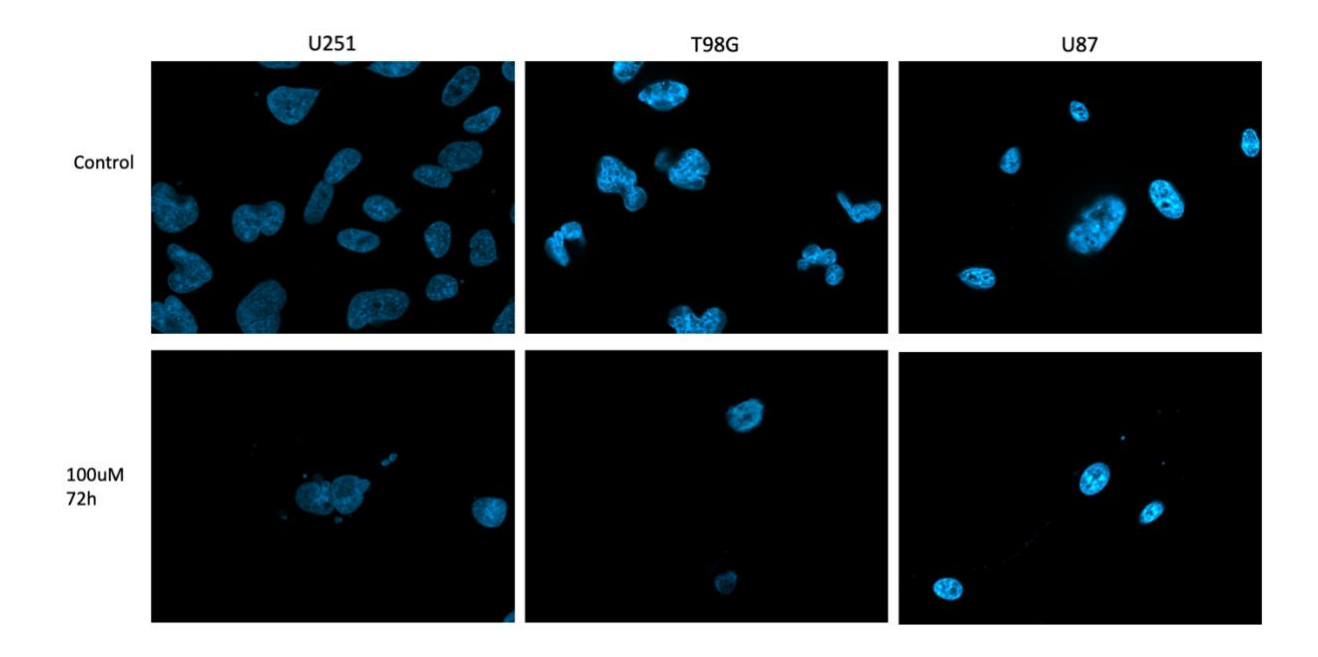


Figure 3.14 Immunofluorescence images of GB cell lines treated with CP-91149, stained with DAPI. Representative images showing the chromatin stained with DAPI of untreated and treated U251, T98G, and U87 cells. Treatment was with 100μM of CP-91149 for 72h.

4. Discussion

Therapeutic options for the treatment of GB remain limited, with 50% of patients showing little to no improvement when treated with radiotherapy with the addition of temozolomide, the main chemotherapeutic, potentially due to resistance mechanisms (Lee, 2016). Additionally, the progress of finding new and effective treatments has been slow for many reasons, including the inability of compounds to pass the BBB and therefore target the tumour site (Sweeney *et al.*, 2019). Unfortunately, this provides a negative outlook for many patients diagnosed with GB as the prognosis remains poor, and the median survival remains 14.6 months.

The main aim of this project was to investigate the potential of GP as a novel therapeutic target *in vitro* utilising GB cell lines (U251, T98G, and U87) by utilising a GP inhibitor, CP-91149, and observing expression of GP isoforms. The efficacy of GP inhibition as a therapeutic approach was investigated by measuring cell viability, cell migration, and cell cycle distribution following treatment. Additionally, different GP isoform levels were observed through western blot and immunofluorescence to supplement cell viability, cell migration, and cell cycle distribution experiments.

4.1 Levels of GP as Found in Western Blot and Fluorescence

While it is known that there are three isoforms of GP, levels expressed within patient-derived GB cells or GB cell lines have not been well established. Therefore, this project aimed to investigate levels of PYGB, PYGL, and PYGM amongst a variety of GB cell lines to determine which isoform is the most predominant and which of the isoforms, if any, are overexpressed. Findings through western blot analysis and confirmed through immunocytochemistry, suggest that PYGL is expressed at a higher level in U251, T98G, and U87. Additionally, visualization determined that all isoforms of GP were overexpressed in U251 in comparison to the other cell lines tested. This suggests that the liver isoform, PYGL, must have a significant impact on the progression of GB, which could relate back to its specific function. PYGL is mainly responsible for maintaining glycaemic levels, suggesting its

upregulation is advantageous to GB cells as it supplies glucose for the main purpose of promoting growth (Migocka-Patrzałek & Elias, 2021). Through western blot analysis compared to the control, SVG p12, it appears that PYGL is overexpressed in U251 cells. However, when comparing relative expression to SVG p12, it appeared that both the PYGB and PYGM isoforms were overexpressed at a higher level in U251 cells than PYGL expression relative to SVG p12. While it would be expected for the PYGB isoform to be the most abundant within GB, findings that PYGL is the most abundant isoform in GB cell lines are consistent among other studies on PYGL in GB. Findings from Zois *et al* (2022) investigating the protein levels of PYGL and PYGB via western blot analysis amongst GB cell lines support the findings of this study before the expression of PYGL was calculated relative to the control (SVG p12) that U251 cell lines show the highest level of PYGL.

It was not expected for the control cells, SVG p12, to display levels of PYGL that were higher than T98G and U87 cells. A comparison of gene expression data revealed that expression levels of PYGL were upregulated in human GB when compared to normal brain, while there were no differences in the expression of PYGB, and PYGM expression was downregulated in human GB compared to normal brain tissue (Zois *et al.*, 2022). This data corresponds with the raw results of this study showing the expression of each isoform within the GB cell lines, where PYGL was the most abundant and PYGM was expressed at a very low level. However, it does not support the data in this study when expression is shown relative to the control, SVG p12, raising to question of the reliability of the control.

4.2 Effects on Cell Viability

This study found that CP-91149 has a dose-dependent cytotoxic effect on human GB cell lines U251, T98G, and U87 *in vitro*.

SVG p12 cell viability following treatment with CP-91149 had a dose-dependent effect, with the greatest effect on cell viability at 72h and 100 μ M of CP-91149. At lower concentrations of 5 μ M and 10 μ M CP-91149, cell viability increased above 100% across all three time points. This increase reduced as the time point increased. At 100 μ M significant decreases in cell viability were observed, with the lowest cell viability being after 72h of treatment. The findings from SVG p12 cells were unexpected as, theoretically, they wouldn't be as sensitive to GP inhibition. This is because it was expected that SVG p12, due to its non-cancerous nature, would make use of other metabolic pathways rather than aerobic glycolysis, as detailed in the hallmark of metabolic switching (mentioned in section 1.4). However, as shown by its clear reduction in cell viability following GP inhibition, SVG p12 could have been affected by this metabolic switch.

Cell viability of U251 cells following treatment with CP-91149 also had a dose-dependent effect, with a significant reduction in cell viability at 72h and 100 μ M of CP-91149. At lower concentrations of 5 μ M and 10 μ M CP-91149, cell viability increased above 100% across all three time points. At higher concentrations of 50 μ M and 100 μ M significant decreases in cell viability were observed, with the lowest cell viability being after 72h of treatment (19±7%). Compared to the other cell lines, the lowest cell viability was greater than that of SVG p12, T98G, and U87, suggesting greater resistance in this cell line. When comparing these findings to GP levels across cell lines from western blot/immunofluorescence (sections 3.1 and 3.2), U251 displayed the highest expression of GP in all three isoforms. This could indicate a potential link between GP expression and the effectiveness of GP inhibition as a treatment, as the most resistant GB cell line has the greatest GP expression.

Therefore, it could be presumed that GB tumours that exhibit higher GP expression may require higher doses of GP inhibitor or may not benefit as much as those with lower GP expression.

than what was observed in T98G and U87. This observation makes sense when compared to the western blot and immunofluorescence results, which showed that U251 showed the greatest expression of GP amongst the GB cell lines, suggesting it would require a higher dose of inhibitor than T98G and U87 would require. This could be explained by the fact that the U251 cell line is recognised as the more aggressive model (Schulz *et al.*, 2022). While in tumour models U87 cells tend to grow quicker they tend to remain localised, whereas U251 cells have displayed greater levels of migration in tumours. The U251 cell line was established decades ago, meaning its highly infiltrative and invasive growth pattern could be explained by genetic and biological changes due to high passages from long-term culture. Since U251 is known to be more aggressive and has displayed greater resistance to GP inhibition in this study, it could be concluded that there is a correlation between the "Warburg effect" (mentioned in section 1.3) and the tumour phenotype, with greater upregulation of glycolysis occurring in more aggressive cancer cells (Hanahan & Weinberg, 2011).

T98G cells exhibited similar dose-dependent reductions in cell viability with a significant decrease in cell viability at 72h and 100 μ M of CP-91149. At lower concentrations of 5 μ M and 10 μ M CP-91149, cell viability was above 100% across all three time points. At higher concentrations of 50 μ M and 100 μ M significant decreases in cell viability were observed, and T98G cells appeared the most sensitive of the GB cell lines to CP-91149 (72h treatment, 100 μ M: 3.5±6%). Compared to western blot/immunofluorescence analysis (sections 3.1 and 3.2), GP levels in T98G cells were significantly lower across all isoforms, and specifically in PYGL T98G showed the least expression. Therefore, in contrast to U251 cells, it could be determined that a lower level of GP expression in GB cells results in greater sensitivity to GP inhibitors as a treatment.

As with the other GB cell lines, U87 demonstrated a similar reaction to CP-91149, with a dose dependent decrease in cell viability that was statistically significant at higher concentrations of 50μM and 100μM. At lower concentrations of 5μM and 10μM CP-91149, cell viability was above 100% across all three time points. U87 cell viability after 72h with 100μM was between that observed in T98G and U251 cells (16±9%). When looking at western blot/immunofluorescence data of GP expression in U87 cells, it appears that U87 expresses the least amount of PYGB and PYGB, and slightly more PYGL expression than T98G cells. Based on the cell viability results, this could suggest that the differences in sensitivity to CP-91149 are most likely linked to PYGL expression specifically as opposed to GP expression as a whole. This further indicates the potential significance of PYGL in GB.

These overall findings from T98G and U87 cells are consistent with findings from Schnier et~al (2003) that found a correlation between glycogen accumulation and growth inhibition following treatment with CP-91149. This study touched on the effect of CP-91149 on glioma cell lines, including T98G and U87 cell lines. After treating cells with 30 μ M of CP-91149, glycogen content in T98G cells increased over twice as much as untreated T98G cells whereas U87 cells displayed a slight decrease in glycogen accumulation after treatment. This was reflected in the cell growth patterns as T98G cells after treatment with 30 μ M of CP-91149 were half as much as untreated T98G cells, whereas U87 cells showed minimal differences in cell growth after treatment. This demonstrates the ability of CP-91149 to inhibit glycogenolysis.

Interestingly, the effect of CP-91149 *in vivo* was established by Martin *et al* (1998), by measuring net liver glycogen content and plasma glucose concentration within *ob/ob* mice following treatment with CP-91149. When treated with CP-91149, hepatic glycogen increased 3-fold and plasma glucose was nearly halved when compared to the control. This further supports the inhibition of glycogenolysis following the inhibition of GP.

An unexpected finding was the slight increase in cell viability compared to the control that was observed in all cell lines when treated with lower doses of CP-91149. A potential reason for this could be what is known as the hormetic effect, or hormesis, where low doses may provide a stimulatory effect whereas higher doses have an inhibitory effect (Calabrese, 2008). The stimulatory response has been noted to increase up to 30-60% above the control response, which correlates with the cell viability following treatment at 5-10 μ M CP-91149. This aspect is a key finding that would be of importance to consider when determining a therapeutic dose for future research as these low doses that increase cell viability are likely to stimulate tumour growth.

4.5 Inhibitor Effect on Colony Formation

The clonogenic assay involves seeding a low density of cells to achieve single cells in order to observe the ability of the cell to form colonies, demonstrating survival and proliferation, in the presence of a drug treatment.

When treated with CP-91149, at a concentration of $10\mu M$ there was no difference in colony growth in both U251 and U87 when compared to the respective control, suggesting this dose was too low to elicit an inhibitory response. This was expected considering prior cell viability results. However, when treated with $50\mu M$ CP-91149 there was an observed difference in colony formation for both cell lines.

U251 colonies following treatment with $50\mu M$ CP-91149 appeared to yield as many colonies as the control and $10\mu M$ treatment, however, individual colonies at this greater treatment concentration are much smaller. Given that U251 cells also exhibited the greatest level of GP expression from western blot/fluorescence analysis (sections 3.1 and 3.2) and appeared to be the more resistant cell line in cell viability assays (section 3.3), it could be assumed that U251 cells

possess a quality that allows them to have greater survival against GP inhibition, but their growth is limited.

Conversely, U87 colonies in $50\mu M$ treatment appeared to grow to a similar size to colonies in the control and $10\mu M$ treatment conditions, however, there seemed to be fewer of these colonies present at a higher concentration. This suggests that GP inhibition suppresses survival in some U87 colonies, but some colonies can evade this, a reflection of the heterogeneous nature of glioblastoma.

These differences observed in U251 and U87 cells could indicate inhibition of their characteristics. For instance, as mentioned in section 4.2, U251 cells are known to be more aggressive and infiltrative than U87 cells (Schulz *et al.*, 2022). Since a characteristic of U251 cells is greater migration, this could explain why results from the Clonogenic assay (Figure 3.6) show U251 cells having a similar number of colonies compared to the control. On the other hand, U87 cells usually remain localised but grow quicker, explaining why in the Clonogenic assay, following the highest concentration of CP-91149, U87 cells displayed fewer colonies but they were of similar size to the control.

Due to the novelty of GP as a target for GB, there is a lack of research regarding the effect of GP inhibition in gliomas. However, research supports the reduction of colonies following GP inhibition within other cancer cell lines. In the context of ovarian and renal cancer, $20\mu M$ of CP-91149 induced no change in colony formation but $100\mu M$ caused a significant decrease in colony formation (Khan *et al.*, 2023).

4.3 Combination Treatment Effect on Cell Viability

To investigate whether GP inhibition could sensitise GB cell lines to TMZ treatment, a combination of CP-91149 and TMZ was administered to SVG p12, U251, T98G, and U87 cell lines. Concentrations of CP-91149 (20 μ M and 50 μ M) were selected from initial cell viability results that yielded approximately 80-50% cell viability following treatment. TMZ concentrations were selected following prior tests of varying concentrations from 5-400 μ M and two that produced a very slight reduction in cell viability (50 μ M and 100 μ M) were selected for combination treatment.

Results following combination treatment were highly variable across all four cell lines and all time points. While CP-91149 alone consistently demonstrated a dose-dependent effect, a dose-dependent effect with TMZ either alone or in combination was not clear. When observing TMZ treatment alone, cells given 100µM had greater cell viability than cells given 50µM, which is unexpected considering the mechanism of action for TMZ. Then, in combination treatments cell viability results were highly inconsistent and often showed greater cell viability than cells treated with CP-91149 alone, demonstrating no clear synergistic or additive effect.

Temozolomide within *in vitro* research has proven to be highly inconsistent. For example, Pyko *et al.*, (2013) used TMZ concentrations 50, 100, 200, and 400 μ M on T98G cells and when TMZ was used alone for a total treatment time of 144h, cell viability in concentrations 50 μ M and 100 μ M only reduced very minimally to approximately 90%. These findings are similar to what was observed in this study where T98G cell viability showed minimal reductions to approximately 90%. On the other hand, when treating U87 cells with TMZ alone for 144h, cell viability reduced to approximately 60% when treated with 50 μ M and 100 μ M. This does not reflect the results from this project, where treatment of U87 cells with 50 μ M and 100 μ M TMZ had no effect on cell viability. Alternatively, Alonso *et al.*, (2007) measured cell viability of TMZ for 72h have observed cell viability reduction to approximately 80% following treatment with 50 μ M and 100 μ M TMZ. These differences could be due

to differences in protocol and/or treatment times, however, this demonstrates a variety in results of TMZ treatment alone.

However, while TMZ alone (and in combination with many other drugs) shows poor results and low potency on GB cells *in vitro*, it is worth noting that TMZ is usually administered to patients to sensitise the tumour to radiotherapy (Stupp protocol) rather than acting effectively independently. This further highlights the importance of the discovery of new and effective drugs for the treatment of GB.

Overall, these results suggest that a combination therapy of CP-91149 with TMZ would not be effective for GB treatment. A possible explanation for this could involve the incompatibility of CP-91149 and TMZ's different mechanisms of action. TMZ aims to induce apoptosis by indirect DNA damage via methylation, causing a mismatch (Arora & Somasundaram, 2019). On the other hand, results from this study suggest GP inhibition with CP-91149 suppresses proliferation but does not induce apoptosis. Unfortunately, the exact mechanism of CP-91149 is unknown. Because inhibition of GP results in glycogen accumulation and a lack of glucose for the cell to maintain metabolic processes that generate energy to support growth and division, the cell would likely undergo apoptosis due to lack of energy (Garcia, Jain, & Aghi, 2021). Schnier *et al.*, (2003) treated A549 non-small cell lung carcinoma cells with CP-91149 and observed glycogen accumulation, growth inhibition, and cell cycle disruption in a concentration-dependent manner. This supports that CP-91149 can inhibit glycogenolysis in cancer cells and confirms that there is a cytotoxic effect associated.

4.4 Inhibitor Effect on Migration

Cell migration in response to inhibition of GP using CP-91149 was assessed by a wound healing assay. Investigation of the effect of GP inhibition on GB cell migration was important due to the highly infiltrative nature of GB tumours. Since GB cells often migrate from the primary site, tumours become extremely complicated to remove by surgical resection, leading to poor prognosis and high rates of recurrence. Therefore, identifying effective treatments that may also help reduce cell migration could be essential in the progression of GB therapeutic research. Results show that the rate of migration in both T98G and U251 cell lines was reduced following treatment with CP-91149 in a dose-dependent manner, where the migration rate was comparatively lower at $50\mu M$ than at $10\mu M$.

As mentioned in section 4.2, U251 cells appeared to be more resistant, which explains why a greater rate of migration was observed in $10\mu M$ treatment of U251 cells compared to T98G cells, i.e., following 24h of treatment with $10\mu M$ CP-91149 U251 percentage migration was 62.5% while T98G percentage migration was 52%. This could be because U251 cells are recognised as highly infiltrative and have a high rate of migration in tumours (Schulz *et al.*, 2022).

However, in the higher concentration of CP-91149 ($50\mu M$), the rate of migration measured in T98G and U251 cells was very similar (after 24h the percentage migration of T98G was 43.6% and the percentage migration of U251 was 43.8%). This dose was more effective in reducing cell viability in viability assays; therefore, it is appropriate that it displays greater effectiveness in reducing migration. These findings show that CP-91149 is effective in suppressing migration in GB cells. Therefore, this suggests that GP inhibition has the potential to aid in the prevention of the spread of GB within the brain and also potentially suppress the metastasis of GB.

The effect of GP inhibition on GB cell migration is not well known. As observed by Zhan *et al.*, (2021), A549 lung cancer cell lines overexpress PYGB and knockdown of PYGB in A549 cells caused a significant reduction in cell migration after 24h and inhibited invasion. This supports the findings from the wound healing assay in this project as it suggests limiting GP activity by inhibition would decrease the rate of migration in cancer cells.

4.6 Inhibitor Effect on Cell Cycle

Inhibition of GP reduced cell viability, migration, and colony formation in GB cell lines. The mechanism of action however was unknown, therefore, the effect of GP inhibition on the cell cycle was investigated using propidium iodide staining followed by flow cytometry. Propidium iodide stains the DNA, allowing for a distinction between stages of the cell cycle (G1, S phase, G2, and late apoptosis sub-G1) by the level of fluorescence indicated by the amount of DNA in the cell. This showed that 48h treatment of U251, T98G, and U87 cell lines with $10\mu M$, $50\mu M$, and $100\mu M$ of CP-91149 displayed minimal or no significant differences in the cell cycle distribution (Figure 3.13). This was unexpected and suggests that GP inhibition with CP-91149 does not induce apoptosis or cell cycle arrest in GB cell lines, therefore there must be an alternative explanation for the reduction in viability observed.

Within models of hepatocellular carcinoma (HCC), Barot *et al* (2019) observed CP-91149 had a concentration-dependent effect on the cell cycle and induced cell cycle arrest in the S phase when treated with 100µM which was not clearly visible within GB cell lines in this study. However, Barot also investigated apoptosis following treatment with CP-91149 in HepG2 cells utilising the addition of markers of apoptosis such as annexin V-FITC, which binds to phosphatidylserine that is exposed extracellularly on apoptotic cells. This showed that HepG2 cells showed a decrease in healthy cells

and an increase in early apoptotic cells, but limited changes in the number of late apoptosis (sub-G1)/necrotic cells, in a dose-dependent manner following treatment with CP-91149. This finding in particular relates to the findings in GB cells following treatment with CP-91149, which displayed limited changes in the distribution of cells in sub-G1.

Furthermore, it is known that interruption of metabolic processes using metabolic inhibitors elicits cell cycle arrest and apoptosis, as reported by Lee *et al.*, (2004) when using the GP inhibitor CP-320626 on MIA pancreatic adenocarcinoma cells. Findings included a reduction in macromolecular synthesis required for cellular proliferation, which occurred in lower concentrations before apoptotic markers were present. More in-depth analysis of the metabolic pathways following GP inhibition reveals restriction of glycogenolysis results in cell cycle arrest and apoptosis in a dose-dependent manner within pancreatic cancer cells through the MAPK pathway and increased expression of P53 (Ma *et al.*, 2012). This demonstrates the complicated integrated network between metabolic pathways and signalling pathways, but also the potential mechanism of action for CP-91149.

A potential reason why these findings do not correlate with results from this project could be due to the biological differences between GB cancer cells and other cancer cells such as HCC/pancreatic adenocarcinoma cells. Interestingly, in hepatocellular carcinoma, a PYGB overexpression has been identified and it is associated with poor prognosis in patients with the disease (Cui *et al.*, 2020). On the other hand, this study suggests that PYGL is overexpressed in GB cells, presenting a potential reason why these cells respond differently to GP inhibition.

Another reason could be due to the amount of time cells were exposed to the treatment. For example, Knizhnik *et al.*, (2013) investigated apoptosis of GB cell lines Ln-229 and U87 following treatment with TMZ for up to 144h and found that apoptosis was not significantly observed until 120h whereas autophagy was observed within 72h. This suggests that 48h treatment of CP-91149 in

GB cells could also be too short to observe late apoptosis. However, 48h treatment was enough to detect a reduction in mitochondrial activity based on cell viability assays utilising resazurin, a blue dye that is reduced by the mitochondria of healthy cells to a red fluorescent dye, as shown in figure 3.5. This could suggest that apoptosis may have been in the early stages after 48h since mitochondrial dysfunction occurs in early apoptosis (Elmore, 2007).

A DAPI assay was performed as a quick experiment to investigate DNA fragmentation, which would present in late apoptosis (sub-G1), after 72h treatment with 100µM of CP-91149 in order to gain more insight following results from the cell cycle analysis assay. DAPI works by binding to DNA at A-T-rich regions, thus providing visual analysis by fluorescence of nuclear morphology, allowing observation of changes following treatments (Wallberg, Tenev, & Meier, 2016). Observed differences after treatment within U251, T98G, and U87 cell lines included a reduction in the cell density, but no clear DNA fragmentation. This aligns with cell cycle analysis results which showed only a small percentage of cells were in sub-G1 and no differences in the distribution of cells in sub-G1 across all treatment concentrations were observed, suggesting late apoptosis did not occur. However, the reduction in cell density suggests CP-91149 could be affecting proliferation.

An alternative strategy for cell death includes autophagy, the process by which the cell will self-degrade intercellular components in response to extracellular stressors (Rodriguez-Rocha *et al.*, 2011). Anti-cancer treatments have the potential to promote autophagy, however, this could either be a cytotoxic response resulting in cell death or a protective response that allows the cancer cell to survive (Thorburn, Thamm, & Gustafson, 2014). This process would be worth investigating in the context of GP inhibition within GB in parallel with apoptosis investigation to rationalise why CP-91149 reduces cell viability in GB cell lines.

These points suggest the importance of exploring further parameters of apoptosis investigation before concluding that apoptosis has not occurred. However, it must also be considered that other

mechanisms of cell death, such as autophagy, could be occurring when GB cells are treated with a GP inhibitor.

4.7 Conclusion

The results from this project suggest an upregulation of GP *in vitro*, most predominantly the PYGL isoform only in U251 GB cells. Findings also show that inhibition of GP with CP-91149 has a cytotoxic effect on GB cell lines as there is a dose-dependent reduction in cell viability. Combination treatment of CP-91149 with temozolomide was less effective than when CP-91149 was administered alone. CP-91149 inhibited the rate of migration of both U251 and T98G cells in a dose-dependent manner. Cell cycle analysis of U251, T98G, and U87 following 48h treatment with CP-91149 showed minimal changes, suggesting GP inhibition may not induce apoptosis. From cell viability and migration assay results, GP inhibition as a therapeutic approach for GB has potential and it would be expected that CP-91149 would inhibit the growth of GB tumours *in vivo*.

4.8 Limitations

As with many studies, this project has several limitations that are worth taking into consideration. Firstly, the findings from SVG p12 cells were unexpected as, theoretically, they wouldn't be as sensitive to GP inhibition. This is because it was expected that SVG p12, due to its non-cancerous nature, would make use of other metabolic pathways rather than aerobic glycolysis, as detailed in the hallmark of metabolic switching (mentioned in section 1.4). However, as shown by its clear reduction in cell viability following GP inhibition, SVG p12 could have been affected by this metabolic switch. Explanations for this could come from the origins of SVG p12 cells. SVG p12 is a normal human foetal glial cell line that has been immortalised and found to contain the BK polyomavirus (Henricksen *et al.*, 2014). Due to the nature of viral infections, it results in mutations within the host cell genome to optimise replication and alter the cell cycle. As a result, this means that SVG p12 as a control may not be a reliable control glial cell line as it may not behave similarly to

normal cells and instead may share some properties with cancerous cells, thus it may not yield results considered 'normal'. This knowledge must be taken into consideration when comparing data and could explain the unexpected results. Furthermore, a limitation when using SVG p12 as a control glial cell line for human adult GB cell lines such as U251, T98G, and U87, is that SVG p12 is of foetal origin (Major *et al.*, 1985). This needs to be considered as it is likely that there will be differences observed that may potentially be due to the differences between foetal and adult cells. For example, PYGB is more highly expressed in foetal tissue than in adult tissue, with levels decreasing in most adult tissues as PYGB ratios are determined specifically to the tissue type after development (Sato *et al.*, 1976; Migocka-Patrzałek & Elias, 2021). This further illustrates the limitations that can arise when using an immortalised foetal cell line, such as SVG p12, as a control.

Replacing SVG p12 with an alternative glial control cell for all future experiments would be an ideal step towards more realistic comparisons against the GB cell lines. For example, a widely recommended control for *in vitro* studies is normal human astrocyte primary cells. This is because astrocytes are the most common cell type within the central nervous system and is the cell type from which glioblastoma originates, making them the most representative single-cell culture (Gradisnik & Velnar, 2023). The gold standard of *in vitro* GB culture models is patient-derived (PD) cells rather than immortalised glioma cells (Caragher, Chalmers, & Gomez-Roman, 2019). This is because most of these cell lines, such as U251 and U87, were established decades ago and there have been reports that current cell lines have genetically drifted from the tumour of origin, raising questions about the validity of these cell lines for GB research (Allen *et al.*, 2016; Torsvik *et al.*, 2014). However, PD cells are highly difficult to obtain and also extremely challenging to culture. Additionally, there remain limitations with cultured malignant glioma cell lines, including PD cells. For instance, supplementation in classic cell lines has been shown to induce astrocytic differentiation resulting in transcriptional and epigenomic changes that do not reflect the human disease (Lee *et al.*, 2006; Peng *et al.*, 2021).

Additionally, cell viability assays showed high variability which could be a result of not being able to maintain consistent use of the same set of pipettes when seeding, making drug solutions, and adding resazurin solution for the assay. This is because cell viability assays are highly sensitive, therefore minimal changes could have a large impact on the replicability of results (Larsson *et al.*, 2020).

While the results from this experiment were valuable, there were a lot of optimisations required which made completing this experiment highly time-consuming. Firstly, the migration assay aims to measure migration of the wound closure and not the proliferation of cells into the gap, therefore serum starving was used as a cost-effective method to minimise the proliferation of the cells (Jonkman et al., 2014). However, when initially testing different cell densities to obtain a monolayer of cells and providing serum-free media there was difficulty in maintaining the monolayer of U87 cells. Only the U87 cells would consistently form clumps and detach from the plate following the addition of serum-free media despite efforts to ensure the cell surface was washed gently, testing on cells obtained from a different vial, and switching to a low serum (0.5% FBS) alternative. This phenomenon could be explained if the U87 cells had a low tolerance for serum starvation as reducing or removing the serum from the medium can elicit some undesirable changes in signalling pathways in some cell lines (Pirkmajer & Chibalin, 2011). Due to time constraints, the wound healing assay was to be continued only using T98G and U251 cells. Furthermore, the wound healing assay lacked automation, meaning there will have been a higher level of variability in results for several reasons. For instance, it wouldn't be possible to fully replicate the same width of the scratch each time when done manually. Additionally, imaging of the exact same area of the wound was challenging since the plate would have to be transferred back into an incubator after each round of imaging. While efforts were made to capture the same area, it could not be guaranteed that the

exact same spot across all time points was imaged, especially after 24h when the gap closed almost entirely.

When conducting the Clonogenic assay there was some variability observed that was unexplained despite maintaining the same methodology. This could be due to changes in the incubator that cells were stored in for the 2-week duration, which was unavoidable due to the previous incubator breaking. This could have provided a slight difference in the environment, such as a different humidity. Unfortunately, obtaining multiple repeats within the given time frame was also difficult due to the length of the assay. Additionally, quantification of the results proved difficult as colonies had overgrown, overlapping each other, making it difficult to count the number of colonies. Therefore, in future research, this assay could be repeated more and with additional concentrations (e.g., 100µM) to generate a wider range of results that truly reflect the effectiveness of the treatment. Also, optimisation of the protocol to achieve a more quantifiable result would be ideal. This could be achieved by testing different lengths of incubation. The Clonogenic assay has proven to be a highly variable method of testing a drug treatment, with differences in factors such as seeding density or cell type yielding heavily skewed results (Brix *et al.*, 2020). This further demonstrates the importance of collecting more independent replicates for highly variable techniques such as this assay.

4.9 Future Work

Despite the significant amount of work carried out for this project, many questions remain regarding the mechanism of CP-91149. The vast complexity of GB and the tumour microenvironment is incredibly challenging to replicate in experiments using current culture systems *in vitro*. This is because a GB tumour microenvironment comprises a diverse population of endothelial cells, microglia, neurons, and astrocytes and develops in a heterogeneous 3D manner (Caragher, Chalmers, & Gomez-Roman, 2019). Additional factors in GB tumours include oxygen and nutrient variability and a brain-specific extracellular matrix, as well as the BBB and heterogeneous nature of GB tumours. This is not the case in 2D single-cell cultures, which maintain consistent oxygen and nutrient levels, and adhere to a stiff plastic flask in a monolayer of cells. This means the response to treatment in these simplified models may not reflect the response from a real GB tumour.

Unfortunately, this issue is difficult to address since an accurate 3D multicellular GB model would be extremely difficult to achieve.

A deeper understanding of the role of GP in GB cells could be acquired through the utilisation of siRNA to knock down the expression of GP. Cells in which GP expression has been silenced could be used in parallel to cells treated with CP-91149 or other effective GP inhibitors in future experiments and results could be compared to determine the effectiveness GP inhibition as a therapeutic in GB. Additional experiments to investigate other parameters of apoptosis or autophagy would be worthwhile to pinpoint the effect of GP inhibition on GB cells. Apoptosis could be identified by using markers such as annexin V in addition to PI staining in flow cytometric analysis of treated cells. An additional method of identifying apoptosis would be through a caspase assay, which would detect the activation of caspase enzymes during the process (Huang *et al.*, 2023). This would target early apoptosis more specifically as opposed to PI staining followed by flow cytometry. Autophagy could also be investigated by measuring the level of markers such as GFP-LC3 using flow cytometry (Yoshii & Mizushima, 2017). Additionally, a glycogen assay could also provide further insight by establishing

the levels of stored glycogen before and after inhibition with CP-91149 using a glycogen assay kit.

This would confirm the efficacy of CP-91149 as a GP inhibitor if glycogen levels were greater in cells treated with CP-91149.

The precise molecular mechanism of action following GP inhibition is still not clear. Instead, the effect of glycogen in promoting cancer progression in hypoxic conditions is only known, therefore it is to be assumed that preventing the use of glycogen would offer the opposite effects. Glycogen fuels a range of malignant phenotypes, including proliferation and migration, protection from oxidative stress and senescence, histone acetylation, and chemoresistance (Khan *et al.*, 2020; Zois & Harris, 2016). Zhan *et al.*, (2021) observed an overexpression of PYGB in non-small-cell lung carcinoma (NSCLC) and associated the overexpression with an increased activity of the PI3K/AKT pathway, a key signalling pathway related to the progression of NSCLC. As the PI3K/AKT signalling cascade is also activated in GB, this knowledge could be applied to the mechanism of action of PYGB, and the other GP isoforms (Langhans *et al.*, 2017). This further demonstrates the complexity of the involvement of GP in several signalling networks that could all be affected following GP inhibition, lending to the cytotoxic abilities of a GP inhibitor such as CP-91149.

Future research on GP inhibition could go beyond the use of GB cell lines due to the controversies surrounding their suitability as a model. Advancements in GB models are still being developed but show promise in providing more accurate models for research (Caragher, Chalmers, & Gomez-Roman, 2019). One novel system that allows for a more dynamic and non-static microenvironment is microfluidic systems, which involves culturing primary GB cells within a network of hydrogel tubes with circulating media (Li *et al.*, 2018). These cells were able to self-develop from single cells into clusters, spheroids, and then a mass of cells. It has been suggested that tumour-specific cells could be cultured in this manner and then used directly from the system for use in drug testing. Another system being investigated is "mini-brains", which involves growing

pluripotent stem cells into a cerebral organoid through the utilisation of changes in media and additives (Ogawa *et al.*, 2018). These systems expand the ability of *in vitro* models in GB research, providing promising potential in generating accurate data in early research stages. Unfortunately, the disadvantages of these models mainly include low cost-efficiency and time efficiency due to optimisation. However, these options for *in vitro* systems would be reasonable to consider in the progress of drug screening following success in the more simplified models.

To aid the progression of research on GP inhibition in GB, it would be necessary to investigate the ability of GP inhibitors to cross the BBB. This could be achieved by screening the compound of interest using an *in vitro* BBB model. Ideally, 3D models, such as microfluidic or chip-based models, would be the most accurate representations of the BBB to generate the most realistic results (Shah & Dong, 2022). This aspect of future research would be imperative since a compound that cannot cross the BBB in sufficient quantities would not be beneficial in the treatment of a brain neoplasia such as GB.

Further research could include the use of *in vivo* animal models to establish the effect of GP inhibition on a living organism rather than cells that have been cultured. This methodology most commonly utilises mouse models. Mouse models can include many variations, but mice that naturally acquire GB (spontaneous GB mouse models) are uncommon, therefore xenograft or genetically modified mice are often used in GB research (Jin *et al.*, 2021). Xenograft mice are immunocompromised mice that have had human GB cells/tissue transplanted to induce GB.

However, these models may not be as representative as others since they do not have a fully intact immune system. Mice models that may be more representative, with a working immune system, are genetically modified through methods such as viral vectors to induce overexpression of oncogenes or mutation of tumour suppressor genes. This would be a necessary step to validate the efficacy of a novel therapeutic such as GP inhibitors before clinical trials.

5. References

- Abe, H., Natsumeda, M., Kanemaru, Y., Watanabe, J., Tsukamoto, Y., *et al.* (2018). MGMT Expression Contributes to Temozolomide Resistance in H3K27M-Mutant Diffuse Midline Gliomas and MGMT Silencing to Temozolomide Sensitivity in IDH-Mutant Gliomas, *Neurologia medico-chirurgica*, 58(7), 290–295.
- Allen, M., Bjerke, M., Edlund, H., Nelander, S., and Westermark, B. (2016). Origin of the U87MG glioma cell line: Good news and bad news. *Sci. Transl. Med.* 354(8), 354.
- Alonso, M. M., Gomez-Manzano, C., Bekele, B. N., Yung, W. K., and Fueyo, J. (2007). Adenovirus-based strategies overcome temozolomide resistance by silencing the O6-methylguanine-DNA methyltransferase promoter. *Cancer research*, *67*(24), 11499–11504.
- Arora, A., and Somasundaram, K. (2019). Glioblastoma vs temozolomide: can the red queen race be won?, *Cancer biology & therapy*, *20*(8), 1083–1090.
- Barot, S., Abo-Ali, E.M., Zhou, D.L., Palaguachi, C., and Dukhande, V.V. (2019). Inhibition of glycogen catabolism induces intrinsic apoptosis and augments multikinase inhibitors in hepatocellular carcinoma cells, *Experimental Cell Research*, 381(2), 288-300.
- Brix, N., Samaga, D., Hennel, R. et al. (2020) The clonogenic assay: robustness of plating efficiency-based analysis is strongly compromised by cellular cooperation. Radiat Oncol 15, 248.
- Brown, T. J., Brennan, M. C., Li, M., Church, E. W., Brandmeir, N. J., *et al.* (2016). Association of the Extent of Resection With Survival in Glioblastoma: A Systematic Review and Meta-analysis. *JAMA oncology*, *2*(11), 1460–1469.
- Caragher, S., Chalmers, A. J., and Gomez-Roman, N. (2019). Glioblastoma's Next Top Model: Novel Culture Systems for Brain Cancer Radiotherapy Research. *Cancers*, 11(1), 44.
- Calabrese, E. J. (2008). Hormesis and medicine. *British journal of clinical pharmacology*, *66*(5), 594–617.
- Crerar, M. M., Karlsson, O., Fletterick, R. J., and Hwang, P. K. (1995). Chimeric muscle and brain glycogen phosphorylases define protein domains governing isozyme-specific responses to allosteric activation. *The Journal of biological chemistry*, *270*(23), 13748–13756.
- Cui, G., Wang, H., Liu, W., Xing, J., Song, W. *et al.* (2020). Glycogen Phosphorylase B Is Regulated by miR101-3p and Promotes Hepatocellular Carcinoma Tumorigenesis. *Frontiers in cell and developmental biology*, *8*, 566494.
- Elmore S. (2007). Apoptosis: a review of programmed cell death. *Toxicologic pathology*, *35*(4), 495–516.
- Ferraro, G., Mozzicafreddo, M., Ettari, R., Corsi, L., and Monti, M. C. (2022). A Proteomic Platform Unveils the Brain Glycogen Phosphorylase as a Potential Therapeutic Target for Glioblastoma Multiforme. *International journal of molecular sciences*, 23(15), 8200.
- Garcia, J. H., Jain, S., and Aghi, M. K. (2021). Metabolic Drivers of Invasion in Glioblastoma. *Frontiers in cell and developmental biology*, *9*, 683276.

- Gilard, V., Tebani, A., Dabaj, I., Laquerrière, A., Fontanilles, M., et al. (2021). Diagnosis and Management of Glioblastoma: A Comprehensive Perspective. *Journal of personalized medicine*, 11(4), 258.
- Grabowski, M. M., Recinos, P. F., Nowacki, A. S., Schroeder, J. L., Angelov, L., *et al.* (2014). Residual tumor volume versus extent of resection: predictors of survival after surgery for glioblastoma. *Journal of neurosurgery*, *121*(5), 1115–1123.
- Gradisnik, L., and Velnar, T. (2023). Astrocytes in the central nervous system and their functions in health and disease: A review. *World journal of clinical cases*, *11*(15), 3385–3394.
- Grech, N., Dalli, T., Mizzi, S., Meilak, L., Calleja, N., and Zrinzo, A. (2020). Rising Incidence of Glioblastoma Multiforme in a Well-Defined Population. Cureus, 12(5).
- Hanahan, D., and Weinberg, R.A. (2011). Hallmarks of cancer: the next generation, *Cell, 144*(5), 646–674.
- Henriksen, S., Tylden, G. D., Dumoulin, A., Sharma, B. N., Hirsch, H. H., and Rinaldo, C. H. (2014). The human fetal glial cell line SVG p12 contains infectious BK polyomavirus. *Journal of virology*, 88(13), 7556–7568.
- Huang, Y. K., Chang, K. C., Li, C. Y., Lieu, A. S., and Lin, C. L. (2023). AKR1B1 Represses Glioma Cell Proliferation through p38 MAPK-Mediated Bcl-2/BAX/Caspase-3 Apoptotic Signaling Pathways. *Current issues in molecular biology*, *45*(4), 3391–3405.
- Inno, A., Di Noia, V., D'Argento, E., Modena, A., and Gori, S. (2016). State of the art of chemotherapy for the treatment of central nervous system metastases from non-small cell lung cancer, *Translational lung cancer research*, *5*(6), 599–609.
- Jacobs, S. S., Fox, E., Dennie, C., Morgan, L. B., McCully, C. L., and Balis, F. M. (2005). Plasma and cerebrospinal fluid pharmacokinetics of intravenous oxaliplatin, cisplatin, and carboplatin in nonhuman primates. Clinical cancer research: an official journal of the American Association for Cancer Research, 11(4), 1669–1674.
- Jakobs, S., Fridrich, D., Hofem, S., Pahlke, G., and Eisenbrand, G. (2006). Natural flavonoids are potent inhibitors of glycogen phosphorylase, *Molecular nutrition & food research*, *50*(1), 52–57.
- Jena, L., McErlean, E., and McCarthy, H. (2020). Delivery across the blood-brain barrier: nanomedicine for glioblastoma multiforme, *Drug delivery and translational research*, 10(2), 304–318.
- Jin F, Jin-Lee HJ, Johnson AJ. Mouse Models of Experimental Glioblastoma. In: Debinski W, editor. Gliomas [Internet]. Brisbane (AU): Exon Publications; 2021 Apr 30. Chapter 2. Available from: https://www.ncbi.nlm.nih.gov/books/NBK570698/
- Jonkman, J. E., Cathcart, J. A., Xu, F., Bartolini, M. E., Amon, J. E., Stevens, K. M., and Colarusso, P. (2014). An introduction to the wound healing assay using live-cell microscopy. *Cell adhesion & migration*, *8*(5), 440–451.

- Khan, T., Kryza, T., He, Y., Gunter, J.H., Gough, M., et al. (2023). Glycogen phosphorylase inhibition alongside taxol chemotherapy synergistically elicits ferroptotic cell death in clear cell ovarian and kidney cancers.
- Khan, T., Sullivan, M. A., Gunter, J. H., Kryza, T., Lyons, N., et al. (2020). Revisiting Glycogen in Cancer: A Conspicuous and Targetable Enabler of Malignant Transformation. *Frontiers in oncology*, 10, 592455.
- Lane, L. A., Nadeau, O. W., Carlson, G. M., and Robinson, C. V. (2012). Mass spectrometry reveals differences in stability and subunit interactions between activated and nonactivated conformers of the $(\alpha\beta\gamma\delta)4$ phosphorylase kinase complex. *Molecular & cellular proteomics : MCP, 11*(12), 1768–1776.
- Langhans, J., Schneele, L., Trenkler, N., von Bandemer, H., Nonnenmacher, L., et al. (2017). The effects of PI3K-mediated signalling on glioblastoma cell behaviour. *Oncogenesis*, 6(11), 398.
- Larsson, P., Engqvist, H., Biermann, J. et al. (2020) Optimization of cell viability assays to improve replicability and reproducibility of cancer drug sensitivity screens. *Sci Rep*, 10, 5798
- Lee, J., Kotliarova, S., Kotliarov, Y., Li, A., Su, Q., *et al.* (2006). Tumor stem cells derived from glioblastomas cultured in bFGF and EGF more closely mirror the phenotype and genotype of primary tumors than do serum-cultured cell lines. *Cancer cell*, *9*(5), 391–403.
- Lee, S.Y. (2016). Temozolomide resistance in glioblastoma multiforme, *Genes & diseases*, 3(3), 198–210. doi: 10.1016/j.gendis.2016.04.007.
- Lee, W. N., Guo, P., Lim, S., Bassilian, S., Lee, S. T., *et al.* (2004). Metabolic sensitivity of pancreatic tumour cell apoptosis to glycogen phosphorylase inhibitor treatment. *British journal of cancer*, *91*(12), 2094–2100.
- Li, Q., Lin, H., Rauch, J. et al. (2018) Scalable Culturing of Primary Human Glioblastoma Tumor-Initiating Cells with a Cell-Friendly Culture System. Sci Rep 8, 3531
- Lillpopp, L., Tzikas, S., Ojeda, F., Zeller, T., Baldus, S., *et al.* (2012). Prognostic information of glycogen phosphorylase isoenzyme BB in patients with suspected acute coronary syndrome. *The American journal of cardiology*, *110*(9), 1225–1230.
- Louis, D. N., Perry, A., Reifenberger, G., von Deimling, A., Figarella-Branger, *et al.* (2016). The 2016 World Health Organization Classification of Tumors of the Central Nervous System: a summary. *Acta neuropathologica*, *131*(6), 803–820.
- Louis, D. N., Wesseling, P., Aldape, K., Brat, D. J., Capper, D., et al. (2020). cIMPACT-NOW update 6: new entity and diagnostic principle recommendations of the cIMPACT-Utrecht meeting on future CNS tumor classification and grading. *Brain pathology (Zurich, Switzerland)*, 30(4), 844–856.
- Louis, D.N., Perry, A., Wesseling, P., Brat, D.J., Cree, I.A., et al. (2021). The 2021 WHO Classification of Tumors of the Central Nervous System: a summary, Neuro-Oncology, 23(8), 1231–1251.

- Ma, D., Wang, J., Zhao, Y., Lee, W. N., Xiao, J., *et al.* (2012). Inhibition of glycogen phosphorylation induces changes in cellular proteome and signaling pathways in MIA pancreatic cancer cells. *Pancreas*, *41*(3), 397–408.
- Major, E. O., Miller, A. E., Mourrain, P., Traub, R. G., de Widt, E., and Sever, J. (1985). Establishment of a line of human fetal glial cells that supports JC virus multiplication. *Proceedings of the National Academy of Sciences of the United States of America*, 82(4), 1257–1261.
- Martin, M.H., Hoover, D.J., Armento, S.J., Stock, I.A., McPherson, R.K., *et al.* (1998). Discovery of human liver glycogen phosphorylase inhibitor that lowers blood glucose in vivo, *Proceedings of the National Academy of Sciences*, *95*, 1776-1781.
- Mathieu, C., Dupret, J.M., and Rodrigues Lima, F. (2017). The structure of brain glycogen phosphorylase-from allosteric regulation mechanisms to clinical perspectives, *The FEBS journal*, *284*(4), 546–554.
- Mathomes, R. T., Koulas, S. M., Tsialtas, I., Stravodimos, G., Welsby, P. J., *et al.* (2023). Multidisciplinary docking, kinetics and X-ray crystallography studies of baicalein acting as a glycogen phosphorylase inhibitor and determination of its' potential against glioblastoma in cellular models. *Chemico-biological interactions*, *382*, 110568.
- McKinnon, C., Nandhabalan, M., Murray, S. A., and Plaha, P. (2021). Glioblastoma: clinical presentation, diagnosis, and management. *BMJ (Clinical research ed.)*, *374*, n1560.
- Migocka-Patrzałek, M., and Elias, M. (2021). Muscle Glycogen Phosphorylase and Its Functional Partners in Health and Disease, *Cells (Basel, Switzerland)*, 10(4), 883–.
- Miller, K. D., Ostrom, Q. T., Kruchko, C., Patil, N., Tihan, T., *et al.* (2021). Brain and other central nervous system tumor statistics, 2021. *CA: a cancer journal for clinicians*, 71(5), 381–406.
- Molinaro, A. M., Hervey-Jumper, S., Morshed, R. A., Young, J., Han, S. J., *et al.* (2020). Association of Maximal Extent of Resection of Contrast-Enhanced and Non-Contrast-Enhanced Tumor With Survival Within Molecular Subgroups of Patients With Newly Diagnosed Glioblastoma. *JAMA oncology*, *6*(4), 495–503.
- Nadeau, O. W., Fontes, J. D., and Carlson, G. M. (2018). The regulation of glycogenolysis in the brain. *The Journal of biological chemistry*, *293*(19), 7099–7107.
- Naifeh J, Dimri M, Varacallo M. Biochemistry, Aerobic Glycolysis. [Updated 2023 Apr 9]. In: StatPearls [Internet]. Treasure Island (FL): StatPearls Publishing; 2024 Jan-. Available from: https://www.ncbi.nlm.nih.gov/books/NBK470170/
- Niewald, M., Berdel, C., Fleckenstein, J., Licht, N., Ketter, R., and Rübe, C. (2011). Toxicity after radiochemotherapy for glioblastoma using temozolomide--a retrospective evaluation. *Radiation oncology (London, England)*, *6*, 141.
- Noch, E.K., Ramakrishna, R. and Magge, R. (2018). Challenges in the Treatment of Glioblastoma: Multisystem Mechanisms of Therapeutic Resistance, World neurosurgery, 116, 505–517.
- Ogawa, J., Pao, G.M., Shokhirev, M.N., and Verma, I.M. (2018). Glioblastoma Model Using Human Cerebral Organoids. *Cell Rep.* 23, 1220–1229.

- Paredes-Flores MA, Rahimi N, Mohiuddin SS. Biochemistry, Glycogenolysis. [Updated 2024 Jan 9]. In: StatPearls [Internet]. Treasure Island (FL): StatPearls Publishing; 2024 Jan-. Available from: https://www.ncbi.nlm.nih.gov/books/NBK554417/
- Park, J. H., and Lee, H. K. (2022). Current Understanding of Hypoxia in Glioblastoma Multiforme and Its Response to Immunotherapy. *Cancers*, *14*(5), 1176.
- Peng, D., Gleyzer, R., Tai, W. H., Kumar, P., Bian, Q., et al. (2021). Evaluating the transcriptional fidelity of cancer models. *Genome medicine*, 13(1), 73.
- Philips, A., Henshaw, D. L., Lamburn, G., and O'Carroll, M. J. (2018). Brain Tumours: Rise in Glioblastoma Multiforme Incidence in England 1995-2015 Suggests an Adverse Environmental or Lifestyle Factor. *Journal of environmental and public health*, 2018, 7910754.
- Pirkmajer, S., & Chibalin, A. V. (2011). Serum starvation: caveat emptor. *American journal of physiology. Cell physiology*, 301(2), C272–C279.
- Posti, J. P., Bori, M., Kauko, T., Sankinen, M., Nordberg, J., et al. (2015). Presenting symptoms of glioma in adults. *Acta neurologica Scandinavica*, 131(2), 88–93.
- Pyko, I.V., Nakada, M., Sabit, H., Teng, L., Furuyama, N., *et al.* (2013). Glycogen synthase kinase 3β inhibition sensitizes human glioblastoma cells to temozolomide by affecting O 6 -methylguanine DNA methyltransferase promoter methylation via c-Myc signaling , *Carcinogenesis*, 34(10), 2206–2217.
- Rao, V. M., Parker, L., Levin, D. C., Sunshine, J., and Bushee, G. (2001). Use trends and geographic variation in neuroimaging: nationwide medicare data for 1993 and 1998. *AJNR. American journal of neuroradiology*, 22(9), 1643–1649.
- Rick, J., Chandra, A. and Aghi, M.K. (2018). Tumor treating fields: a new approach to glioblastoma therapy, *J Neurooncol* 137, 447–453.
- Rodriguez-Rocha, H., Garcia-Garcia, A., Panayiotidis, M. I., and Franco, R. (2011). DNA damage and autophagy. *Mutation research*, *711*(1-2), 158–166.
- Sakoda, H., Fujishiro, M., Fujio, J., Shojima, N., Ogihara, T., *et al.* (2005). Glycogen debranching enzyme association with beta-subunit regulates AMP-activated protein kinase activity. *American journal of physiology. Endocrinology and metabolism*, *289*(3), E474–E481.
- Sato, K., Satoh, K., Sato, T., Imai, F., and Morris, H. P. (1976). Isozyme patterns of glycogen phosphorylase in rat tissues and transplantable hepatomas. *Cancer research*, *36*(2 Pt 1), 487–495.
- Schnier, J.B., Nishi, K., Monks, A., Gorin, F.A., and Bradbury, E.M. (2003). Inhibition of glycogen phosphorylase (GP) by CP-91,149 induces growth inhibition correlating with brain GP expression, *Biochemical and Biophysical Research Communications*, 309 (1).
- Schnier, J. B., Nishi, K., Gumerlock, P. H., Gorin, F. A., and Bradbury, E. M. (2005). Glycogen synthesis correlates with androgen-dependent growth arrest in prostate cancer. *BMC urology*, *5*, 6.

- Shihan, M. H., Novo, S. G., Le Marchand, S. J., Wang, Y., and Duncan, M. K. (2021). A simple method for quantitating confocal fluorescent images. *Biochemistry and biophysics reports*, 25, 100916.
- Shukla, G., Alexander, G. S., Bakas, S., Nikam, R., Talekar, K., *et al.* (2017). Advanced magnetic resonance imaging in glioblastoma: a review. *Chinese clinical oncology*, *6*(4), 40. https://doi.org/10.21037/cco.2017.06.28
- Singh, N., Miner, A., Hennis, L., and Mittal, S. (2021). Mechanisms of temozolomide resistance in glioblastoma a comprehensive review, *Cancer drug resistance*, *4*, 17–43.
- Strobel, H., Baisch, T., Fitzel, R., Schilberg, K., Siegelin, M. D., et al. (2019). Temozolomide and Other Alkylating Agents in Glioblastoma Therapy, *Biomedicines*, 7(3), 69.
- Stupp, R., Mason, W. P., van den Bent, M. J., Weller, M., Fisher, B., *et al.* (2005). Radiotherapy plus concomitant and adjuvant temozolomide for glioblastoma. *The New England journal of medicine*, *352*(10), 987–996.
- Stupp, R., Hegi, M.E., Mason, W.P., van den Bent, M.J., Taphoorn, M.J.B. *et al.* (2009). Effects of radiotherapy with concomitant and adjuvant temozolomide versus radiotherapy alone on survival in glioblastoma in a randomised phase III study: 5-year analysis of the EORTC-NCIC trial, *The Lancet Oncology*, 10(5), 459-466.
- Sweeney, M.D., Zhao, Z., Montagne, A., Nelson, A.R, and Zlokovic, B.V. (2019). Blood-Brain Barrier: From Physiology to Disease and Back, Physiol. Rev., 99, 21-78.
- Thakkar, J.P., Dolecek, T.A., Horbinski, C., Ostrom, Q.T., Lightner, D. D., Barnholtz-Sloan, J.S., et al. (2014). Epidemiologic and molecular prognostic review of glioblastoma, Cancer epidemiology, biomarkers & prevention: a publication of the American Association for Cancer Research, cosponsored by the American Society of Preventive Oncology, 23(10), 1985–1996.
- Thorburn, A., Thamm, D. H., and Gustafson, D. L. (2014). Autophagy and cancer therapy. *Molecular pharmacology*, *85*(6), 830–838.
- Torsvik, A., Stieber, D., Enger, P. Ø., Golebiewska, A., Molven, A., *et al.* (2014). U-251 revisited: genetic drift and phenotypic consequences of long-term cultures of glioblastoma cells. *Cancer medicine*, *3*(4), 812–824.
- Wallberg, F., Tenev, T., and Meier, P. (2016). Analysis of Apoptosis and Necroptosis by Fluorescence-Activated Cell Sorting. *Cold Spring Harbor protocols*, *2016*(4), pdb.prot087387.
- Weller, M., van den Bent, M., Preusser, M., Le Rhun, E., Tonn, J. C., et al. (2021). EANO guidelines on the diagnosis and treatment of diffuse gliomas of adulthood. *Nature reviews. Clinical oncology*, 18(3), 170–186.
- WHO Classification of Tumours Editorial Board. World Health Organization Classification of Tumours of the Central Nervous System. 5th ed.Lyon: International Agency for Research on Cancer; 2021.

- Wu, W., Klockow, J. L., Zhang, M., Lafortune, F., Chang, E., et al. (2021). Glioblastoma multiforme (GBM): An overview of current therapies and mechanisms of resistance. *Pharmacological research*, 171, 105780.
- Yang, C., Wang, H., Shao, M., Chu, F., He, Y., et al. (2024). Brain-Type Glycogen Phosphorylase (PYGB) in the Pathologies of Diseases: A Systematic Review. *Cells*, 13(3), 289.
- Yang, P., Zhang, W., Wang, Y., Peng, X., Chen, B., et al. (2015). IDH mutation and MGMT promoter methylation in glioblastoma: results of a prospective registry, Oncotarget, 6(38), 40896–40906.
- Yoshii, S. R., and Mizushima, N. (2017). Monitoring and Measuring Autophagy. *International journal of molecular sciences*, 18(9), 1865.
- Zhai, L., Feng, L., Xia, L., Yin, H., and Xiang, S. (2016). Crystal structure of glycogen debranching enzyme and insights into its catalysis and disease-causing mutations. *Nature communications*, *7*, 11229.
- Zhan, Y., Chen, R., Wang, T., Shan, S., and Zhu, H. (2021). Glycogen phosphorylase B promotes cell proliferation and migration through PI3K/AKT pathway in non-small cell lung cancer. *Experimental lung research*, 47(3), 111–120.
- Zikou, A., Sioka, C., Alexiou, G. A., Fotopoulos, A., Voulgaris, S., and Argyropoulou, M. I. (2018). Radiation Necrosis, Pseudoprogression, Pseudoresponse, and Tumor Recurrence: Imaging Challenges for the Evaluation of Treated Gliomas. *Contrast media & molecular imaging*, 2018, 6828396.
- Zois, C.E. and Harris, A.L. (2016). Glycogen metabolism has a key role in the cancer microenvironment and provides new targets for cancer therapy, *Journal of molecular medicine* (*Berlin, Germany*), 94(2), 137–154.
- Zois, C. E., Hendriks, A. M., Haider, S., Pires, E., Bridges, E., *et al.* (2022). Liver glycogen phosphorylase is upregulated in glioblastoma and provides a metabolic vulnerability to high dose radiation. *Cell death & disease*, *13*(6), 573.

6. Appendices

Appendix 1

Recipes for western blot buffers.

RIPA buffer

```
50 mM Tris
```

5 mM EDTA

150 mM NaCl

1 % Triton X-100

0.1 % Sodium deoxycholate

0.1 % SDS

Loading buffer (4X)

8% SDS

20% 2-mercaptoethanol

40% glycerol

0.008% bromophenol blue

0.250 M Tris-HCl

pH = 6.8

Running buffer

25 mM Tris base

190 mM glycine

0.1% SDS

```
pH = 8.3
```

Transfer buffer

25 mM Tris base

190 mM glycine

20% methanol

pH = 8.3

TBS (Tris-buffered saline)

For 1 L 10X TBS:

24 g Tris-HCl (formula weight: 157.6 g)

5.6 g Tris base (formula weight: 121.1 g)

88 g NaCl (formula weight: 58.4 g)

pH = 7.6

- 1. For a 1x solution, mix 1 part 10x with 9 parts distilled water and pH to 7.6 again.
- 2. The final molar concentrations of the 1x solution are 20 mM Tris and 150 mM NaCl.

TBS-T (Tris-buffered saline, 0.1% Tween 20)

For 1 L:

100 mL of TBS 10x

900 mL distilled water

1 mL Tween 20

Appendix 2

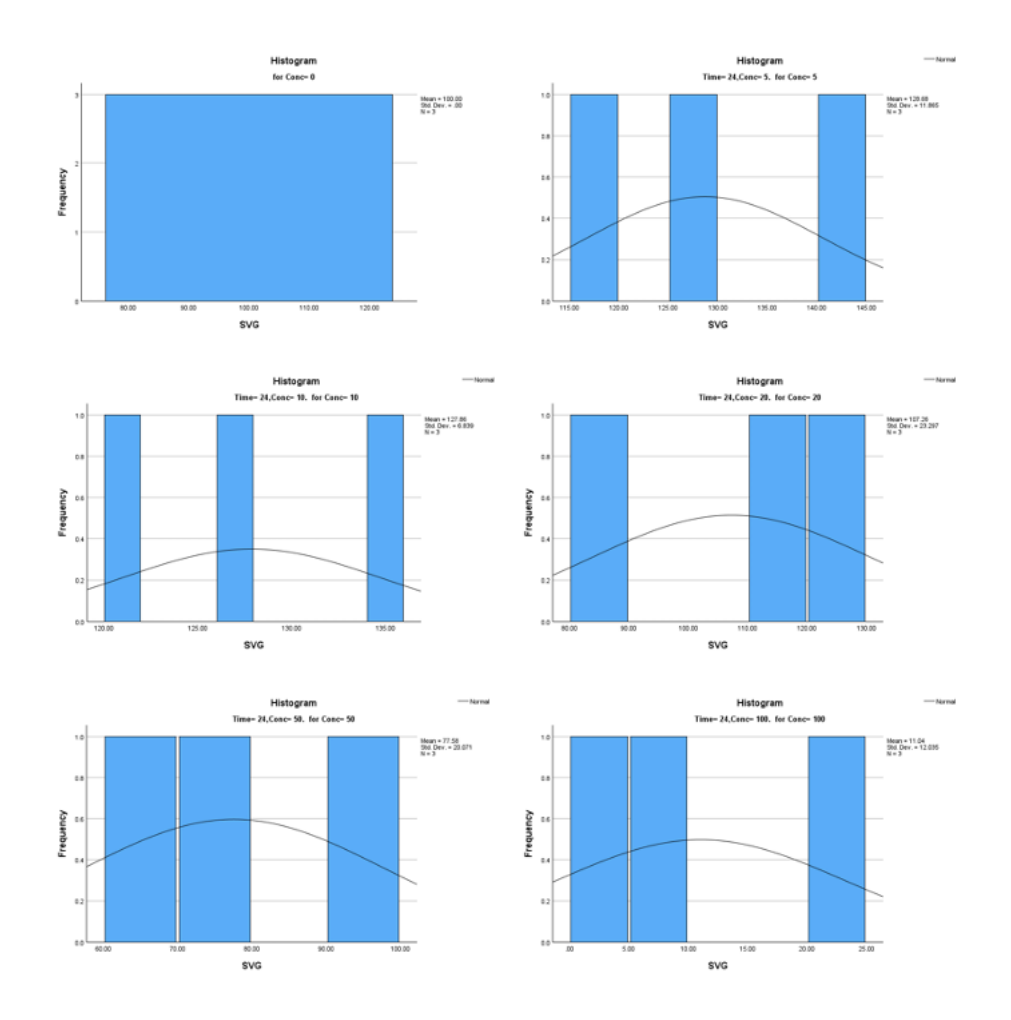
Statistical analysis for 24h treatment cell viability of SVG, U251, T98G, and U87.

Tests of Normality

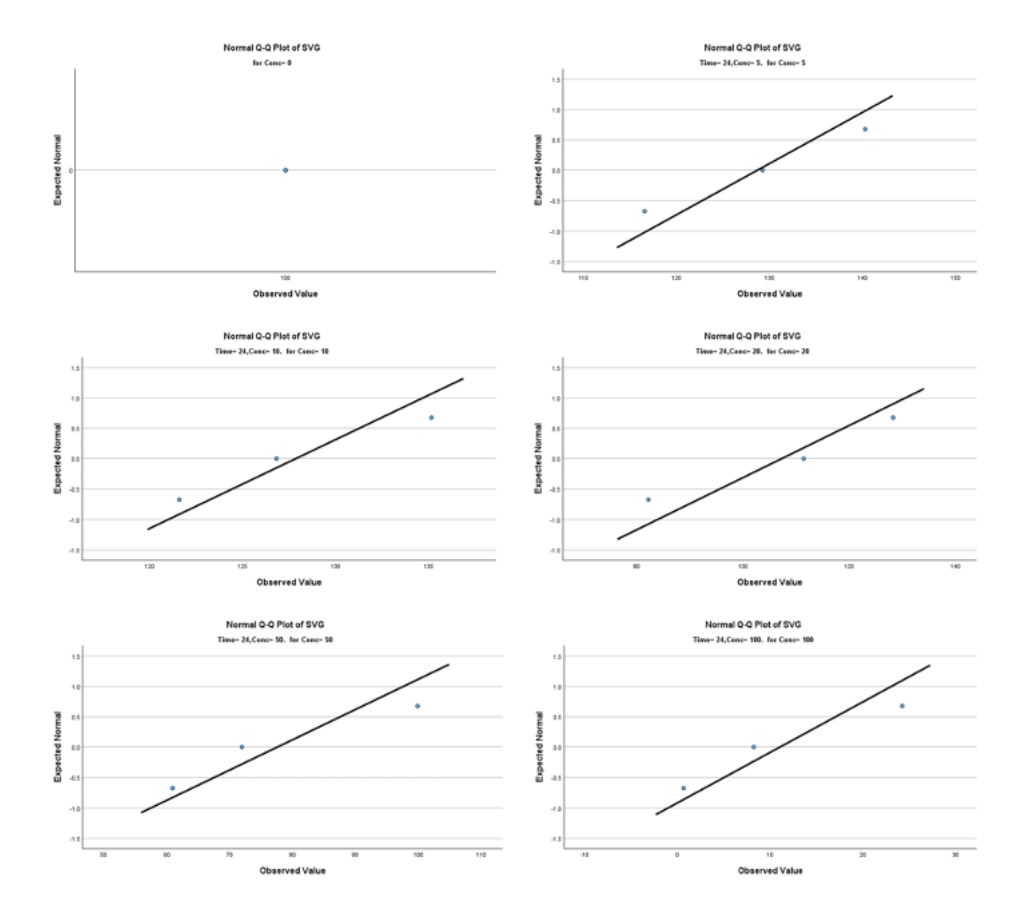
		Kolmogorov-Smirnov ^a		Shapiro-Wilk			
	Conc	Statistic	df	Sig.	Statistic	df	Sig.
SVG	0		3			3	
	5	.185	3		.998	3	.922
	10	.227	3		.983	3	.749
	20	.237	3		.976	3	.705
	50	.277	3		.941	3	.532
	100	.259	3		.959	3	.610
U251	0		3			3	
	5	.194	3		.997	3	.888
	10	.362	3		.804	3	.125
	20	.276	3		.942	3	.535
	50	.374	3		.776	3	.058
	100	.203	3		.994	3	.849
T98G	0		3			3	
	5	.359	3		.811	3	.142
	10	.338	3		.852	3	.246
	20	.287	3		.930	3	.488
	50	.253	3		.964	3	.638
	100	.357	3		.815	3	.151
U87	0		3			3	
	5	.250	3		.967	3	.649
	10	.350	3		.829	3	.187
	20	.370	3		.785	3	.080
	50	.368	3		.791	3	.093
	100	.261	3		.957	3	.601

a. Lilliefors Significance Correction

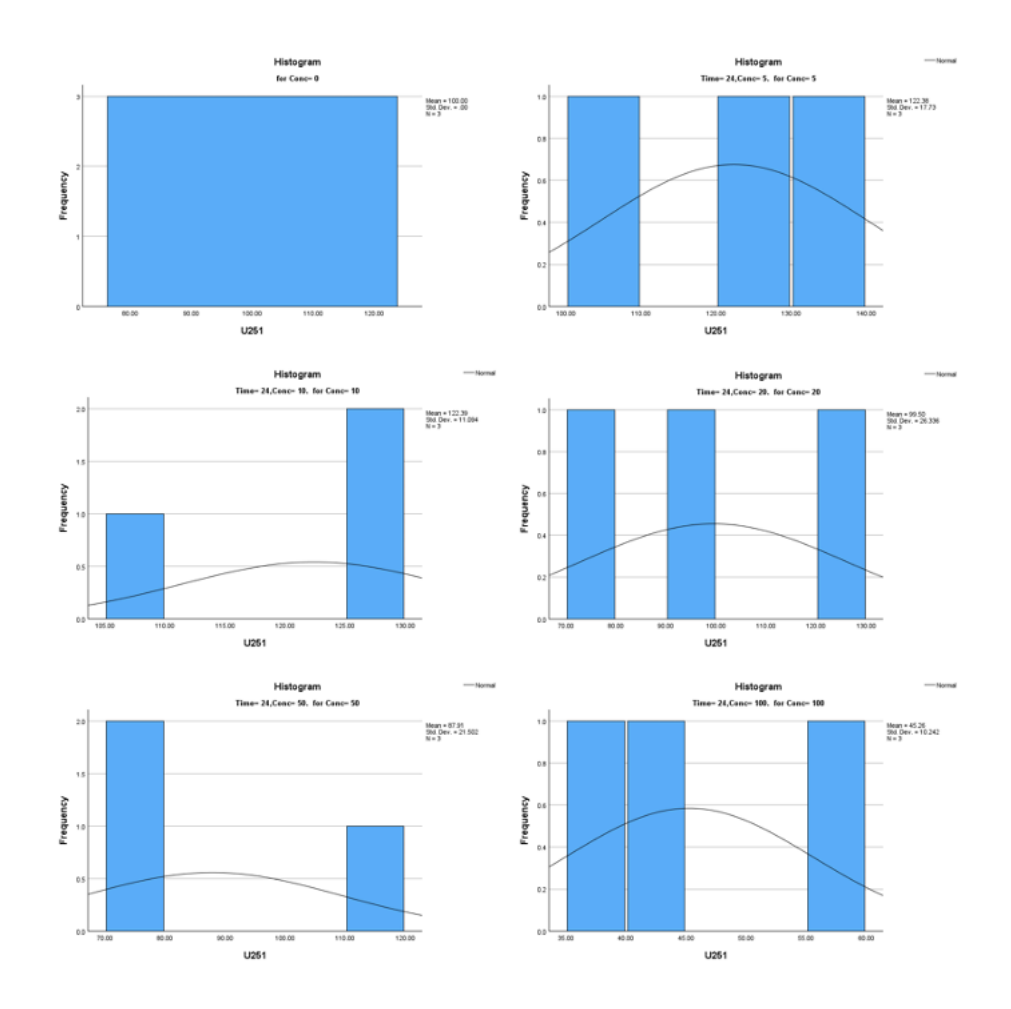
Shapiro-Wilk for 24h treatment cell viability of SVG, U251, T98G, and U87



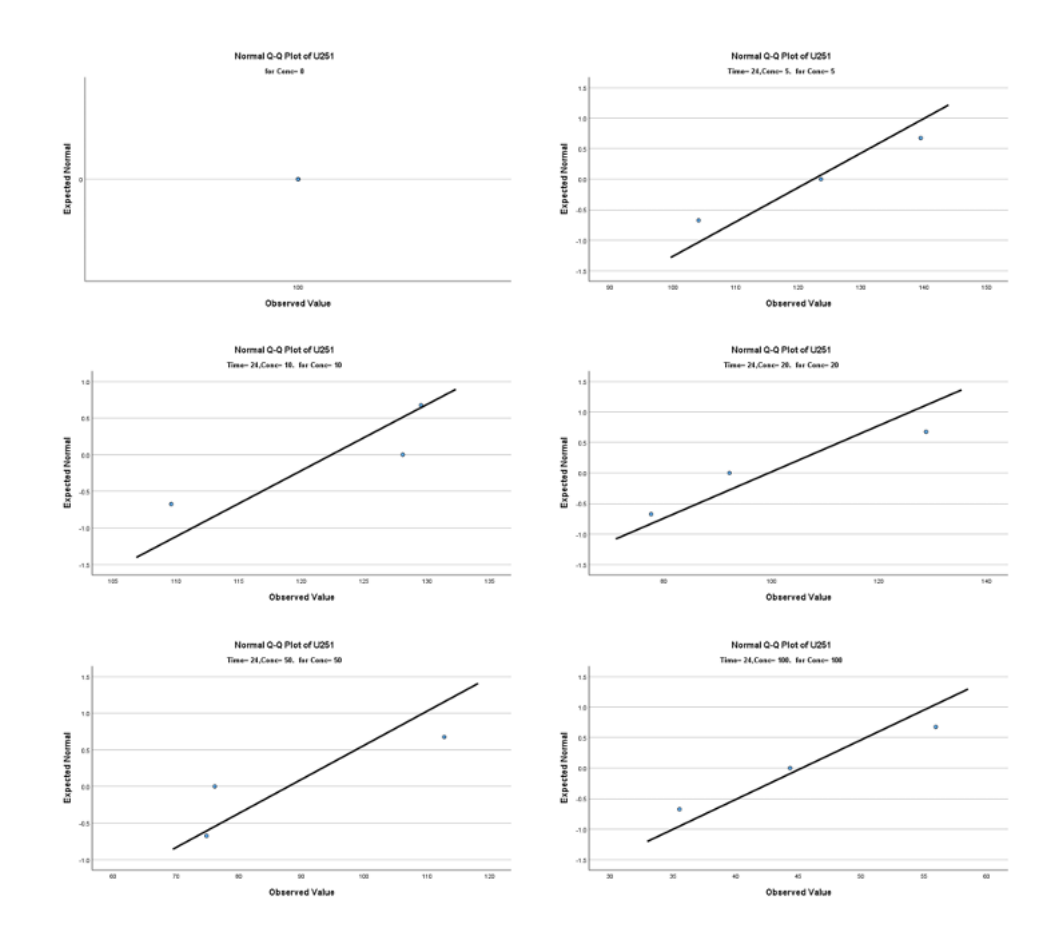
Tests of normality histograms for 24h treatment cell viability of SVG



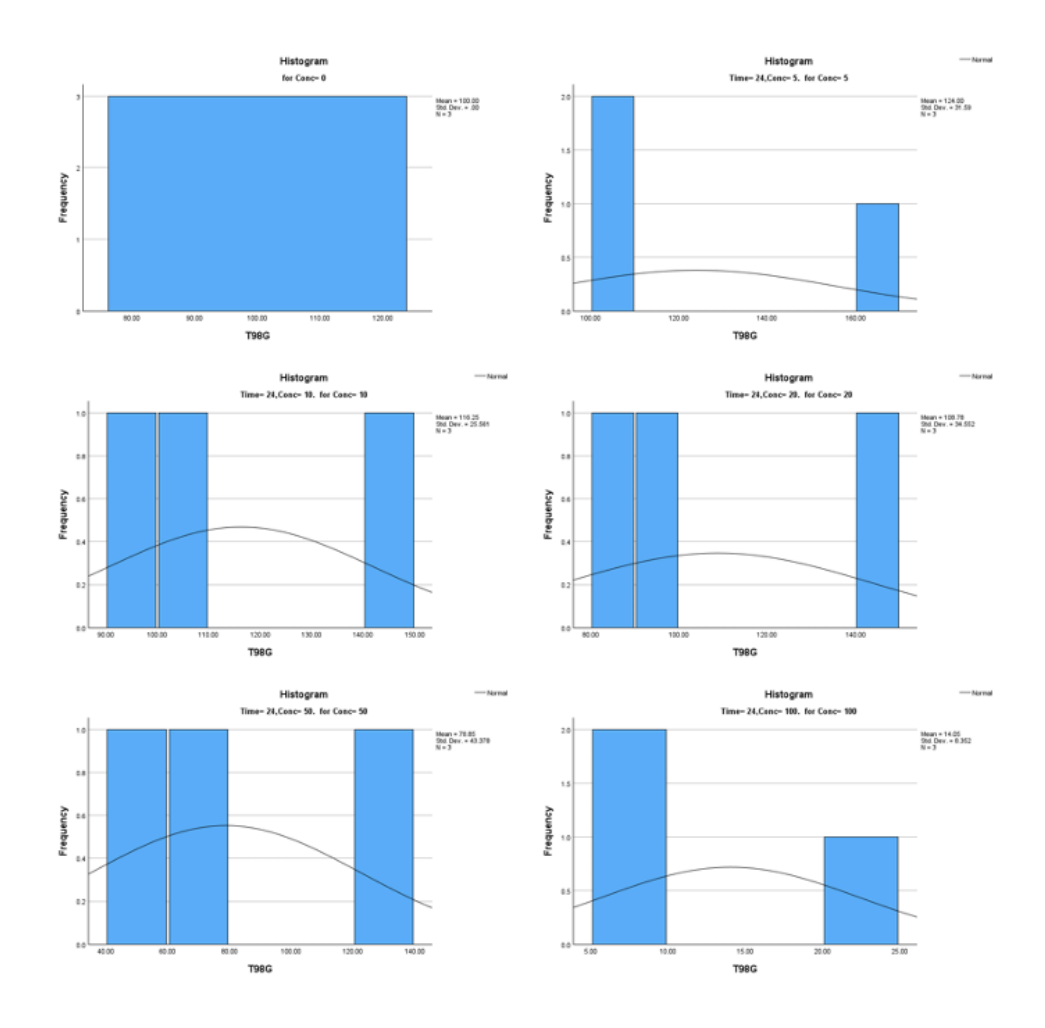
Tests of normality Q-Q plots for 24h treatment cell viability of SVG



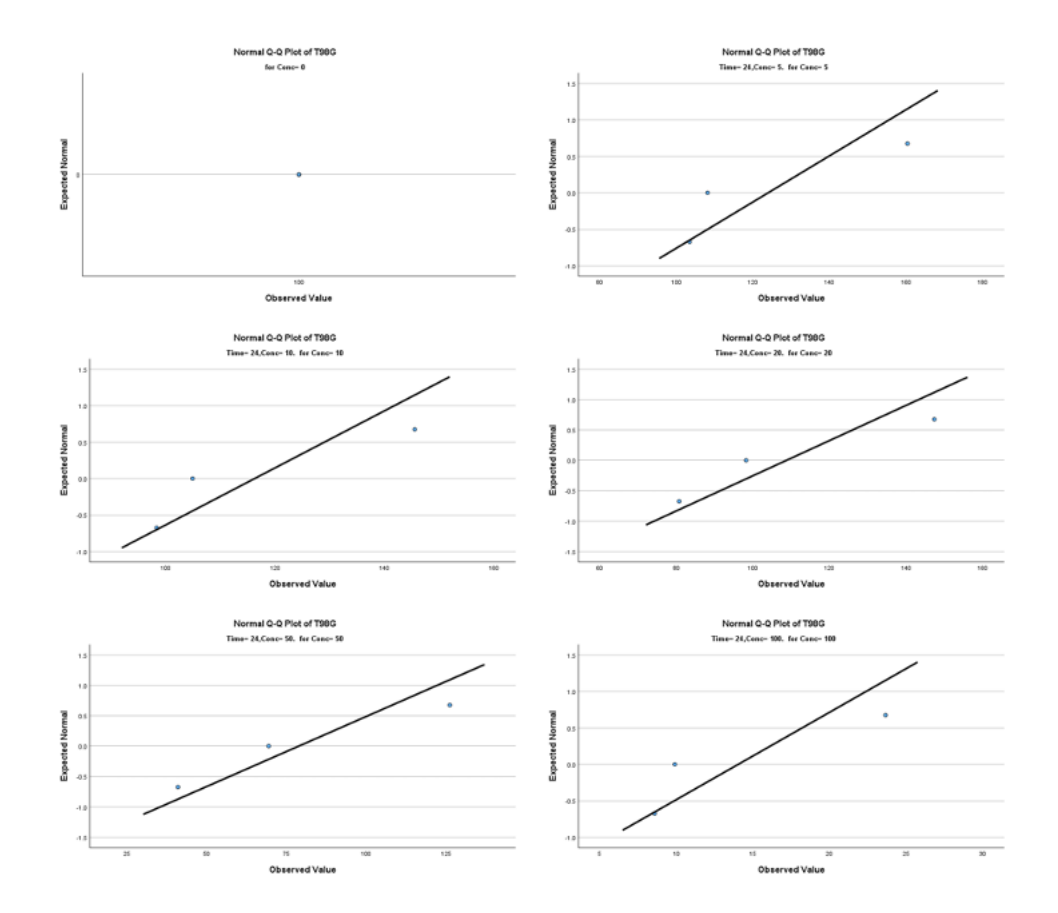
Tests of normality histograms for 24h treatment cell viability of U251



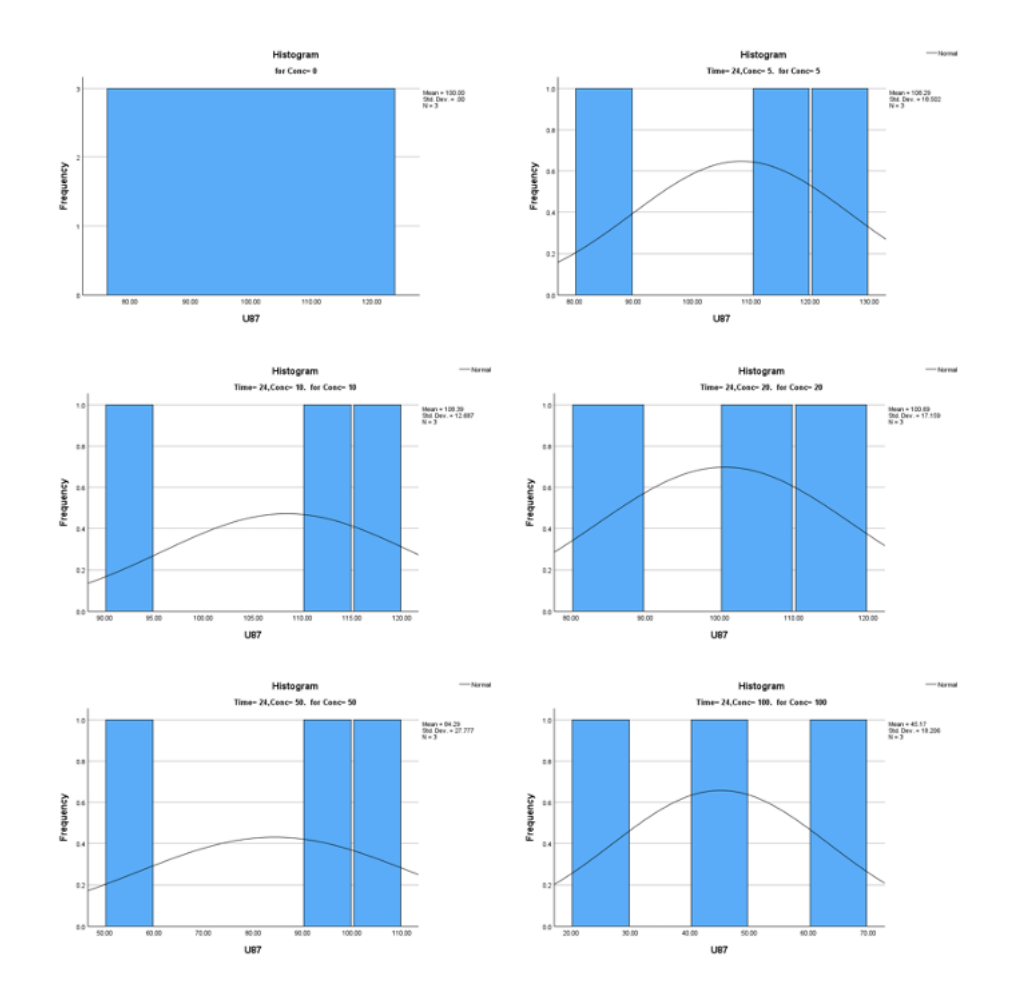
Tests of normality Q-Q plots for 24h treatment cell viability of U251



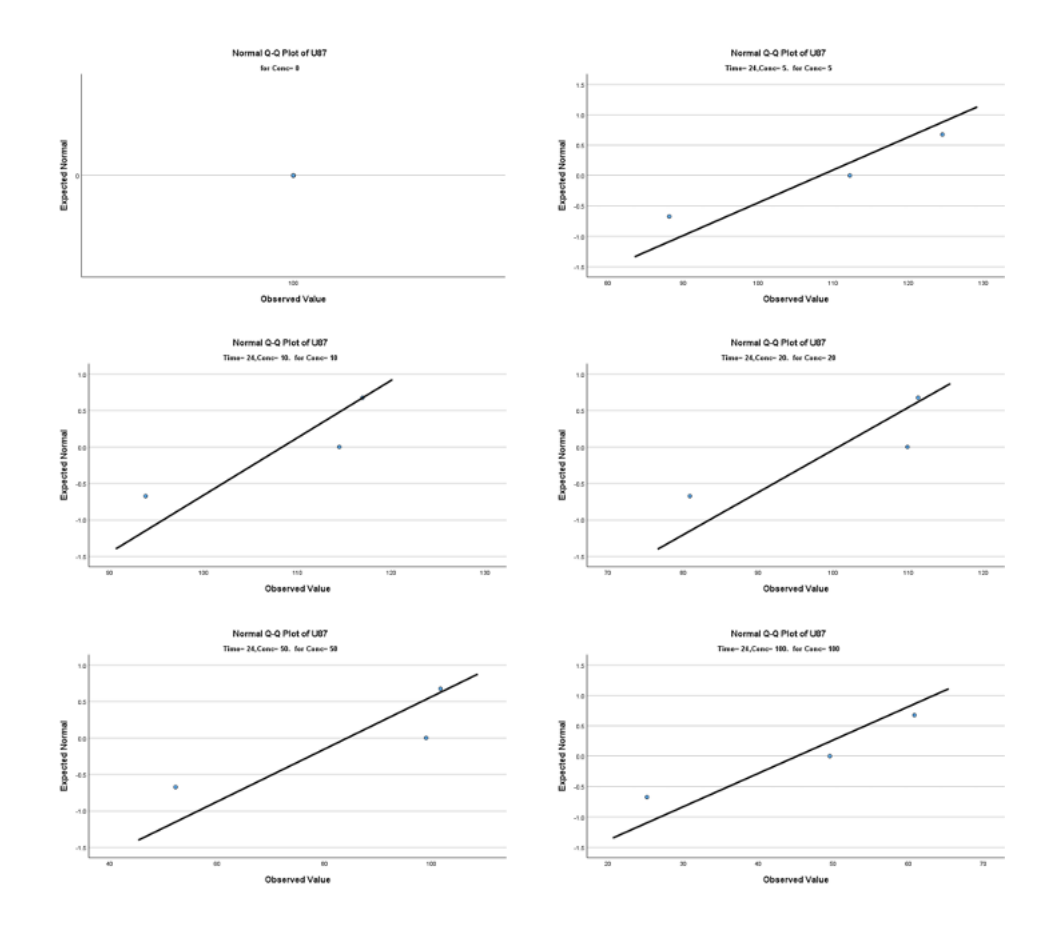
Tests of normality histograms for 24h treatment cell viability of T98G



Tests of normality Q-Q plot for 24h treatment cell viability of T98G



Tests of normality histograms for 24h treatment cell viability of U87



Tests of normality Q-Q plots for 24h treatment cell viability of U87

ANOVA

		Sum of Squares	df	Mean Square	F	Sig.
SVG	Between Groups	29075.029	5	5815.006	27.302	<.001
	Within Groups	2555.877	12	212.990		
	Total	31630.906	17			
U251	Between Groups	12179.982	5	2435.996	8.606	.001
	Within Groups	3396.512	12	283.043		
	Total	15576.494	17			
T98G	Between Groups	24571.994	5	4914.399	6.147	.005
	Within Groups	9593.163	12	799.430		
	Total	34165.156	17			
U87	Between Groups	8764.941	5	1752.988	5.534	.007
	Within Groups	3801.516	12	316.793		
	Total	12566.457	17			

One-way ANOVA for 24h treatment of SVG, U251, T98G, and U87.

.

Tests of Homogeneity of Variances

		Levene Statistic	df1	df2	Sig.
SVG	Based on Mean	2.500	5	12	.090
	Based on Median	1.028	5	12	.444
	Based on Median and with adjusted df	1.028	5	6.389	.473
	Based on trimmed mean	2.380	5	12	.101
U251	Based on Mean	2.851	5	12	.064
	Based on Median	.625	5	12	.684
	Based on Median and with adjusted df	.625	5	6.407	.688
	Based on trimmed mean	2.602	5	12	.081
T98G	Based on Mean	3.363	5	12	.040
	Based on Median	.737	5	12	.610
	Based on Median and with adjusted df	.737	5	7.965	.616
	Based on trimmed mean	3.051	5	12	.053
U87	Based on Mean	3.147	5	12	.048
	Based on Median	.405	5	12	.836
	Based on Median and with adjusted df	.405	5	6.264	.830
	Based on trimmed mean	2.729	5	12	.072

Levene's F-test for 24h treatment of SVG, U251, T98G, and U87.

Appendix 3

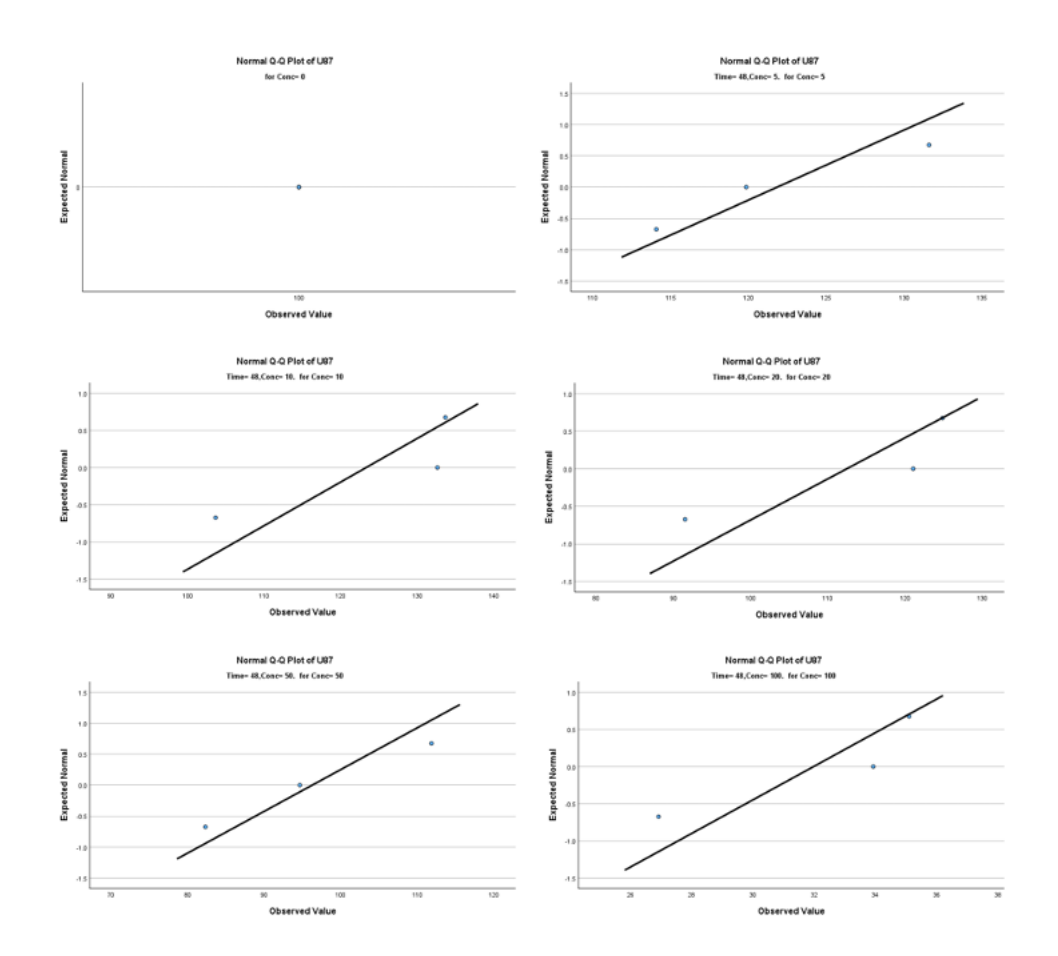
Statistical analysis for 48h treatment cell viability of SVG, U251, T98G, and U87.

Tests of Normality

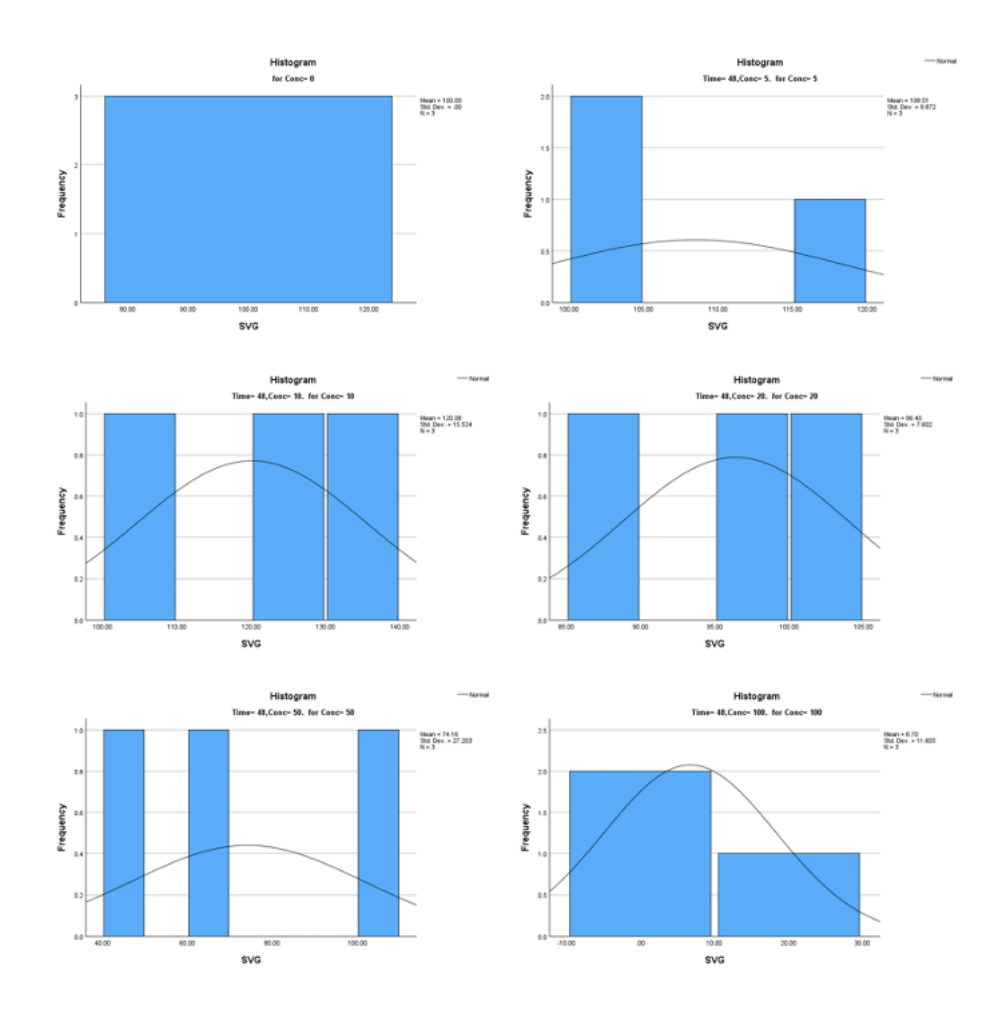
		Kolmogorov-Smirnov ^a		Shapiro-Wilk			
	Conc	Statistic	df	Sig.	Statistic	df	Sig.
SVG	0		3			3	
	5	.371	3		.785	3	.078
	10	.261	3		.957	3	.600
	20	.209	3		.992	3	.826
	50	.233	3		.979	3	.722
	100	.385	3		.750	3	<.001
U251	0		3			3	
	5	.361	3		.807	3	.131
	10	.286	3		.931	3	.494
	20	.288	3		.928	3	.482
	50	.216	3		.989	3	.796
	100	.288	3		.928	3	.482
T98G	0		3			3	
	5	.300	3		.912	3	.426
	10	.276	3		.942	3	.534
	20	.191	3		.997	3	.899
	50	.352	3		.825	3	.176
	100	.385	3		.750	3	<.001
U87	0		3			3	
	5	.255	3		.963	3	.629
	10	.374	3		.776	3	.058
	20	.348	3		.834	3	.199
	50	.210	3		.991	3	.819
	100	.337	3		.855	3	.253

a. Lilliefors Significance Correction

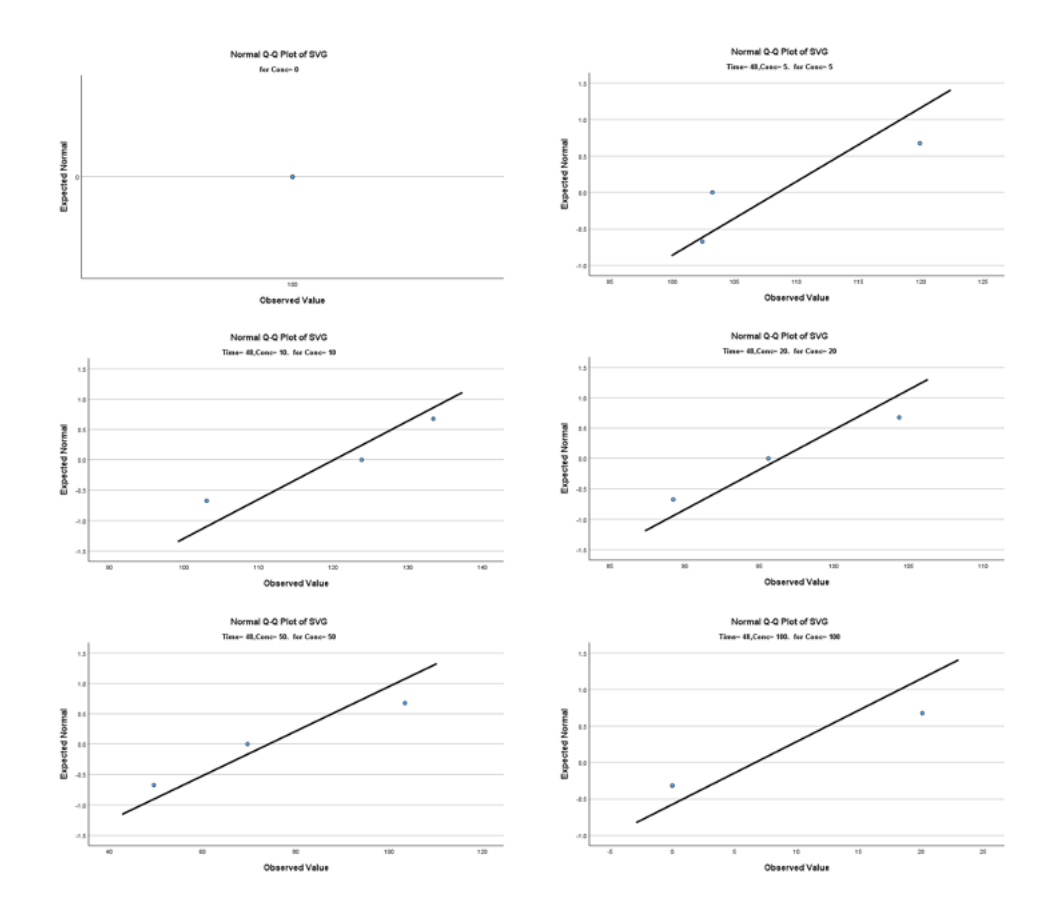
Shapiro-Will test for 48h treatment cell viability of SVG, U251, T98G, and U87.



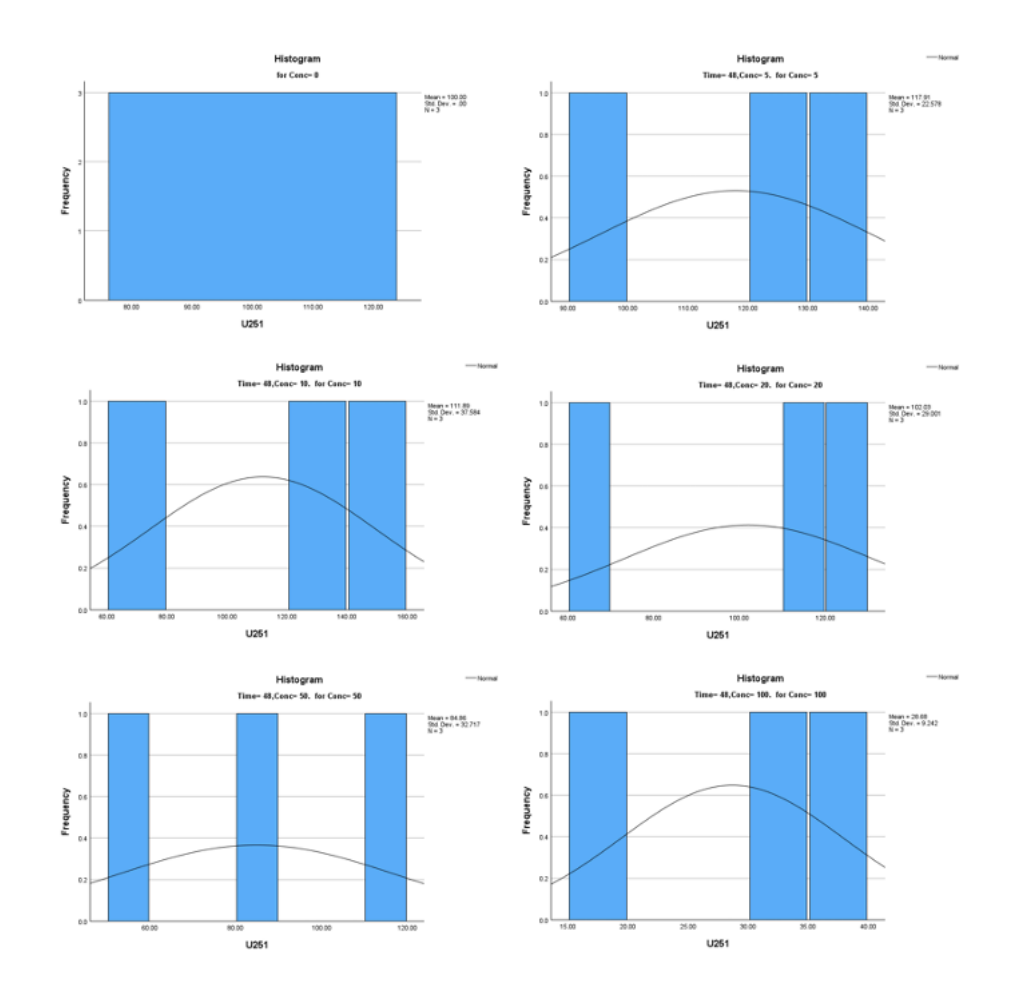
Tests of normality Q-Q plots for 48h treatment cell viability of SVG.



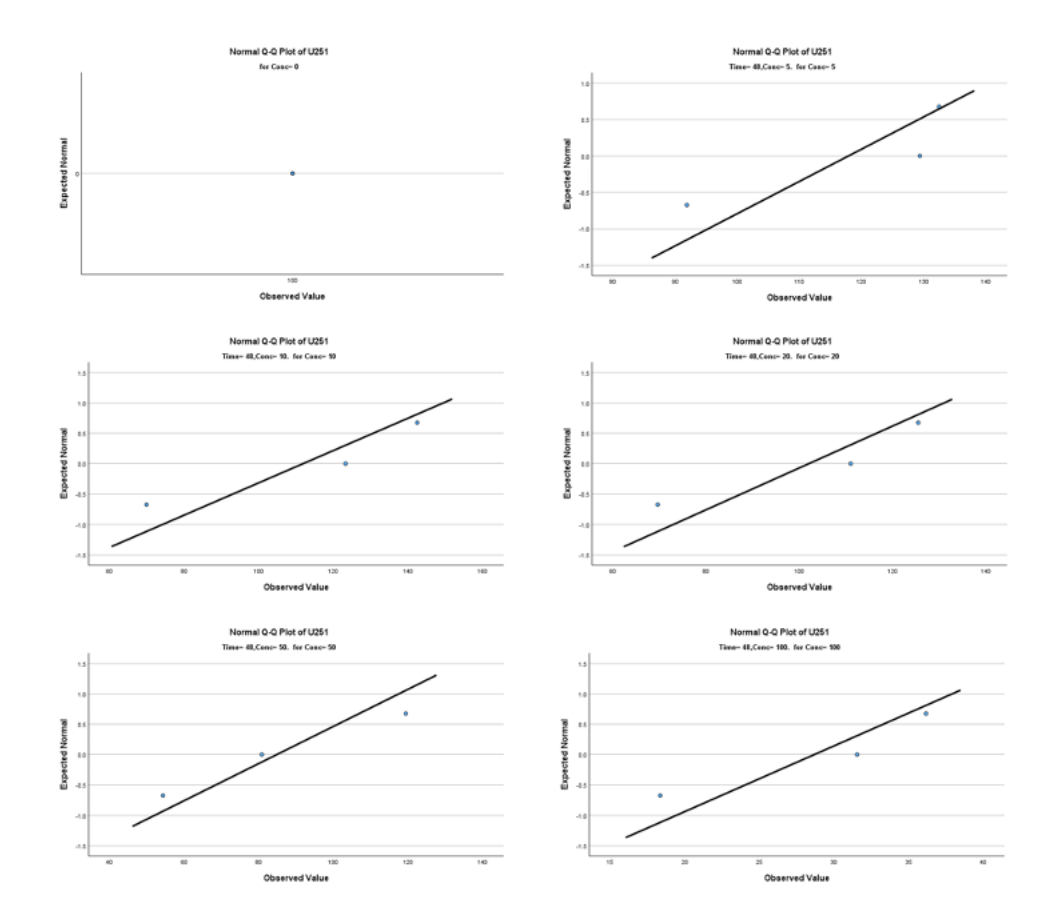
Tests of normality histograms for 48h treatment cell viability of SVG.



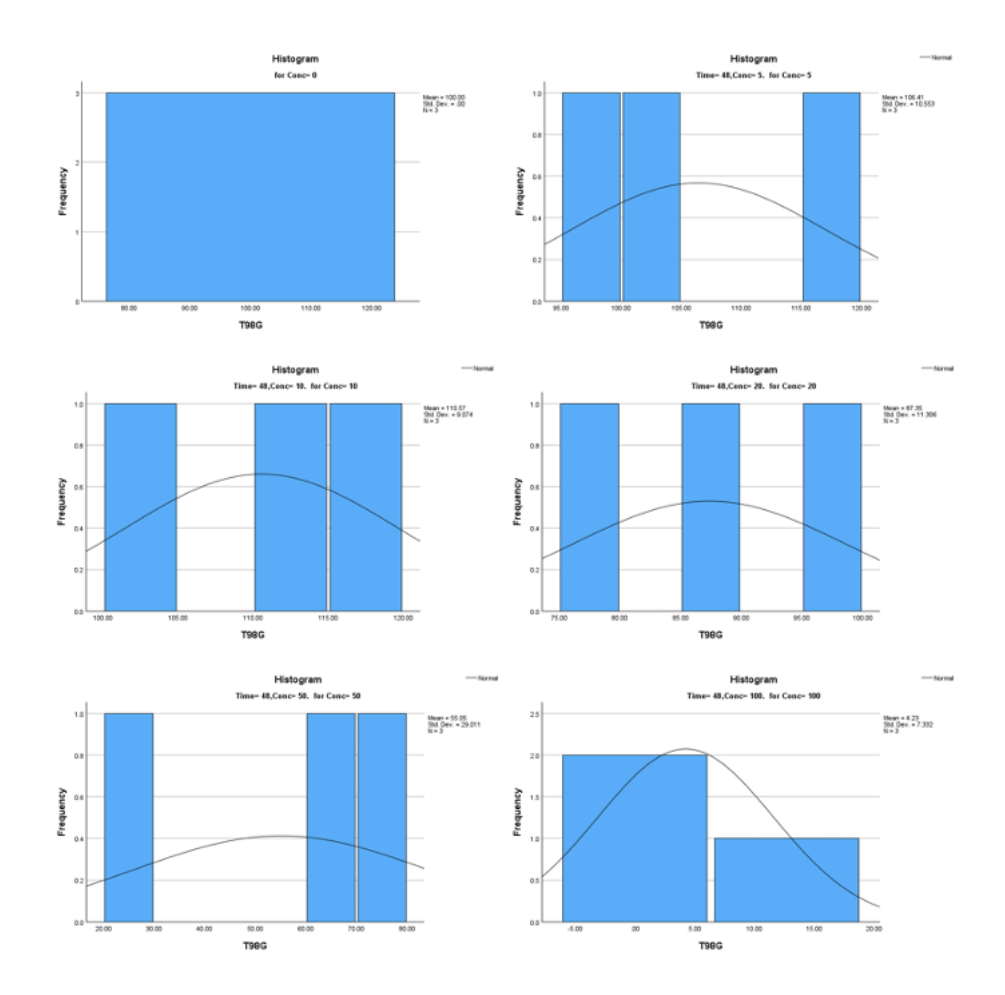
Tests of normality Q-Q plots for 48h treatment cell viability of U251.



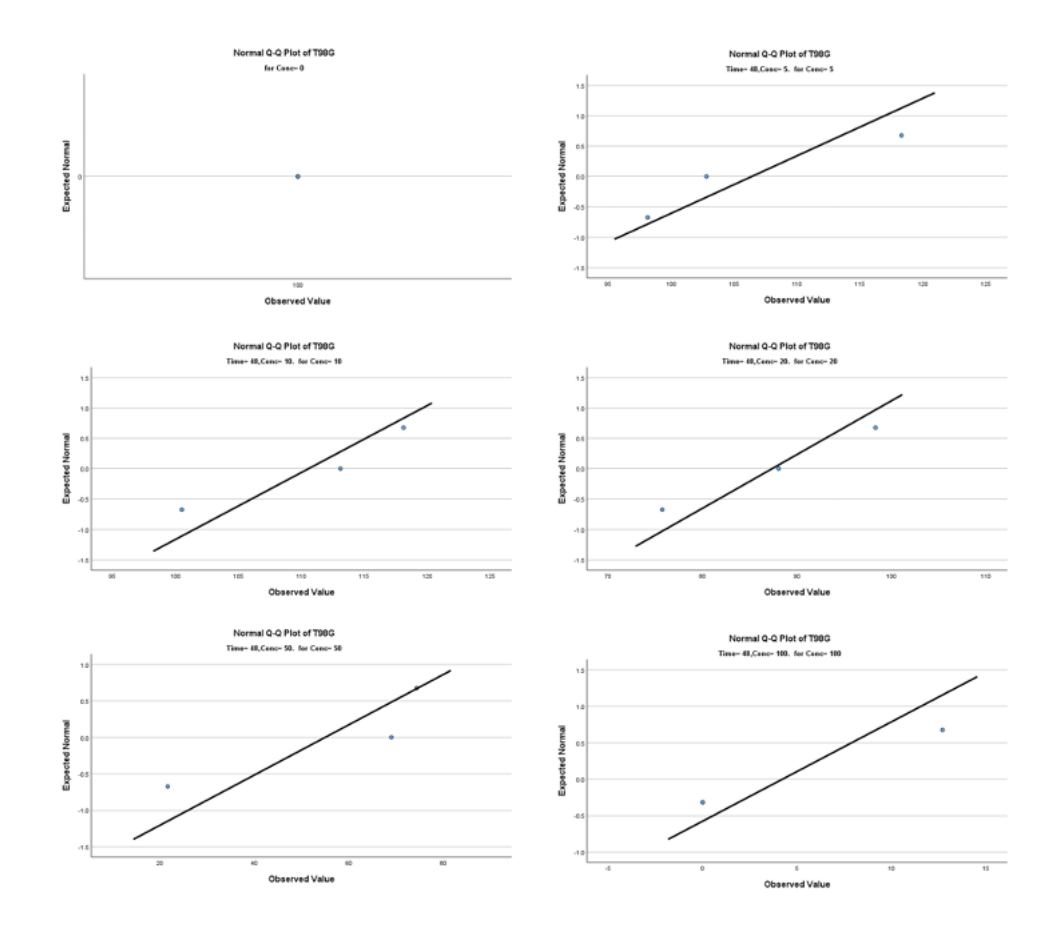
Tests of normality histograms for 48h treatment cell viability of U251.



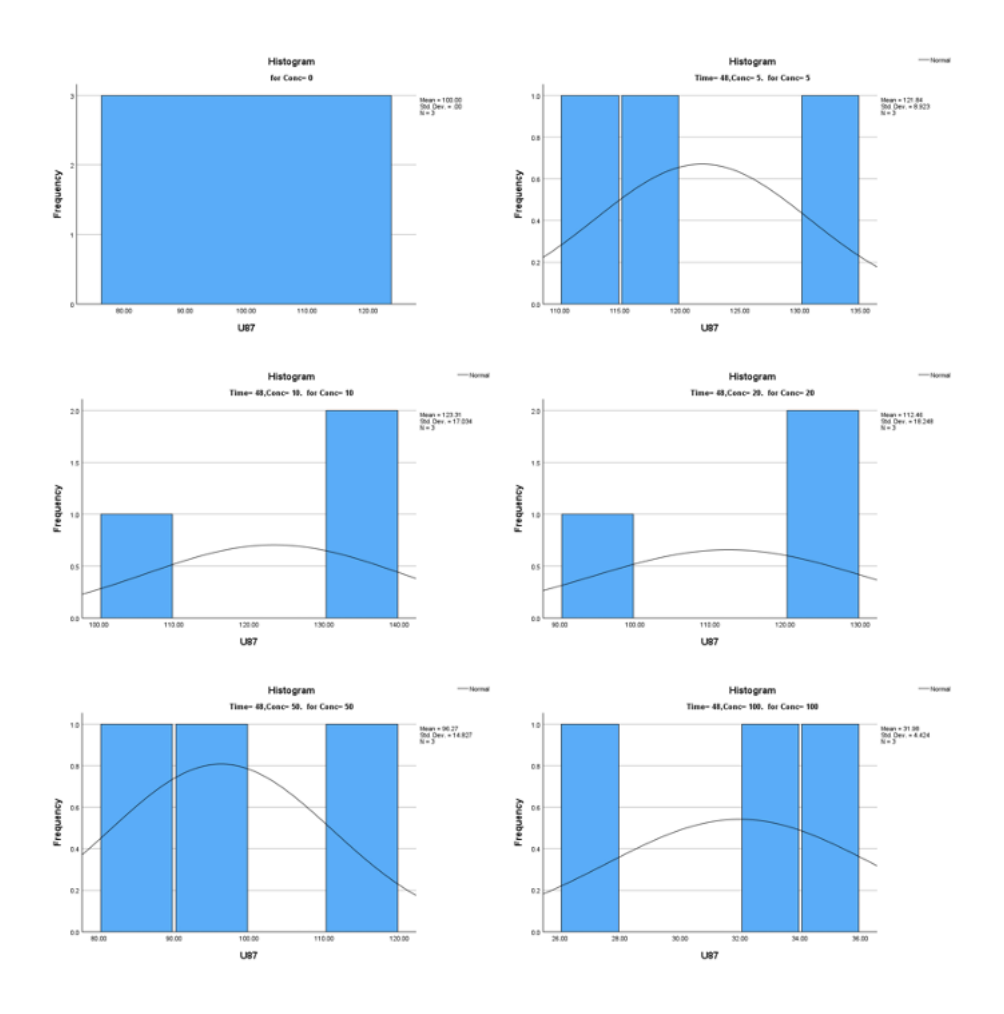
Tests of normality Q-Q plots for 48h treatment cell viability of T98G.



Tests of normality histograms for 48h treatment cell viability of T98G.



Tests of normality Q-Q plots for 48h treatment cell viability of U87.



Tests of normality histograms for 48h treatment cell viability of U87.

ANOVA

		Sum of Squares	df	Mean Square	F	Sig.
SVG	Between Groups	25150.923	5	5030.185	23.748	<.001
	Within Groups	2541.779	12	211.815		
	Total	27692.701	17			
U251	Between Groups	15851.843	5	3170.369	4.854	.012
	Within Groups	7838.320	12	653.193		
	Total	23690.163	17			
T98G	Between Groups	25213.179	5	5042.636	24.862	<.001
	Within Groups	2433.856	12	202.821		
	Total	27647.036	17			
U87	Between Groups	17347.100	5	3469.420	22.095	<.001
	Within Groups	1884.302	12	157.025		
	Total	19231.402	17			

One-way ANOVA for 48h treatment cell viability of SVG, U251, T98G, and U87.

Tests of Homogeneity of Variances

		Levene Statistic	df1	df2	Sig.
SVG	Based on Mean	2.921	5	12	.059
	Based on Median	1.021	5	12	.447
	Based on Median and with adjusted df	1.021	5	6.762	.473
	Based on trimmed mean	2.753	5	12	.070
U251	Based on Mean	2.799	5	12	.067
	Based on Median	.787	5	12	.579
	Based on Median and with adjusted df	.787	5	7.777	.588
	Based on trimmed mean	2.594	5	12	.082
T98G	Based on Mean	5.606	5	12	.007
	Based on Median	.701	5	12	.633
	Based on Median and with adjusted df	.701	5	3.296	.658
	Based on trimmed mean	4.853	5	12	.012
U87	Based on Mean	3.729	5	12	.029
	Based on Median	.558	5	12	.730
	Based on Median and with adjusted df	.558	5	5.837	.731
	Based on trimmed mean	3.291	5	12	.042

Levene's F-test for 48h treatment cell viability of SVG, U251, T98G, and U87.

Appendix 4

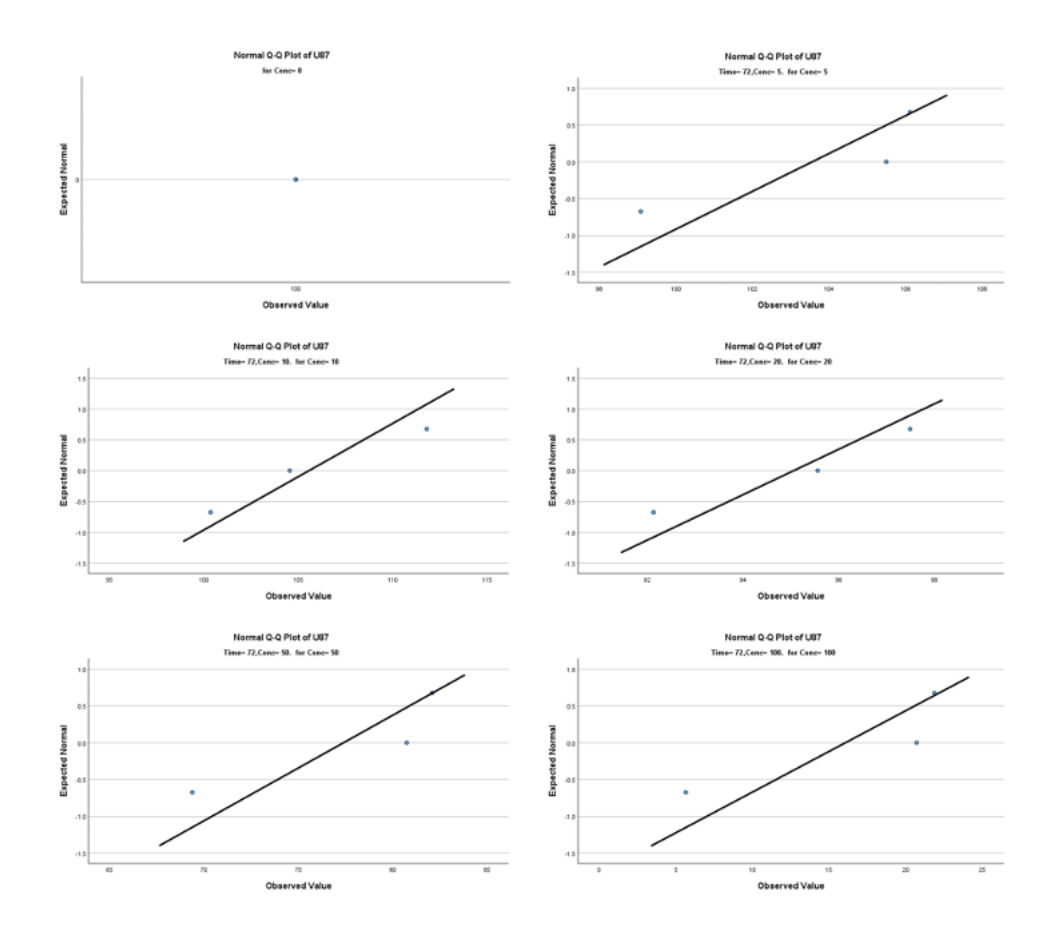
Statistical analysis for 72h treatment cell viability of SVG, U251, T98G, and U87.

Tests of Normality

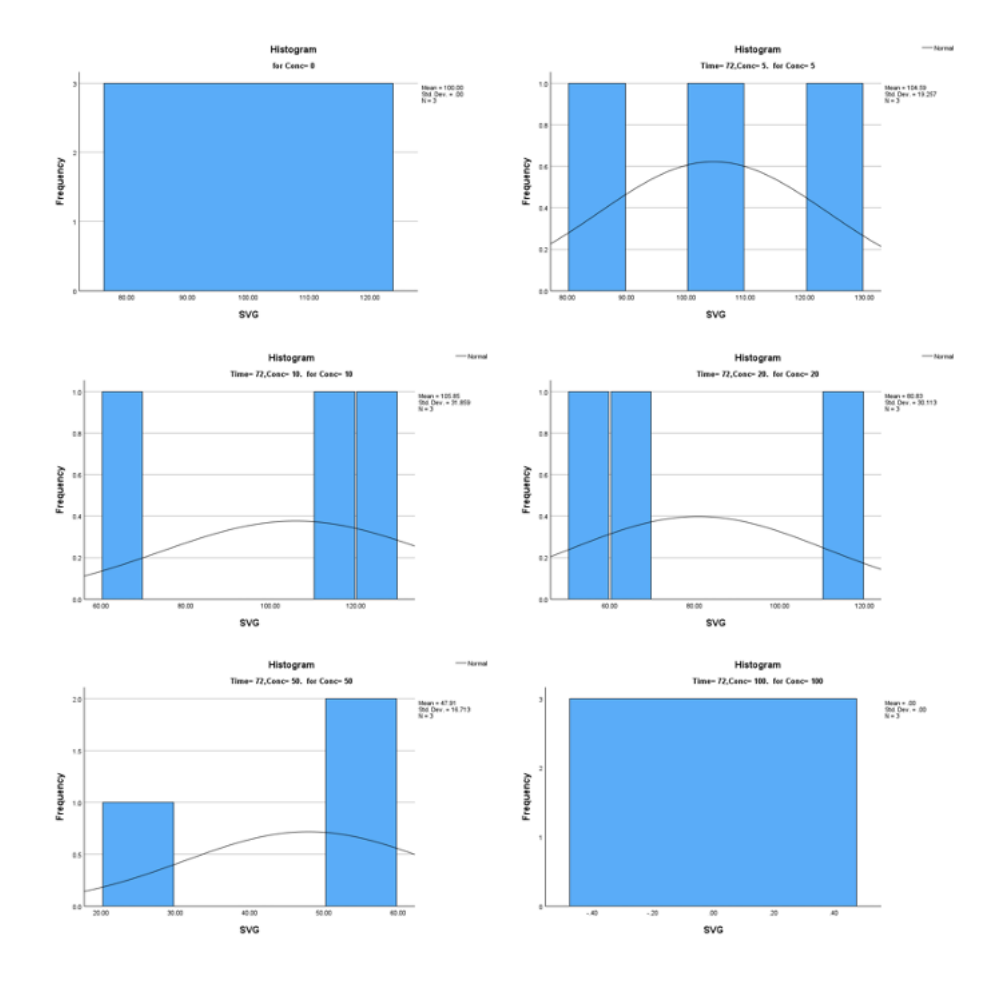
		Kolmogorov-Smirnov ^a			Shapiro-Wilk		
	Conc	Statistic	df	Sig.	Statistic	df	Sig.
SVG	0		3			3	
	5	.259	3		.959	3	.611
	10	.323	3		.878	3	.320
	20	.322	3		.880	3	.326
	50	.358	3		.812	3	.145
	100		3			3	
U251	0		3			3	
	5	.296	3		.918	3	.445
	10	.243	3		.972	3	.679
	20	.181	3		.999	3	.942
	50	.337	3		.855	3	.254
	100	.287	3		.930	3	.489
T98G	0		3			3	
	5	.297	3		.917	3	.442
	10	.315	3		.892	3	.359
	20	.243	3		.973	3	.682
	50	.294	3		.921	3	.455
	100	.385	3		.750	3	<.001
U87	0		3			3	
	5	.357	3		.816	3	.152
	10	.237	3		.977	3	.707
	20	.240	3		.975	3	.694
	50	.351	3		.828	3	.184
	100	.362	3		.803	3	.122

a. Lilliefors Significance Correction

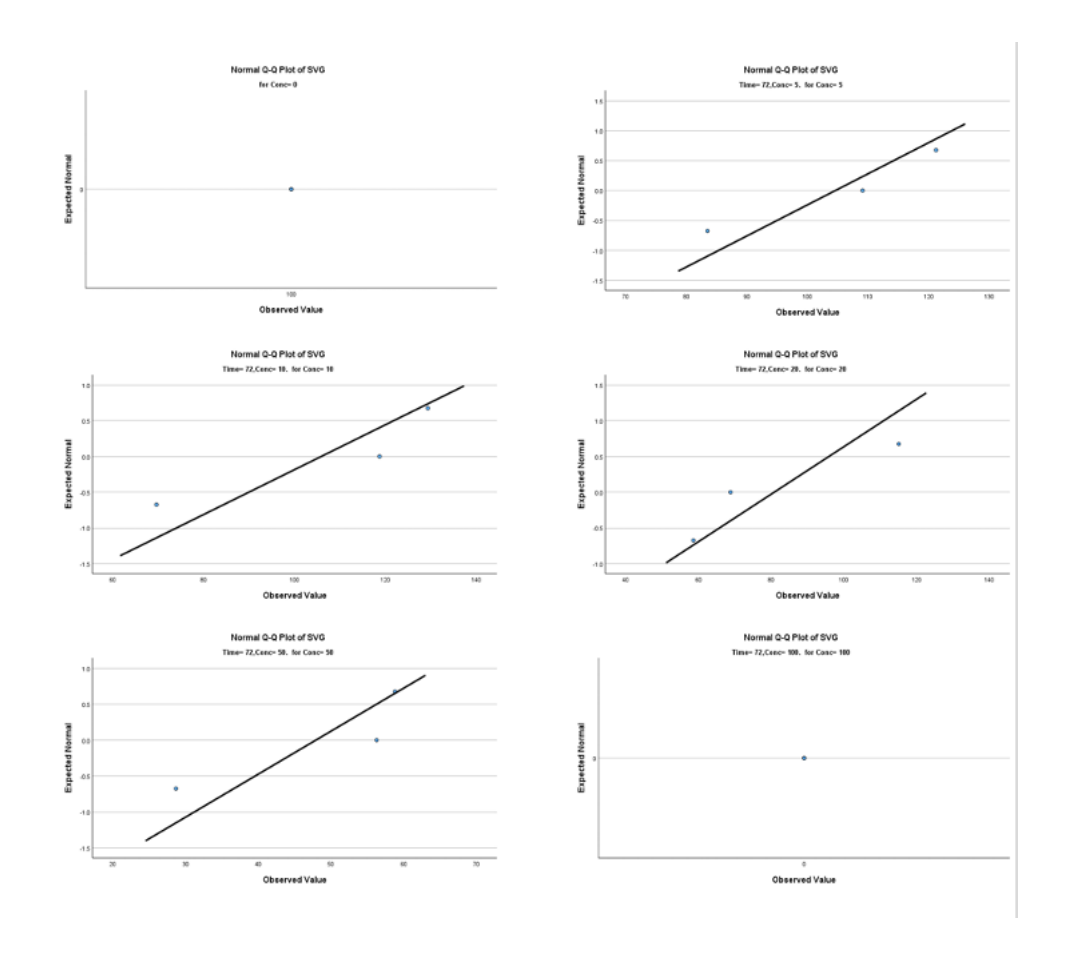
Shapiro-Wilk test for 72h treatment cell viability of SVG, U251, T98G, and U87.



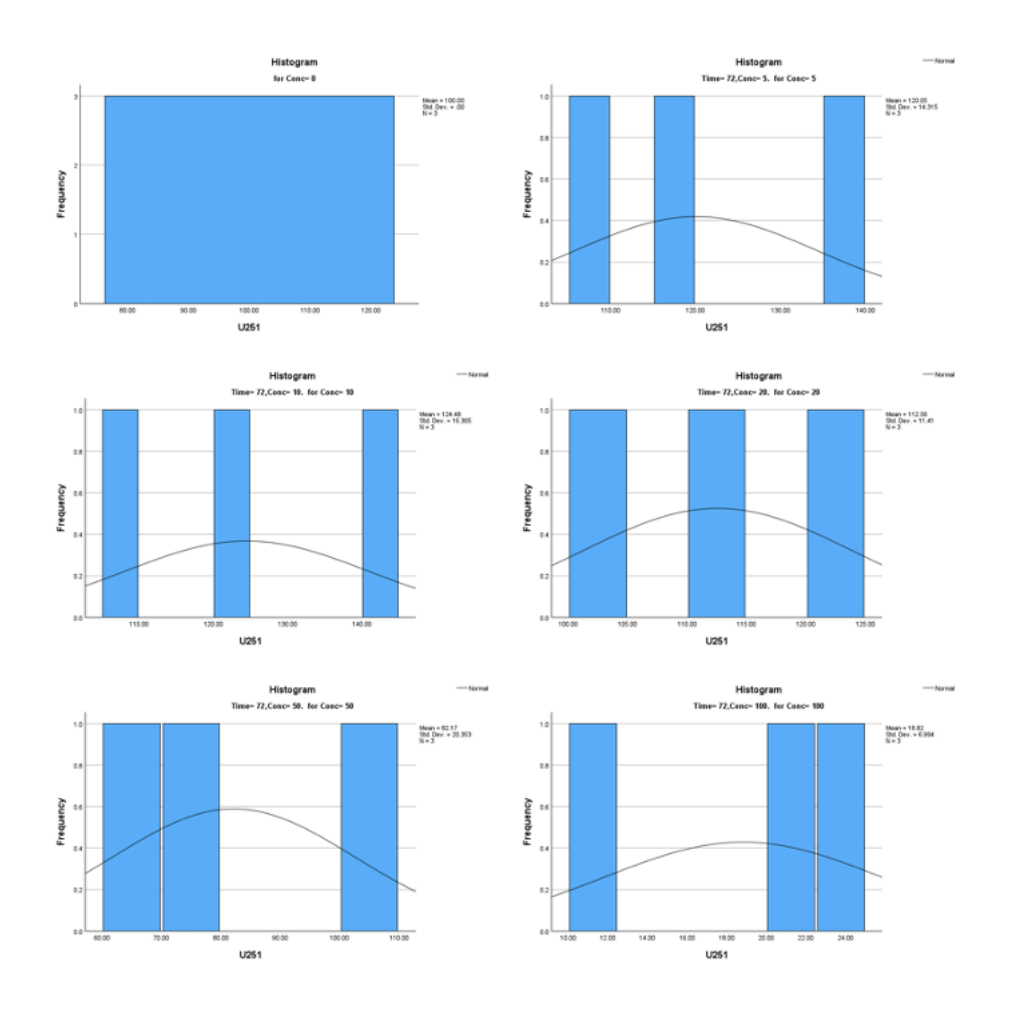
Tests of normality Q-Q plots for 72h treatment cell viability of SVG.



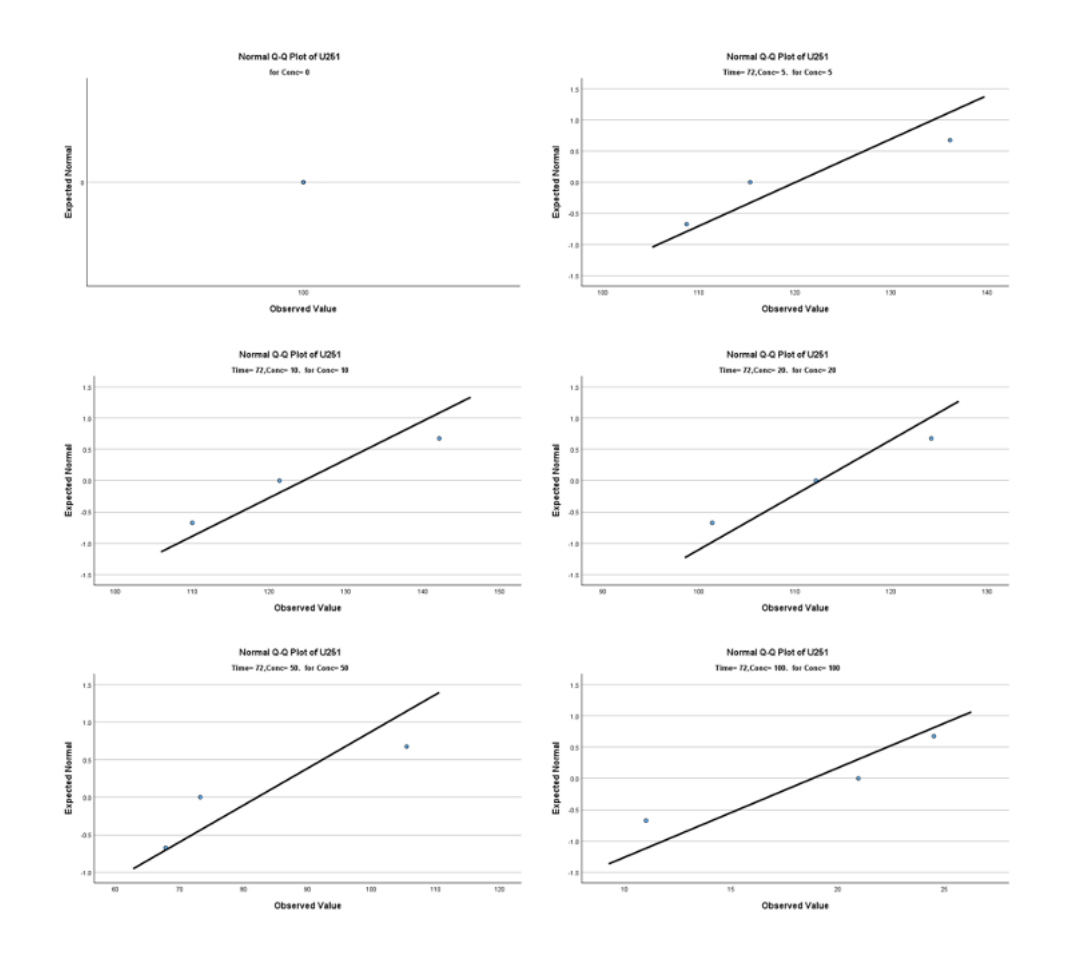
Tests of normality histograms for 72h treatment cell viability of SVG.



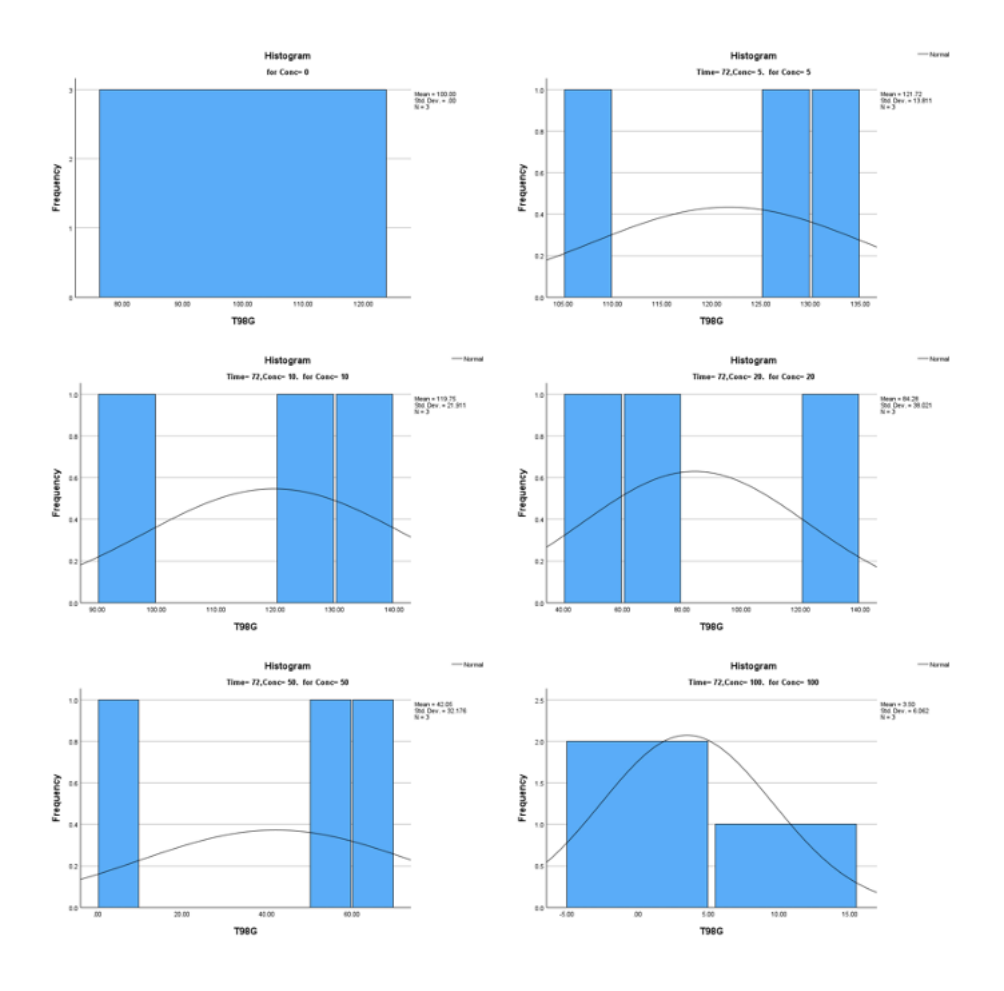
Tests of normality Q-Q plots for 72h treatment cell viability of U251.



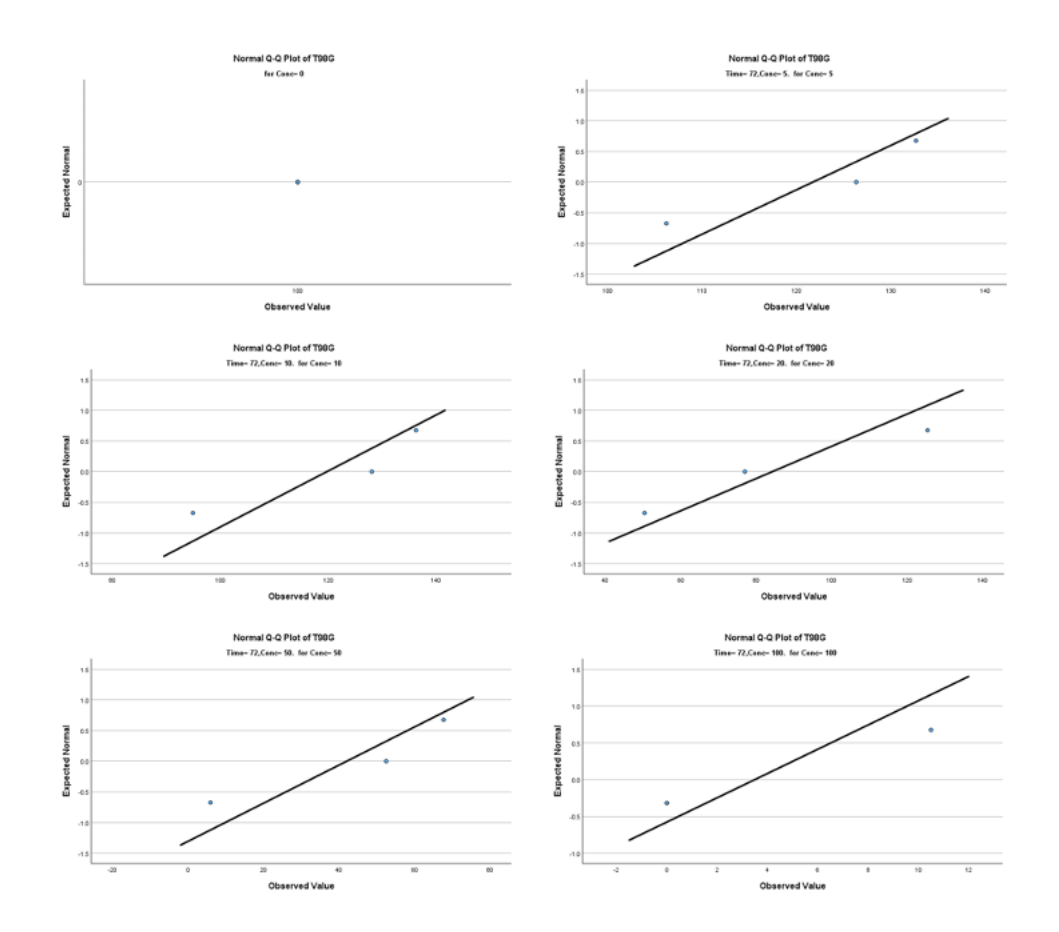
Tests of normality histograms for 72h treatment cell viability of U251.



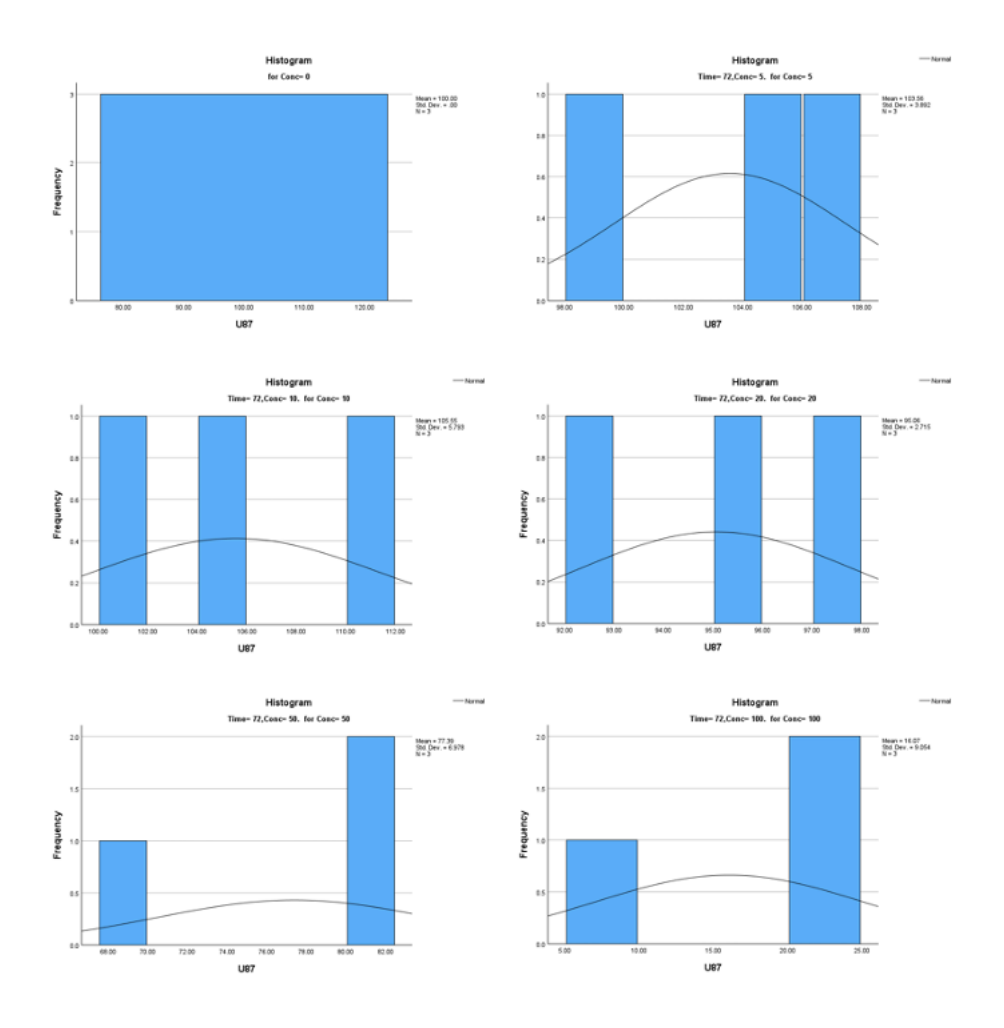
Tests of normality Q-Q plots for 72h treatment cell viability of T98G.



Tests of normality histograms for 72h treatment cell viability of T98G.



Tests of normality Q-Q plots for 72h treatment cell viability of U87.



Tests of normality histograms for 72h treatment cell viability of U87.

ANOVA

		Sum of Squares	df	Mean Square	F	Sig.
SVG	Between Groups	26476.579	5	5295.316	12.353	<.001
	Within Groups	5143.899	12	428.658		
	Total	31620.478	17			
U251	Between Groups	23321.324	5	4664.265	26.299	<.001
	Within Groups	2128.231	12	177.353		
	Total	25449.554	17			
T98G	Between Groups	33057.173	5	6611.435	12.441	<.001
	Within Groups	6376.866	12	531.406		
	Total	39434.040	17			
U87	Between Groups	17629.317	5	3525.863	113.283	<.001
	Within Groups	373.493	12	31.124		
	Total	18002.809	17			

One-way ANOVA for 72h treatment.

Tests of Homogeneity of Variances

		Levene Statistic	df1	df2	Sig.
SVG	Based on Mean	5.461	5	12	.008
	Based on Median	.832	5	12	.551
	Based on Median and with adjusted df	.832	5	6.256	.569
	Based on trimmed mean	4.789	5	12	.012
U251	Based on Mean	2.791	5	12	.067
	Based on Median	.634	5	12	.678
	Based on Median and with adjusted df	.634	5	5.979	.683
	Based on trimmed mean	2.554	5	12	.085
T98G	Based on Mean	3.588	5	12	.032
	Based on Median	1.067	5	12	.425
	Based on Median and with adjusted df	1.067	5	6.632	.454
	Based on trimmed mean	3.335	5	12	.041
U87	Based on Mean	4.203	5	12	.019
	Based on Median	.494	5	12	.775
	Based on Median and with adjusted df	.494	5	5.592	.772
	Based on trimmed mean	3.612	5	12	.032

Levene's F-test for 72h treatment.

Appendix 5

Post-hoc tests for cell viability data of SVG, U251, T98G, and U87.

Multiple Comparisons

Dependent Variable: Viability

Bonferroni

		Mean			95% Confide	ence Interval
(I) Time	(J) Time	Difference (I-J)	Std. Error	Sig.	Lower Bound	Upper Bound
Time, 24h	Time, 48h	7.7622	5.62225	.528	-6.3555	21.8799
	Time, 72h	18.8717	5.62225	.006	4.7540	32.9894
Time, 48h	Time, 24h	-7.7622	5.62225	.528	-21.8799	6.3555
	Time, 72h	11.1094	5.62225	.168	-3.0083	25.2271
Time, 72h	Time, 24h	-18.8717 [*]	5.62225	.006	-32.9894	-4.7540
	Time, 48h	-11.1094	5.62225	.168	-25.2271	3.0083

Based on observed means.

The error term is Mean Square(Error) = 284.488.

Bonferroni post-hoc tests for cell viability of SVG at 24h, 48h, and 72h.

^{*.} The mean difference is significant at the .05 level.

Dependent Variable: Viability

Bonferroni

		Mean			95% Confide	ence Interval
(I) Concentration	(J) Concentration	Difference (I-J)	Std. Error	Sig.	Lower Bound	Upper Bound
Control	5uM	-28.6833	11.91609	.496	-72.1638	14.7972
	10uM	-27.8633	11.91609	.563	-71.3438	15.6172
	20uM	-7.2567	11.91609	1.000	-50.7372	36.2238
	50uM	22.4233	11.91609	1.000	-21.0572	65.9038
	100uM	88.9633	11.91609	<.001	45.4828	132.4438
5uM	Control	28.6833	11.91609	.496	-14.7972	72.1638
	10uM	.8200	11.91609	1.000	-42.6605	44.3005
	20uM	21.4267	11.91609	1.000	-22.0538	64.9072
	50uM	51.1067	11.91609	.016	7.6262	94.5872
	100uM	117.6467*	11.91609	<.001	74.1662	161.1272
10uM	Control	27.8633	11.91609	.563	-15.6172	71.3438
	5uM	8200	11.91609	1.000	-44.3005	42.6605
	20uM	20.6067	11.91609	1.000	-22.8738	64.0872
	50uM	50.2867 [*]	11.91609	.018	6.8062	93.7672
	100uM	116.8267*	11.91609	<.001	73.3462	160.3072
20uM	Control	7.2567	11.91609	1.000	-36.2238	50.7372
	5uM	-21.4267	11.91609	1.000	-64.9072	22.0538
	10uM	-20.6067	11.91609	1.000	-64.0872	22.8738
	50uM	29.6800	11.91609	.426	-13.8005	73.1605
	100uM	96.2200 [*]	11.91609	<.001	52.7395	139.7005
50uM	Control	-22.4233	11.91609	1.000	-65.9038	21.0572
	5uM	-51.1067 [*]	11.91609	.016	-94.5872	-7.6262
	10uM	-50.2867 [*]	11.91609	.018	-93.7672	-6.8062
	20uM	-29.6800	11.91609	.426	-73.1605	13.8005
	100uM	66.5400 [*]	11.91609	.002	23.0595	110.0205
100uM	Control	-88.9633 [*]	11.91609	<.001	-132.4438	-45.4828
	5uM	-117.6467 [*]	11.91609	<.001	-161.1272	-74.1662
	10uM	-116.8267 [*]	11.91609	<.001	-160.3072	-73.3462
	20uM	-96.2200 [*]	11.91609	<.001	-139.7005	-52.7395
	50uM	-66.5400 [*]	11.91609	.002	-110.0205	-23.0595

Based on observed means.

The error term is Mean Square(Error) = 212.990.

Bonferroni post-hoc tests for 24h cell viability of SVG doses 0, 5, 10, 20, 50, and $100\mu M$.

^{*.} The mean difference is significant at the .05 level.

Dependent Variable: Viability

Bonferroni

Domenom						
		Mean			95% Confide	
(I) Concentration	(J) Concentration	Difference (I-J)	Std. Error	Sig.	Lower Bound	Upper Bound
Control	5uM	-8.5100	11.88318	1.000	-51.8704	34.8504
	10uM	-20.0767	11.88318	1.000	-63.4371	23.2837
	20uM	3.6000	11.88318	1.000	-39.7604	46.9604
	50uM	25.8433	11.88318	.755	-17.5171	69.2037
	100uM	93.3000*	11.88318	<.001	49.9396	136.6604
5uM	Control	8.5100	11.88318	1.000	-34.8504	51.8704
	10uM	-11.5667	11.88318	1.000	-54.9271	31.7937
	20uM	12.1100	11.88318	1.000	-31.2504	55.4704
	50uM	34.3533	11.88318	.203	-9.0071	77.7137
	100uM	101.8100	11.88318	<.001	58.4496	145.1704
10uM	Control	20.0767	11.88318	1.000	-23.2837	63.4371
	5uM	11.5667	11.88318	1.000	-31.7937	54.9271
	20uM	23.6767	11.88318	1.000	-19.6837	67.0371
	50uM	45.9200 [*]	11.88318	.034	2.5596	89.2804
	100uM	113.3767*	11.88318	<.001	70.0163	156.7371
20uM	Control	-3.6000	11.88318	1.000	-46.9604	39.7604
	5uM	-12.1100	11.88318	1.000	-55.4704	31.2504
	10uM	-23.6767	11.88318	1.000	-67.0371	19.6837
	50uM	22.2433	11.88318	1.000	-21.1171	65.6037
	100uM	89.7000	11.88318	<.001	46.3396	133.0604
50uM	Control	-25.8433	11.88318	.755	-69.2037	17.5171
	5uM	-34.3533	11.88318	.203	-77.7137	9.0071
	10uM	-45.9200 [*]	11.88318	.034	-89.2804	-2.5596
	20uM	-22.2433	11.88318	1.000	-65.6037	21.1171
	100uM	67.4567 [*]	11.88318	.002	24.0963	110.8171
100uM	Control	-93.3000 [*]	11.88318	<.001	-136.6604	-49.9396
	5uM	-101.8100 [*]	11.88318	<.001	-145.1704	-58.4496
	10uM	-113.3767 [*]	11.88318	<.001	-156.7371	-70.0163
	20uM	-89.7000 [*]	11.88318	<.001	-133.0604	-46.3396
	50uM	-67.4567 [*]	11.88318	.002	-110.8171	-24.0963

Based on observed means.

The error term is Mean Square(Error) = 211.815.

Bonferroni post-hoc tests for 48h cell viability of SVG doses 0, 5, 10, 20, 50, and $100\mu M$.

^{*.} The mean difference is significant at the .05 level.

Dependent Variable: Viability

Bonferroni

201110110111		Mann			95% Confide	ence Interval
(I) Concentration	(J) Concentration	Mean Difference (I-J)	Std. Error	Sig.	Lower Bound	
Control	5uM	-4.5867	16.90480	1.000	-66.2704	57.0971
00111101	10uM	-5.8533	16.90480	1.000	-67.5371	55.8304
	20uM	19.1667	16.90480	1.000	-42.5171	80.8504
	50uM	52.0867	16.90480	.143	-9.5971	113.7704
	100uM	100.0000*	16.90480	.001	38.3163	161.6837
5uM	Control	4.5867	16.90480	1.000	-57.0971	66.2704
out.	10uM	-1.2667	16.90480	1.000	-62.9504	60.4171
	20uM	23.7533	16.90480	1.000	-37.9304	85.4371
	50uM	56.6733	16.90480	.086	-5.0104	118.3571
	100uM	104.5867*	16.90480	<.001	42.9029	166.2704
10uM	Control	5.8533	16.90480	1.000	-55.8304	67.5371
	5uM	1.2667	16.90480	1.000	-60.4171	62.9504
	20uM	25.0200	16.90480	1.000	-36.6637	86.7037
	50uM	57.9400	16.90480	.075	-3.7437	119.6237
	100uM	105.8533	16.90480	<.001	44.1696	167.5371
20uM	Control	-19.1667	16.90480	1.000	-80.8504	42.5171
	5uM	-23.7533	16.90480	1.000	-85.4371	37.9304
	10uM	-25.0200	16.90480	1.000	-86.7037	36.6637
	50uM	32.9200	16.90480	1.000	-28.7637	94.6037
	100uM	80.8333*	16.90480	.007	19.1496	142.5171
50uM	Control	-52.0867	16.90480	.143	-113.7704	9.5971
	5uM	-56.6733	16.90480	.086	-118.3571	5.0104
	10uM	-57.9400	16.90480	.075	-119.6237	3.7437
	20uM	-32.9200	16.90480	1.000	-94.6037	28.7637
	100uM	47.9133	16.90480	.226	-13.7704	109.5971
100uM	Control	-100.0000 [*]	16.90480	.001	-161.6837	-38.3163
	5uM	-104.5867 [*]	16.90480	<.001	-166.2704	-42.9029
	10uM	-105.8533 [*]	16.90480	<.001	-167.5371	-44.1696
	20uM	-80.8333 [*]	16.90480	.007	-142.5171	-19.1496
	50uM	-47.9133	16.90480	.226	-109.5971	13.7704

Based on observed means.

The error term is Mean Square(Error) = 428.658.

Bonferroni post-hoc tests for 72h cell viability of SVG doses 0, 5, 10, 20, 50, and 100µM.

^{*.} The mean difference is significant at the .05 level.

Multiple Comparisons

Dependent Variable: Viability

Bonferroni

		Mean			95% Confide	ence Interval
(I) Time	(J) Time	Difference (I-J)	Std. Error	Sig.	Lower Bound	Upper Bound
Time, 24h	Time, 48h	5.3461	6.42215	1.000	-10.7802	21.4724
	Time, 72h	3.2278	6.42215	1.000	-12.8985	19.3541
Time, 48h	Time, 24h	-5.3461	6.42215	1.000	-21.4724	10.7802
	Time, 72h	-2.1183	6.42215	1.000	-18.2446	14.0079
Time, 72h	Time, 24h	-3.2278	6.42215	1.000	-19.3541	12.8985
	Time, 48h	2.1183	6.42215	1.000	-14.0079	18.2446

Based on observed means.

The error term is Mean Square(Error) = 371.196.

Bonferroni post-hoc tests for cell viability of U251 24h, 48h, and 72h.

Dependent Variable: Viability

Bonferroni

Bomenom		Mean			95% Confide	ence Interval
(I) Concentration	(J) Concentration	Difference (I-J)	Std. Error	Sig.	Lower Bound	
Control	5uM	-22.3800	13.73663	1.000	-72.5035	27.7435
	10uM	-22.3933	13.73663	1.000	-72.5168	27.7301
	20uM	.5033	13.73663	1.000	-49.6201	50.6268
	50uM	12.0867	13.73663	1.000	-38.0368	62.2101
	100uM	54.7367 [*]	13.73663	.027	4.6132	104.8601
5uM	Control	22.3800	13.73663	1.000	-27.7435	72.5035
	10uM	0133	13.73663	1.000	-50.1368	50.1101
	20uM	22.8833	13.73663	1.000	-27.2401	73.0068
	50uM	34.4667	13.73663	.412	-15.6568	84.5901
	100uM	77.1167 [*]	13.73663	.002	26.9932	127.2401
10uM	Control	22.3933	13.73663	1.000	-27.7301	72.5168
	5uM	.0133	13.73663	1.000	-50.1101	50.1368
	20uM	22.8967	13.73663	1.000	-27.2268	73.0201
	50uM	34.4800	13.73663	.411	-15.6435	84.6035
	100uM	77.1300 [*]	13.73663	.002	27.0065	127.2535
20uM	Control	5033	13.73663	1.000	-50.6268	49.6201
	5uM	-22.8833	13.73663	1.000	-73.0068	27.2401
	10uM	-22.8967	13.73663	1.000	-73.0201	27.2268
	50uM	11.5833	13.73663	1.000	-38.5401	61.7068
	100uM	54.2333 [*]	13.73663	.029	4.1099	104.3568
50uM	Control	-12.0867	13.73663	1.000	-62.2101	38.0368
	5uM	-34.4667	13.73663	.412	-84.5901	15.6568
	10uM	-34.4800	13.73663	.411	-84.6035	15.6435
	20uM	-11.5833	13.73663	1.000	-61.7068	38.5401
	100uM	42.6500	13.73663	.137	-7.4735	92.7735
100uM	Control	-54.7367 [*]	13.73663	.027	-104.8601	-4.6132
	5uM	-77.1167 [*]	13.73663	.002	-127.2401	-26.9932
	10uM	-77.1300 [*]	13.73663	.002	-127.2535	-27.0065
	20uM	-54.2333 [*]	13.73663	.029	-104.3568	-4.1099
	50uM	-42.6500	13.73663	.137	-92.7735	7.4735
Based on observe		.2.000			-2	

Based on observed means.

The error term is Mean Square(Error) = 283.043.

Bonferroni post-hoc tests for 24h cell viability of U251 doses 0, 5, 10, 20, 50, and $100\mu M$.

^{*.} The mean difference is significant at the .05 level.

Dependent Variable: Viability

Bonferroni

		Mean			95% Confide	ence Interval
(I) Concentration	(J) Concentration	Difference (I-J)	Std. Error	Sig.	Lower Bound	Upper Bound
Control	5uM	-17.9100	20.86773	1.000	-94.0540	58.2340
	10uM	-11.8867	20.86773	1.000	-88.0307	64.2574
	20uM	-2.0267	20.86773	1.000	-78.1707	74.1174
	50uM	15.1367	20.86773	1.000	-61.0074	91.2807
	100uM	71.3167	20.86773	.077	-4.8274	147.4607
5uM	Control	17.9100	20.86773	1.000	-58.2340	94.0540
	10uM	6.0233	20.86773	1.000	-70.1207	82.1674
	20uM	15.8833	20.86773	1.000	-60.2607	92.0274
	50uM	33.0467	20.86773	1.000	-43.0974	109.1907
	100uM	89.2267*	20.86773	.016	13.0826	165.3707
10uM	Control	11.8867	20.86773	1.000	-64.2574	88.0307
	5uM	-6.0233	20.86773	1.000	-82.1674	70.1207
	20uM	9.8600	20.86773	1.000	-66.2840	86.0040
	50uM	27.0233	20.86773	1.000	-49.1207	103.1674
	100uM	83.2033 [*]	20.86773	.027	7.0593	159.3474
20uM	Control	2.0267	20.86773	1.000	-74.1174	78.1707
	5uM	-15.8833	20.86773	1.000	-92.0274	60.2607
	10uM	-9.8600	20.86773	1.000	-86.0040	66.2840
	50uM	17.1633	20.86773	1.000	-58.9807	93.3074
	100uM	73.3433	20.86773	.064	-2.8007	149.4874
50uM	Control	-15.1367	20.86773	1.000	-91.2807	61.0074
	5uM	-33.0467	20.86773	1.000	-109.1907	43.0974
	10uM	-27.0233	20.86773	1.000	-103.1674	49.1207
	20uM	-17.1633	20.86773	1.000	-93.3074	58.9807
	100uM	56.1800	20.86773	.294	-19.9640	132.3240
100uM	Control	-71.3167	20.86773	.077	-147.4607	4.8274
	5uM	-89.2267 [*]	20.86773	.016	-165.3707	-13.0826
	10uM	-83.2033 [*]	20.86773	.027	-159.3474	-7.0593
	20uM	-73.3433	20.86773	.064	-149.4874	2.8007
	50uM	-56.1800	20.86773	.294	-132.3240	19.9640

Based on observed means.

The error term is Mean Square(Error) = 653.193.

Bonferroni post-hoc tests for 48h cell viability of U251 doses 0, 5, 10, 20, 50, and $100\mu M$.

^{*.} The mean difference is significant at the .05 level.

Dependent Variable: Viability

Bonferroni

		Mean			95% Confide	ence Interval
(I) Concentration	(J) Concentration	Difference (I-J)	Std. Error	Sig.	Lower Bound	Upper Bound
Control	5uM	-20.0467	10.87359	1.000	-59.7232	19.6299
	10uM	-24.4800	10.87359	.658	-64.1565	15.1965
	20uM	-12.5633	10.87359	1.000	-52.2399	27.1132
	50uM	17.8333	10.87359	1.000	-21.8432	57.5099
	100uM	81.1767	10.87359	<.001	41.5001	120.8532
5uM	Control	20.0467	10.87359	1.000	-19.6299	59.7232
	10uM	-4.4333	10.87359	1.000	-44.1099	35.2432
	20uM	7.4833	10.87359	1.000	-32.1932	47.1599
	50uM	37.8800	10.87359	.068	-1.7965	77.5565
	100uM	101.2233	10.87359	<.001	61.5468	140.8999
10uM	Control	24.4800	10.87359	.658	-15.1965	64.1565
	5uM	4.4333	10.87359	1.000	-35.2432	44.1099
	20uM	11.9167	10.87359	1.000	-27.7599	51.5932
	50uM	42.3133	10.87359	.032	2.6368	81.9899
	100uM	105.6567	10.87359	<.001	65.9801	145.3332
20uM	Control	12.5633	10.87359	1.000	-27.1132	52.2399
	5uM	-7.4833	10.87359	1.000	-47.1599	32.1932
	10uM	-11.9167	10.87359	1.000	-51.5932	27.7599
	50uM	30.3967	10.87359	.243	-9.2799	70.0732
	100uM	93.7400	10.87359	<.001	54.0635	133.4165
50uM	Control	-17.8333	10.87359	1.000	-57.5099	21.8432
	5uM	-37.8800	10.87359	.068	-77.5565	1.7965
	10uM	-42.3133 [*]	10.87359	.032	-81.9899	-2.6368
	20uM	-30.3967	10.87359	.243	-70.0732	9.2799
	100uM	63.3433 [*]	10.87359	.001	23.6668	103.0199
100uM	Control	-81.1767 [*]	10.87359	<.001	-120.8532	-41.5001
	5uM	-101.2233 [*]	10.87359	<.001	-140.8999	-61.5468
	10uM	-105.6567 [*]	10.87359	<.001	-145.3332	-65.9801
	20uM	-93.7400 [*]	10.87359	<.001	-133.4165	-54.0635
	50uM	-63.3433 [*]	10.87359	.001	-103.0199	-23.6668

Based on observed means.

The error term is Mean Square(Error) = 177.353.

Bonferroni post-hoc tests for 72h cell viability of U251 doses 0, 5, 10, 20, 50, and $100\mu M$.

^{*.} The mean difference is significant at the .05 level.

Dependent Variable: Viability

Bonferroni

		Mean			95% Confide	ence Interval
(I) Time	(J) Time	Difference (I-J)	Std. Error	Sig.	Lower Bound	Upper Bound
Time, 24h	Time, 48h	13.0528	7.53672	.276	-5.8722	31.9778
	Time, 72h	11.7700	7.53672	.381	-7.1550	30.6950
Time, 48h	Time, 24h	-13.0528	7.53672	.276	-31.9778	5.8722
	Time, 72h	-1.2828	7.53672	1.000	-20.2078	17.6422
Time, 72h	Time, 24h	-11.7700	7.53672	.381	-30.6950	7.1550
	Time, 48h	1.2828	7.53672	1.000	-17.6422	20.2078

Based on observed means.

The error term is Mean Square(Error) = 511.219.

Bonferroni post-hoc tests for cell viability of T98G 24h, 48h, and 72h.

Dependent Variable: Viability

Bonferroni

Domenom						
		Mean			95% Confide	
(I) Concentration	(J) Concentration	Difference (I-J)	Std. Error	Sig.	Lower Bound	Upper Bound
Control	5uM	-24.0033	23.08579	1.000	-108.2408	60.2341
	10uM	-16.2500	23.08579	1.000	-100.4875	67.9875
	20uM	-8.7800	23.08579	1.000	-93.0175	75.4575
	50uM	21.1533	23.08579	1.000	-63.0841	105.3908
	100uM	85.9533 [*]	23.08579	.044	1.7159	170.1908
5uM	Control	24.0033	23.08579	1.000	-60.2341	108.2408
	10uM	7.7533	23.08579	1.000	-76.4841	91.9908
	20uM	15.2233	23.08579	1.000	-69.0141	99.4608
	50uM	45.1567	23.08579	1.000	-39.0808	129.3941
	100uM	109.9567	23.08579	.007	25.7192	194.1941
10uM	Control	16.2500	23.08579	1.000	-67.9875	100.4875
	5uM	-7.7533	23.08579	1.000	-91.9908	76.4841
	20uM	7.4700	23.08579	1.000	-76.7675	91.7075
	50uM	37.4033	23.08579	1.000	-46.8341	121.6408
	100uM	102.2033	23.08579	.012	17.9659	186.4408
20uM	Control	8.7800	23.08579	1.000	-75.4575	93.0175
	5uM	-15.2233	23.08579	1.000	-99.4608	69.0141
	10uM	-7.4700	23.08579	1.000	-91.7075	76.7675
	50uM	29.9333	23.08579	1.000	-54.3041	114.1708
	100uM	94.7333	23.08579	.022	10.4959	178.9708
50uM	Control	-21.1533	23.08579	1.000	-105.3908	63.0841
	5uM	-45.1567	23.08579	1.000	-129.3941	39.0808
	10uM	-37.4033	23.08579	1.000	-121.6408	46.8341
	20uM	-29.9333	23.08579	1.000	-114.1708	54.3041
	100uM	64.8000	23.08579	.238	-19.4375	149.0375
100uM	Control	-85.9533 [*]	23.08579	.044	-170.1908	-1.7159
	5uM	-109.9567 [*]	23.08579	.007	-194.1941	-25.7192
	10uM	-102.2033 [*]	23.08579	.012	-186.4408	-17.9659
	20uM	-94.7333 [*]	23.08579	.022	-178.9708	-10.4959
	50uM	-64.8000	23.08579	.238	-149.0375	19.4375

Based on observed means.

The error term is Mean Square(Error) = 799.430.

Bonferroni post-hoc tests for 24h cell viability of T98G doses 0, 5, 10, 20, 50, and $100\mu M$.

^{*.} The mean difference is significant at the .05 level.

Dependent Variable: Viability

Bonferroni

		Mean			95% Confide	ence Interval
(I) Concentration	(J) Concentration	Difference (I-J)	Std. Error	Sig.	Lower Bound	Upper Bound
Control	5uM	-6.4067	11.62817	1.000	-48.8366	36.0232
	10uM	-10.5700	11.62817	1.000	-52.9999	31.8599
	20uM	12.6467	11.62817	1.000	-29.7832	55.0766
	50uM	44.9533	11.62817	.034	2.5234	87.3832
	100uM	95.7667 [*]	11.62817	<.001	53.3368	138.1966
5uM	Control	6.4067	11.62817	1.000	-36.0232	48.8366
	10uM	-4.1633	11.62817	1.000	-46.5932	38.2666
	20uM	19.0533	11.62817	1.000	-23.3766	61.4832
	50uM	51.3600	11.62817	.013	8.9301	93.7899
	100uM	102.1733 [*]	11.62817	<.001	59.7434	144.6032
10uM	Control	10.5700	11.62817	1.000	-31.8599	52.9999
	5uM	4.1633	11.62817	1.000	-38.2666	46.5932
	20uM	23.2167	11.62817	1.000	-19.2132	65.6466
	50uM	55.5233 [*]	11.62817	.007	13.0934	97.9532
	100uM	106.3367 [*]	11.62817	<.001	63.9068	148.7666
20uM	Control	-12.6467	11.62817	1.000	-55.0766	29.7832
	5uM	-19.0533	11.62817	1.000	-61.4832	23.3766
	10uM	-23.2167	11.62817	1.000	-65.6466	19.2132
	50uM	32.3067	11.62817	.251	-10.1232	74.7366
	100uM	83.1200	11.62817	<.001	40.6901	125.5499
50uM	Control	-44.9533 [*]	11.62817	.034	-87.3832	-2.5234
	5uM	-51.3600 [*]	11.62817	.013	-93.7899	-8.9301
	10uM	-55.5233 [*]	11.62817	.007	-97.9532	-13.0934
	20uM	-32.3067	11.62817	.251	-74.7366	10.1232
	100uM	50.8133 [*]	11.62817	.014	8.3834	93.2432
100uM	Control	-95.7667 [*]	11.62817	<.001	-138.1966	-53.3368
	5uM	-102.1733 [*]	11.62817	<.001	-144.6032	-59.7434
	10uM	-106.3367 [*]	11.62817	<.001	-148.7666	-63.9068
	20uM	-83.1200 [*]	11.62817	<.001	-125.5499	-40.6901
	50uM	-50.8133 [*]	11.62817	.014	-93.2432	-8.3834

Based on observed means.

The error term is Mean Square(Error) = 202.821.

Bonferroni post-hoc tests for 48h cell viability of T98G doses 0, 5, 10, 20, 50, and $100\mu M$.

^{*.} The mean difference is significant at the .05 level.

Dependent Variable: Viability

Bonferroni

		Mean			95% Confide	ence Interval
(I) Concentration	(J) Concentration	Difference (I-J)	Std. Error	Sig.	Lower Bound	Upper Bound
Control	5uM	-21.7233	18.82207	1.000	-90.4030	46.9563
	10uM	-19.7533	18.82207	1.000	-88.4330	48.9263
	20uM	15.7233	18.82207	1.000	-52.9563	84.4030
	50uM	57.9467	18.82207	.143	-10.7330	126.6263
	100uM	96.5000	18.82207	.004	27.8203	165.1797
5uM	Control	21.7233	18.82207	1.000	-46.9563	90.4030
	10uM	1.9700	18.82207	1.000	-66.7097	70.6497
	20uM	37.4467	18.82207	1.000	-31.2330	106.1263
	50uM	79.6700	18.82207	.017	10.9903	148.3497
	100uM	118.2233*	18.82207	<.001	49.5437	186.9030
10uM	Control	19.7533	18.82207	1.000	-48.9263	88.4330
	5uM	-1.9700	18.82207	1.000	-70.6497	66.7097
	20uM	35.4767	18.82207	1.000	-33.2030	104.1563
	50uM	77.7000*	18.82207	.021	9.0203	146.3797
	100uM	116.2533 [*]	18.82207	<.001	47.5737	184.9330
20uM	Control	-15.7233	18.82207	1.000	-84.4030	52.9563
	5uM	-37.4467	18.82207	1.000	-106.1263	31.2330
	10uM	-35.4767	18.82207	1.000	-104.1563	33.2030
	50uM	42.2233	18.82207	.668	-26.4563	110.9030
	100uM	80.7767	18.82207	.016	12.0970	149.4563
50uM	Control	-57.9467	18.82207	.143	-126.6263	10.7330
	5uM	-79.6700 [*]	18.82207	.017	-148.3497	-10.9903
	10uM	-77.7000 [*]	18.82207	.021	-146.3797	-9.0203
	20uM	-42.2233	18.82207	.668	-110.9030	26.4563
	100uM	38.5533	18.82207	.946	-30.1263	107.2330
100uM	Control	-96.5000 [*]	18.82207	.004	-165.1797	-27.8203
	5uM	-118.2233 [*]	18.82207	<.001	-186.9030	-49.5437
	10uM	-116.2533 [*]	18.82207	<.001	-184.9330	-47.5737
	20uM	-80.7767 [*]	18.82207	.016	-149.4563	-12.0970
	50uM	-38.5533	18.82207	.946	-107.2330	30.1263

Based on observed means.

The error term is Mean Square(Error) = 531.406.

Bonferroni post-hoc tests for 72h cell viability of T98G doses 0, 5, 10, 20, 50, and $100\mu M$.

^{*.} The mean difference is significant at the .05 level.

Dependent Variable: Viability

Bonferroni

		Mean			95% Confide	ence Interval
(I) Time	(J) Time	Difference (I-J)	Std. Error	Sig.	Lower Bound	Upper Bound
Time, 24h	Time, 48h	-6.5056	4.32453	.424	-17.3646	4.3535
	Time, 72h	8.1983	4.32453	.198	-2.6607	19.0574
Time, 48h	Time, 24h	6.5056	4.32453	.424	-4.3535	17.3646
	Time, 72h	14.7039	4.32453	.005	3.8448	25.5630
Time, 72h	Time, 24h	-8.1983	4.32453	.198	-19.0574	2.6607
	Time, 48h	-14.7039 [*]	4.32453	.005	-25.5630	-3.8448

Based on observed means.

The error term is Mean Square(Error) = 168.314.

Bonferroni post-hoc tests for cell viability of U87 24h, 48h, 72h.

^{*.} The mean difference is significant at the .05 level.

Dependent Variable: Viability

Bonferroni

		Mean			95% Confide	ence Interval
(I) Concentration	(J) Concentration	Difference (I-J)	Std. Error	Sig.	Lower Bound	Upper Bound
Control	5uM	-8.2933	14.53256	1.000	-61.3210	44.7344
	10uM	-8.3900	14.53256	1.000	-61.4177	44.6377
	20uM	6867	14.53256	1.000	-53.7144	52.3410
	50uM	15.7133	14.53256	1.000	-37.3144	68.7410
	100uM	54.8300 [*]	14.53256	.040	1.8023	107.8577
5uM	Control	8.2933	14.53256	1.000	-44.7344	61.3210
	10uM	0967	14.53256	1.000	-53.1244	52.9310
	20uM	7.6067	14.53256	1.000	-45.4210	60.6344
	50uM	24.0067	14.53256	1.000	-29.0210	77.0344
	100uM	63.1233 [*]	14.53256	.014	10.0956	116.1510
10uM	Control	8.3900	14.53256	1.000	-44.6377	61.4177
	5uM	.0967	14.53256	1.000	-52.9310	53.1244
	20uM	7.7033	14.53256	1.000	-45.3244	60.7310
	50uM	24.1033	14.53256	1.000	-28.9244	77.1310
	100uM	63.2200 [*]	14.53256	.014	10.1923	116.2477
20uM	Control	.6867	14.53256	1.000	-52.3410	53.7144
	5uM	-7.6067	14.53256	1.000	-60.6344	45.4210
	10uM	-7.7033	14.53256	1.000	-60.7310	45.3244
	50uM	16.4000	14.53256	1.000	-36.6277	69.4277
	100uM	55.5167 [*]	14.53256	.037	2.4890	108.5444
50uM	Control	-15.7133	14.53256	1.000	-68.7410	37.3144
	5uM	-24.0067	14.53256	1.000	-77.0344	29.0210
	10uM	-24.1033	14.53256	1.000	-77.1310	28.9244
	20uM	-16.4000	14.53256	1.000	-69.4277	36.6277
	100uM	39.1167	14.53256	.294	-13.9110	92.1444
100uM	Control	-54.8300 [*]	14.53256	.040	-107.8577	-1.8023
	5uM	-63.1233 [*]	14.53256	.014	-116.1510	-10.0956
	10uM	-63.2200 [*]	14.53256	.014	-116.2477	-10.1923
	20uM	-55.5167 [*]	14.53256	.037	-108.5444	-2.4890
	50uM	-39.1167	14.53256	.294	-92.1444	13.9110

Based on observed means.

The error term is Mean Square(Error) = 316.793.

Bonferroni post-hoc tests for 24h cell viability of U87 doses 0, 5, 10, 20, 50, and $100\mu M$.

^{*.} The mean difference is significant at the .05 level.

Dependent Variable: Viability

Bonferroni

		Mean			95% Confide	ence Interval
(I) Concentration	(J) Concentration	Difference (I-J)	Std. Error	Sig.	Lower Bound	Upper Bound
Control	5uM	-21.8400	10.23149	.812	-59.1736	15.4936
	10uM	-23.3100	10.23149	.627	-60.6436	14.0236
	20uM	-12.4567	10.23149	1.000	-49.7902	24.8769
	50uM	3.7300	10.23149	1.000	-33.6036	41.0636
	100uM	68.0167 [*]	10.23149	<.001	30.6831	105.3502
5uM	Control	21.8400	10.23149	.812	-15.4936	59.1736
	10uM	-1.4700	10.23149	1.000	-38.8036	35.8636
	20uM	9.3833	10.23149	1.000	-27.9502	46.7169
	50uM	25.5700	10.23149	.419	-11.7636	62.9036
	100uM	89.8567	10.23149	<.001	52.5231	127.1902
10uM	Control	23.3100	10.23149	.627	-14.0236	60.6436
	5uM	1.4700	10.23149	1.000	-35.8636	38.8036
	20uM	10.8533	10.23149	1.000	-26.4802	48.1869
	50uM	27.0400	10.23149	.322	-10.2936	64.3736
	100uM	91.3267	10.23149	<.001	53.9931	128.6602
20uM	Control	12.4567	10.23149	1.000	-24.8769	49.7902
	5uM	-9.3833	10.23149	1.000	-46.7169	27.9502
	10uM	-10.8533	10.23149	1.000	-48.1869	26.4802
	50uM	16.1867	10.23149	1.000	-21.1469	53.5202
	100uM	80.4733	10.23149	<.001	43.1398	117.8069
50uM	Control	-3.7300	10.23149	1.000	-41.0636	33.6036
	5uM	-25.5700	10.23149	.419	-62.9036	11.7636
	10uM	-27.0400	10.23149	.322	-64.3736	10.2936
	20uM	-16.1867	10.23149	1.000	-53.5202	21.1469
	100uM	64.2867 [*]	10.23149	<.001	26.9531	101.6202
100uM	Control	-68.0167 [*]	10.23149	<.001	-105.3502	-30.6831
	5uM	-89.8567 [*]	10.23149	<.001	-127.1902	-52.5231
	10uM	-91.3267 [*]	10.23149	<.001	-128.6602	-53.9931
	20uM	-80.4733 [*]	10.23149	<.001	-117.8069	-43.1398
	50uM	-64.2867 [*]	10.23149	<.001	-101.6202	-26.9531

Based on observed means.

The error term is Mean Square(Error) = 157.025.

Bonferroni post-hoc tests for 48h cell viability of U251 doses 0, 5, 10, 20, 50, and $100\mu M$.

^{*.} The mean difference is significant at the .05 level.

Dependent Variable: Viability

Bonferroni

		Mean			95% Confide	ence Interval
(I) Concentration	(J) Concentration	Difference (I-J)	Std. Error	Sig.	Lower Bound	Upper Bound
Control	5uM	-3.5600	4.55517	1.000	-20.1813	13.0613
	10uM	-5.5533	4.55517	1.000	-22.1746	11.0680
	20uM	4.9400	4.55517	1.000	-11.6813	21.5613
	50uM	22.6100	4.55517	.005	5.9887	39.2313
	100uM	83.9267*	4.55517	<.001	67.3054	100.5480
5uM	Control	3.5600	4.55517	1.000	-13.0613	20.1813
	10uM	-1.9933	4.55517	1.000	-18.6146	14.6280
	20uM	8.5000	4.55517	1.000	-8.1213	25.1213
	50uM	26.1700 [*]	4.55517	.001	9.5487	42.7913
	100uM	87.4867 [*]	4.55517	<.001	70.8654	104.1080
10uM	Control	5.5533	4.55517	1.000	-11.0680	22.1746
	5uM	1.9933	4.55517	1.000	-14.6280	18.6146
	20uM	10.4933	4.55517	.599	-6.1280	27.1146
	50uM	28.1633	4.55517	<.001	11.5420	44.7846
	100uM	89.4800 [*]	4.55517	<.001	72.8587	106.1013
20uM	Control	-4.9400	4.55517	1.000	-21.5613	11.6813
	5uM	-8.5000	4.55517	1.000	-25.1213	8.1213
	10uM	-10.4933	4.55517	.599	-27.1146	6.1280
	50uM	17.6700	4.55517	.033	1.0487	34.2913
	100uM	78.9867	4.55517	<.001	62.3654	95.6080
50uM	Control	-22.6100 [*]	4.55517	.005	-39.2313	-5.9887
	5uM	-26.1700 [*]	4.55517	.001	-42.7913	-9.5487
	10uM	-28.1633 [*]	4.55517	<.001	-44.7846	-11.5420
	20uM	-17.6700 [*]	4.55517	.033	-34.2913	-1.0487
	100uM	61.3167*	4.55517	<.001	44.6954	77.9380
100uM	Control	-83.9267 [*]	4.55517	<.001	-100.5480	-67.3054
	5uM	-87.4867 [*]	4.55517	<.001	-104.1080	-70.8654
	10uM	-89.4800 [*]	4.55517	<.001	-106.1013	-72.8587
	20uM	-78.9867 [*]	4.55517	<.001	-95.6080	-62.3654
	50uM	-61.3167 [*]	4.55517	<.001	-77.9380	-44.6954

Based on observed means.

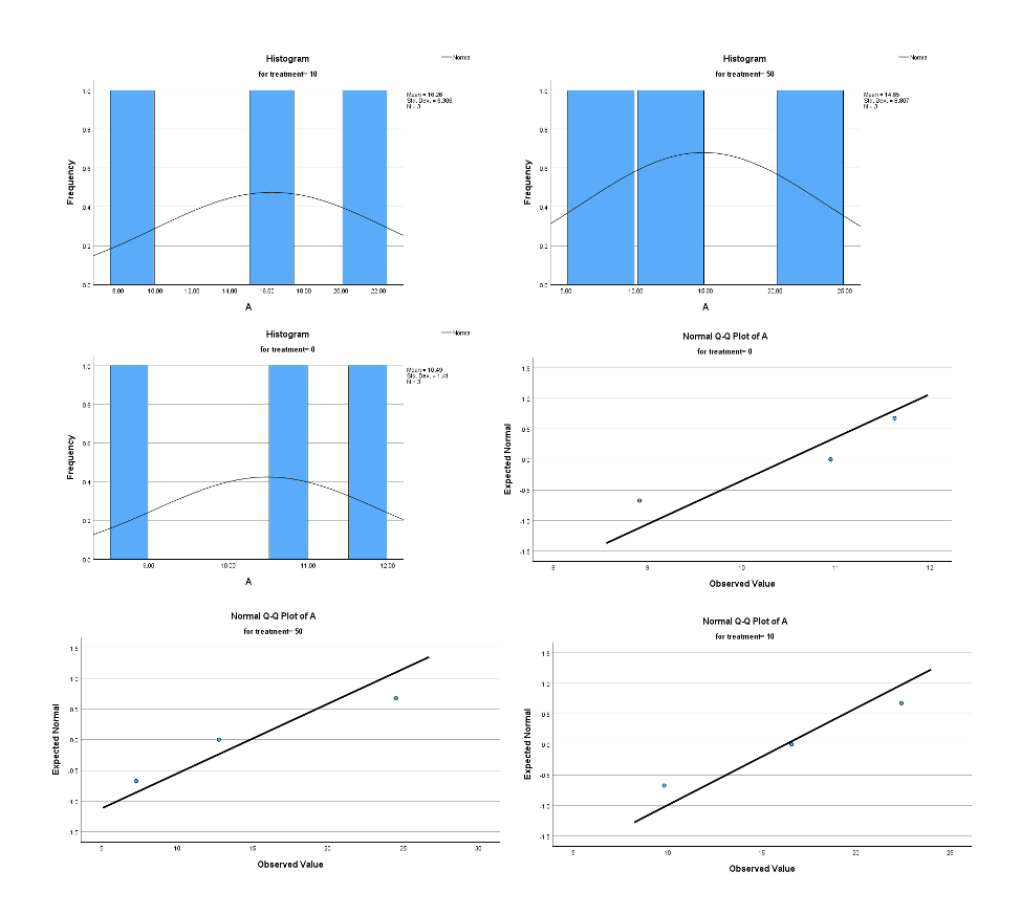
The error term is Mean Square(Error) = 31.124.

Bonferroni post-hoc tests for 72h cell viability of U251 doses 0, 5, 10, 20, 50, and $100\mu M$.

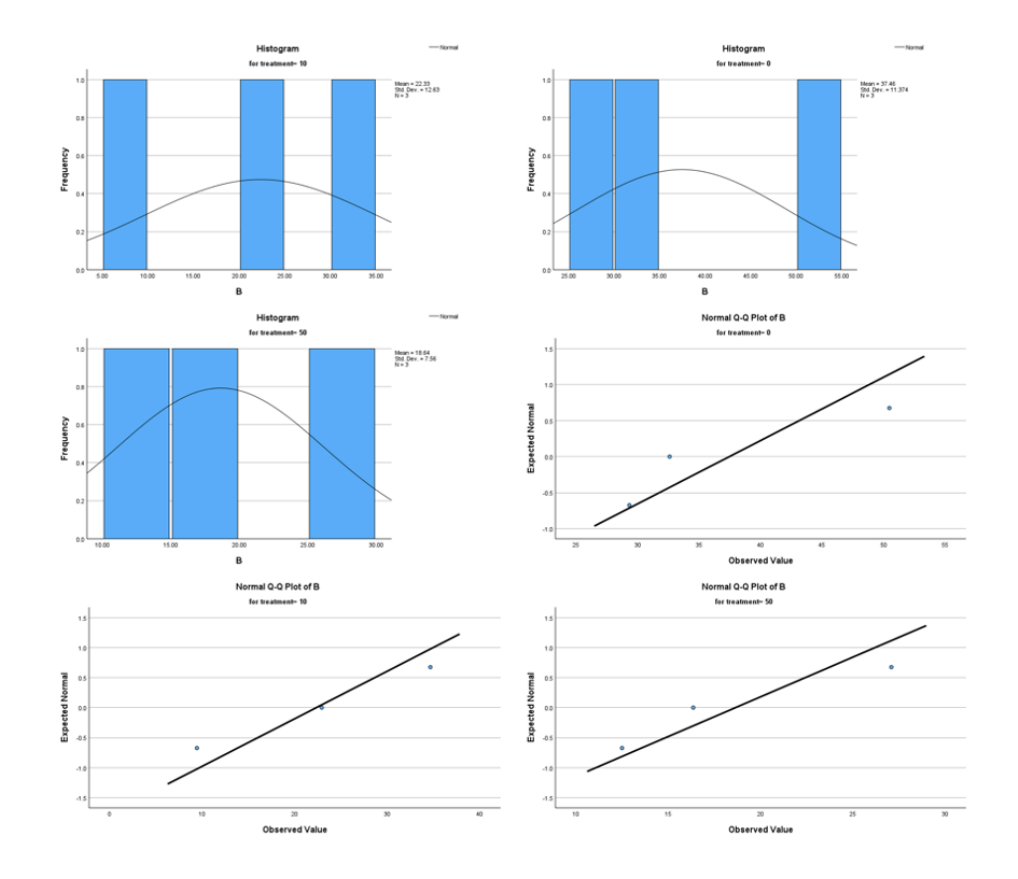
^{*.} The mean difference is significant at the .05 level.

Appendix 6

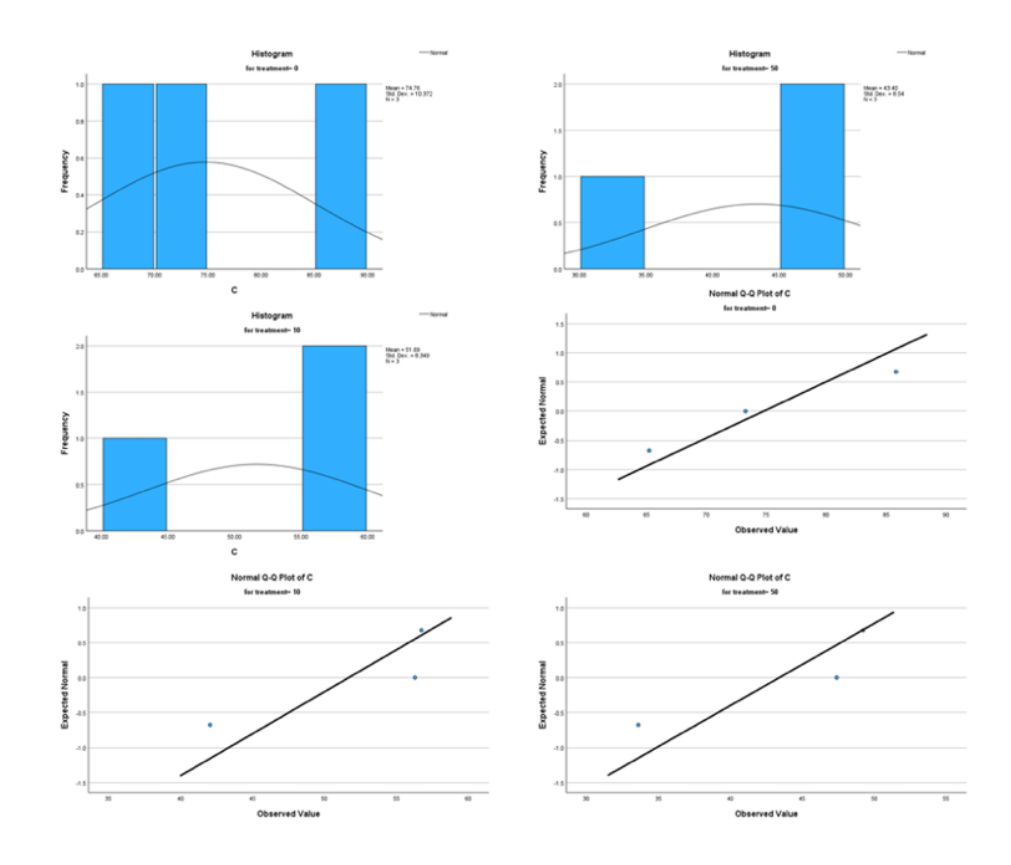
Statistical analysis for wound healing assay results of T98G.



Tests of normality histograms and Q-Q plots for wound healing assay results of T98G 4h.



Tests of normality histograms and Q-Q plots for wound healing assay results of T98G 8h.



Tests of normality histograms and Q-Q plots for wound healing assay results of T98G 24h.

Tests of Normality

		Kolmogorov-Smirnov ^a			Shapiro-Wilk		
	treatment	Statistic	df	Sig.	Statistic	df	Sig.
Α	0	.292	3		.924	3	.465
	10	.186	3		.998	3	.918
	50	.260	3		.958	3	.605
В	0	.332	3		.863	3	.276
	10	.185	3		.998	3	.923
	50	.286	3		.931	3	.493
С	0	.224	3		.984	3	.760
	10	.376	3		.773	3	.051
	50	.346	3		.837	3	.207

a. Lilliefors Significance Correction

Shapiro-Wilk test for wound healing assay results of T98G. 4h (A), 8h (B), 24h (C).

ANOVA

		Sum of Squares	df	Mean Square	F	Sig.
Α	Between Groups	54.223	2	27.112	.682	.541
	Within Groups	238.643	6	39.774		
	Total	292.866	8			
В	Between Groups	596.875	2	298.438	2.587	.155
	Within Groups	692.062	6	115.344		
	Total	1288.937	8			
С	Between Groups	1584.233	2	792.116	9.498	.014
	Within Groups	500.412	6	83.402		
	Total	2084.645	8			

One-way ANOVA for wound healing assay results of T98G.

Tests of Homogeneity of Variances

		Levene Statistic	df1	df2	Sig.
А	Based on Mean	2.400	2	6	.171
	Based on Median	1.122	2	6	.385
	Based on Median and with adjusted df	1.122	2	3.500	.420
	Based on trimmed mean	2.303	2	6	.181
В	Based on Mean	.364	2	6	.709
	Based on Median	.166	2	6	.851
	Based on Median and with adjusted df	.166	2	5.057	.852
	Based on trimmed mean	.346	2	6	.721
С	Based on Mean	.055	2	6	.947
	Based on Median	.062	2	6	.940
	Based on Median and with adjusted df	.062	2	5.787	.940
	Based on trimmed mean	.056	2	6	.946

Levene's F-test for wound healing assay results of T98G.

Multiple Comparisons

Dependent Variable: Migration

Bonferroni

		Mean			95% Confidence Interval	
(I) Concentration	(J) Concentration	Difference (I-J)	Std. Error	Sig.	Lower Bound	Upper Bound
Control	10uM	23.0733	7.45663	.064	-1.4400	47.5867
	50uM	31.3567*	7.45663	.017	6.8433	55.8700
10uM	Control	-23.0733	7.45663	.064	-47.5867	1.4400
	50uM	8.2833	7.45663	.927	-16.2300	32.7967
50uM	Control	-31.3567 [*]	7.45663	.017	-55.8700	-6.8433
	10uM	-8.2833	7.45663	.927	-32.7967	16.2300

Based on observed means.

The error term is Mean Square(Error) = 83.402.

Bonferroni post-hoc for wound healing assay results of T98G concentrations.

^{*.} The mean difference is significant at the .05 level.

Dependent Variable: Migration

Bonferroni

	Mean				95% Confidence Interval	
(I) Time	(J) Time	Difference (I-J)	Std. Error	Sig.	Lower Bound	Upper Bound
Time, 4h	Time, 8h	-12.2811 [*]	4.20334	.027	-23.3743	-1.1879
	Time, 24h	-42.7522 [*]	4.20334	<.001	-53.8455	-31.6590
Time, 8h	Time, 4h	12.2811*	4.20334	.027	1.1879	23.3743
	Time, 24h	-30.4711 [*]	4.20334	<.001	-41.5643	-19.3779
Time, 24h	Time, 4h	42.7522 [*]	4.20334	<.001	31.6590	53.8455
	Time, 8h	30.4711*	4.20334	<.001	19.3779	41.5643

Based on observed means.

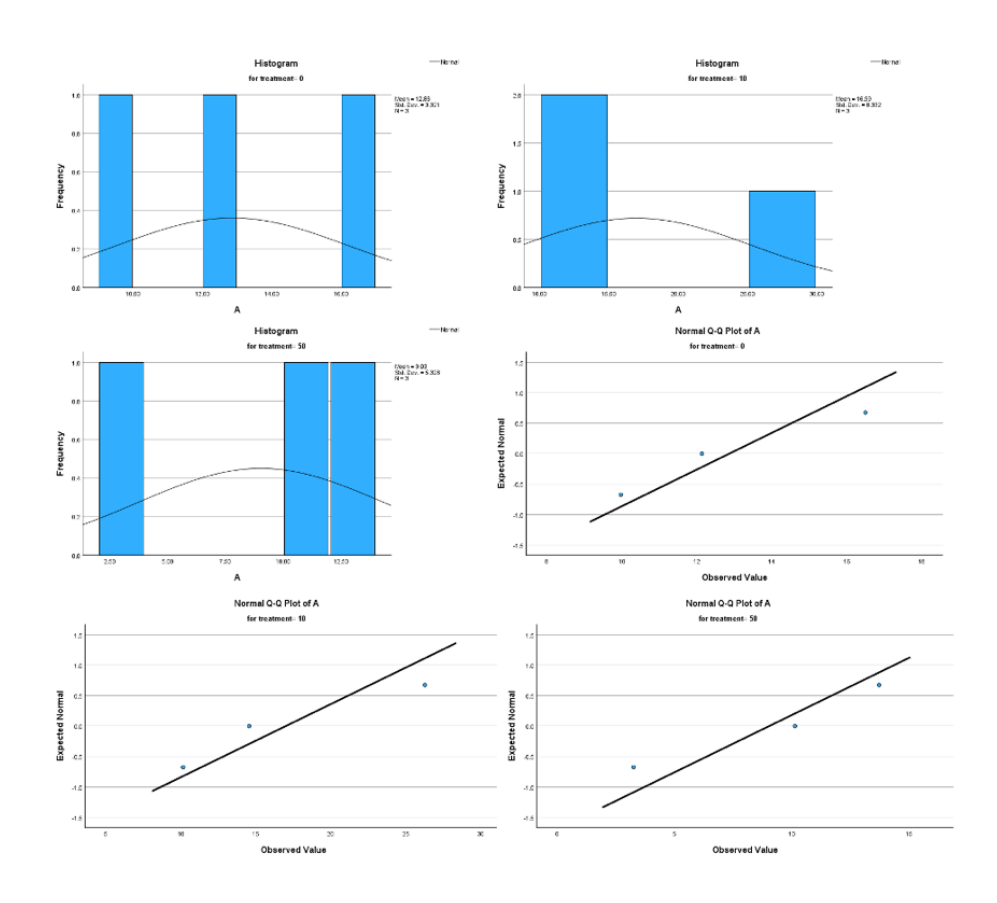
The error term is Mean Square(Error) = 79.506.

Bonferroni post-hoc for wound healing assay results of T98G timepoints.

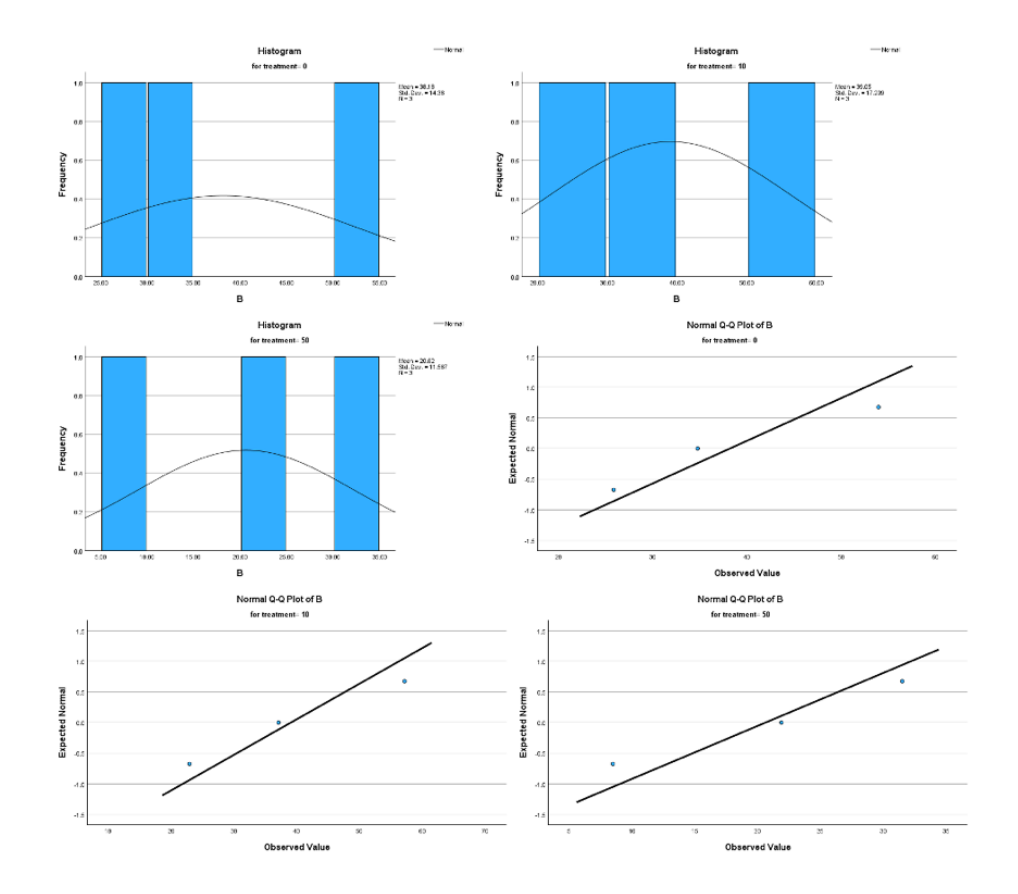
^{*.} The mean difference is significant at the .05 level.

Appendix 7

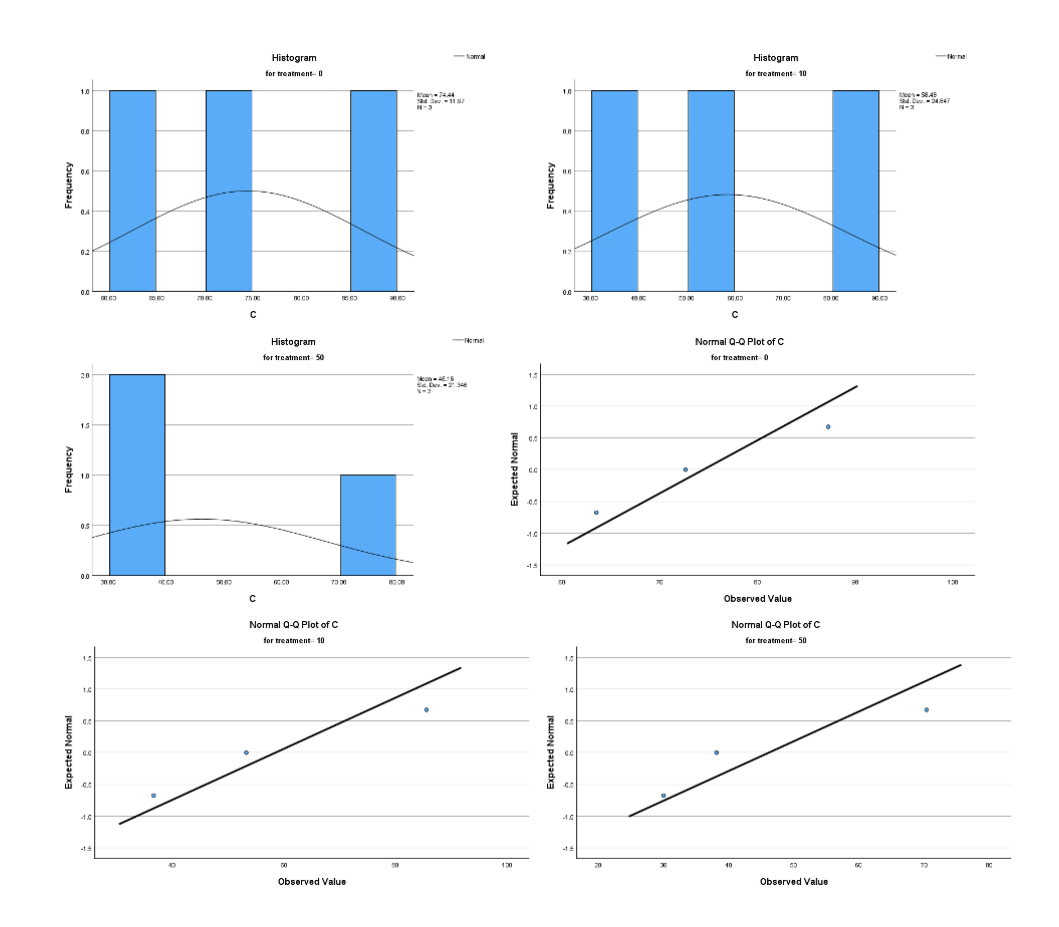
Statistical analysis for wound healing assay results of U251.



Tests of normality histograms and Q-Q plots for wound healing assay results of U251 4h.



Tests of normality histograms and Q-Q plots for wound healing assay results of U251 8h.



Tests of normality histograms and Q-Q plots for wound healing assay results of U251 24h.

Tests of Normality

		Kolmogorov-Smirnov ^a			Shapiro-Wilk			
	treatment	Statistic	df	Sig.	Statistic	df	Sig.	
Α	0	.254	3		.963	3	.633	
	10	.282	3		.936	3	.510	
	50	.248	3		.968	3	.657	
В	0	.261	3		.957	3	.602	
	10	.212	3		.990	3	.811	
	50	.210	3		.991	3	.819	
С	0	.227	3		.982	3	.746	
	10	.250	3		.967	3	.650	
	50	.313	3		.894	3	.366	

a. Lilliefors Significance Correction

Shapiro-Wilk test for wound healing assay results of U251. 4h (A), 8h (B), 24h (C).

ANOVA

		-				
		Sum of Squares	df	Mean Square	F	Sig.
Α	Between Groups	95.085	2	47.543	1.311	.337
	Within Groups	217.650	6	36.275		
	Total	312.735	8			
В	Between Groups	649.033	2	324.516	1.530	.290
	Within Groups	1272.316	6	212.053		
	Total	1921.349	8			
С	Between Groups	1205.967	2	602.984	1.487	.299
	Within Groups	2432.578	6	405.430		
	Total	3638.545	8			

One-way ANOVA for wound healing assay results of U251.

Dependent Variable: Migration

Bonferroni

		Mean			95% Confide	ence Interval
(I) Time	(J) Time	Difference (I-J)	Std. Error	Sig.	Lower Bound	Upper Bound
Time, 4h	Time, 8h	-18.6511 [*]	7.06127	.050	-37.2868	0154
	Time, 24h	-46.7344*	7.06127	<.001	-65.3702	-28.0987
Time, 8h	Time, 4h	18.6511 [*]	7.06127	.050	.0154	37.2868
	Time, 24h	-28.0833 [*]	7.06127	.003	-46.7191	-9.4476
Time, 24h	Time, 4h	46.7344*	7.06127	<.001	28.0987	65.3702
	Time, 8h	28.0833 [*]	7.06127	.003	9.4476	46.7191

Based on observed means.

The error term is Mean Square(Error) = 224.377.

Bonferroni post-hoc for wound healing assay results of U251 timepoints.

^{*.} The mean difference is significant at the .05 level.

Appendix 8

Statistical analysis for cell viability of combination treatment.

Multiple Comparisons

Dependent Variable: Viability

Bonferroni

		Mean			95% Confidence Interval	
(I) Time	(J) Time	Difference (I-J)	Std. Error	Sig.	Lower Bound	Upper Bound
Time, 24h	Time, 48h	6.8456	5.91175	.756	-7.7615	21.4526
	Time, 72h	16.9863 [*]	5.91175	.017	2.3793	31.5933
Time, 48h	Time, 24h	-6.8456	5.91175	.756	-21.4526	7.7615
	Time, 72h	10.1407	5.91175	.276	-4.4663	24.7478
Time, 72h	Time, 24h	-16.9863 [*]	5.91175	.017	-31.5933	-2.3793
	Time, 48h	-10.1407	5.91175	.276	-24.7478	4.4663

Based on observed means.

The error term is Mean Square(Error) = 471.809.

Post-hoc for combination treatment of SVG different timepoints.

Multiple Comparisons

Dependent Variable: Viability

Bonferroni

		Mean			95% Confidence Interval		
(I) Time	(J) Time	Difference (I-J)	Std. Error	Sig.	Lower Bound	Upper Bound	
Time, 24h	Time, 48h	24.7026 [*]	4.69331	<.001	13.1061	36.2990	
	Time, 72h	35.8263 [*]	4.69331	<.001	24.2299	47.4227	
Time, 48h	Time, 24h	-24.7026 [*]	4.69331	<.001	-36.2990	-13.1061	
	Time, 72h	11.1237	4.69331	.064	4727	22.7201	
Time, 72h	Time, 24h	-35.8263 [*]	4.69331	<.001	-47.4227	-24.2299	
	Time, 48h	-11.1237	4.69331	.064	-22.7201	.4727	

Based on observed means.

The error term is Mean Square(Error) = 297.366.

Post-hoc for combination treatment of U251 timepoints.

^{*.} The mean difference is significant at the .05 level.

^{*.} The mean difference is significant at the .05 level.

		Mean			95% Confiden	
I) Concentration	(J) Concentration	Difference (I-J)	Std. Error	Sig.	Lower Bound U	
Control	20uM CP-91149	-8.4467	10.42389	1.000	-47.7888	30.895
	50uM CP-91149	18.5800	10.42389	1.000	-20.7622	57.922
	50uM TMZ	45.4000°	10.42389	.014	6.0578	84.742
	100uM TMZ	33.6267	10.42389	.169	-5.7155	72.968
	20uM CP-91149 + 50uM TMZ	35.5500	10.42389	.112	-3.7922	74.892
	20uM CP-91149 + 100uM TMZ	32.1833	10.42389	.229	-7.1588	71.525
	50uM CP-91149 + 50uM TMZ	32.8100	10.42389	.200	-6.5322	72.152
	50uM CP-91149 + 100uM TMZ	44.3033	10.42389	.017	4.9612	83.645
20uM CP-91149	Control	8.4467	10.42389	1.000	-30.8955	47.788
	50uM CP-91149	27.0267	10.42389	.662	-12.3155	66.368
	50uM TMZ	53.8467	10.42389	.002	14.5045	93.18
	100uM TMZ	42.0733	10.42389	.028	2.7312	81.415
	20uM CP-91149 + 50uM TMZ	43.9967	10.42389	.019	4.6545	83.331
	20uM CP-91149 + 100uM TMZ	40.6300	10.42389	.038	1.2878	79.97
	50uM CP-91149 + 50uM	41.2567	10.42389	.033	1.9145	80.59
	50uM CP-91149 + 100uM	52.7500°	10.42389	.003	13.4078	92.09
50uM CP-91149	TMZ Control	-18.5800	10.42389	1.000	-57.9222	20.76
700m 01-91149	20uM CP-91149	-27.0267	10.42389	.662	-66.3688	12.31
	50uM TMZ	26.8200	10.42389	.690	-12.5222	66.16
	100uM TMZ	15.0467	10.42389	1.000	-24.2955	54.38
	20uM CP-91149 + 50uM	16.9700	10.42389	1.000	-22.3722	56.31
	TMZ					
	20uM CP-91149 + 100uM TMZ	13.6033	10.42389	1.000	-25.7388	52.94
	50uM CP-91149 + 50uM TMZ	14.2300	10.42389	1.000	-25.1122	53.57
	50uM CP-91149 + 100uM TMZ	25.7233	10.42389	.859	-13.6188	65.06
50uM TMZ	Control	-45.4000°	10.42389	.014	-84.7422	-6.05
	20uM CP-91149	-53.8467	10.42389	.002	-93.1888	-14.50
	50uM CP-91149	-26.8200	10.42389	.690	-66.1622	12.52
	100uM TMZ	-11,7733	10.42389	1.000	-51.1155	27.56
	20uM CP-91149 + 50uM TMZ	-9.8500	10.42389	1.000	-49.1922	29.49
	20uM CP-91149 + 100uM TMZ	-13.2167	10.42389	1.000	-52.5588	26.12
	50uM CP-91149 + 50uM	-12.5900	10.42389	1.000	-51.9322	26.75
	TMZ 50uM CP-91149 + 100uM	-1.0967	10.42389	1.000	-40.4388	38.24
100uM TMZ	TMZ Control	-33.6267	10.42389	.169	-72.9688	5.71
	20uM CP-91149	-42.0733	10.42389	.028	-81.4155	-2.73
	50uM CP-91149	-15.0467	10.42389	1.000	-54.3888	24.29
	50uM TMZ	11.7733	10.42389	1.000	-27.5688	51.11
	20uM CP-91149 + 50uM TMZ	1.9233	10.42389	1.000	-37.4188	41.26
	20uM CP-91149 + 100uM TMZ	-1.4433	10.42389	1.000	-40.7855	37.89
	50uM CP-91149 + 50uM TMZ	8167	10.42389	1.000	-40.1588	38.52
	50uM CP-91149 + 100uM TMZ	10.6767	10.42389	1.000	-28.6655	50.01
20uM CP-91149 + 50uM	Control	-35.5500	10.42389	.112	-74.8922	3.79
MZ	20uM CP-91149	-43.9967°	10.42389	.019	-83.3388	-4.65
	50uM CP-91149	-16.9700	10.42389	1.000	-56.3122	22.37
	50uM TMZ	9.8500	10.42389	1.000	-29.4922	49.19
	100uM TMZ	-1.9233	10.42389	1.000	-41.2655	37.41
	20uM CP-91149 + 100uM TMZ	-3.3667	10.42389	1.000	-42.7088	35.97
	50uM CP-91149 + 50uM TMZ	-2.7400	10.42389	1.000	-42.0822	36.60
	50uM CP-91149 + 100uM	8.7533	10.42389	1.000	-30.5888	48.09
20uM CP-91149 + 100uM	TMZ Control	-32.1833	10.42389	.229	-71.5255	7.15
MZ	20uM CP-91149	-40.6300°	10.42389	.038	-79.9722	-1.28
	50uM CP-91149	-13.6033	10.42389	1.000	-52.9455	25.73
	50uM TMZ	13.2167	10.42389	1.000	-26.1255	52.55
	100uM TMZ	1.4433	10.42389	1.000	-37.8988	40.78
	20uM CP-91149 + 50uM TMZ	3.3667	10.42389	1.000	-35.9755	42.70
	50uM CP-91149 + 50uM	.6267	10.42389	1.000	-38.7155	39.96
	TMZ 50uM CP-91149 + 100uM	12.1200	10.42389	1.000	-27.2222	51.46
50uM CP-91149 + 50uM	TMZ Control	-32.8100	10.42389	.200	-72.1522	6.53
MZ	20uM CP-91149	·41.2567	10.42389	.033	-80.5988	-1.91
	50uM CP-91149		10.42389	1.000	-53.5722	25.11
	50uM TMZ		10.42389	1.000	-26.7522	51.93
	100uM TMZ				-38.5255	40.15
	20uM CP-91149 + 50uM		10.42389	1.000	-36.6022	42.08
	20uM CP-91149 + 100uM		10.42389	1.000	-39.9688	38.71
	TMZ 50uM CP-91149 + 100uM		10.42389	1.000	-27.8488	50.83
50uM CP-91149 + 100uM	TMZ Control	-44.3033°	10.42389	.017	-83.6455	-4.96
TMZ	20uM CP-91149	-52.7500		.003	-92.0922	-13.40
	50uM CP-91149			.859	-92.0922 -65.0655	13.40
	50uM CP-91149 50uM TMZ		10.42389			
	100uM TMZ	1.0967 -10.6767	10.42389	1.000	-38.2455	40.43
		-10.6767	10.42389	1.000	-50.0188	28.66
	20uM CP-91149 + 50uM	-8.7533	10.42389	1.000	-48.0955	30.58
		-8.7533	10.42389	1.000	-48.0955 -51.4622	27.22

*. The mean difference is significant at the .ub level

Post-hoc for combination treatment of U251 72h treatment.

Dependent Variable: Viability

Bonferroni

		Mean			95% Confide	ence Interval
(I) Time	(J) Time	Difference (I-J)	Std. Error	Sig.	Lower Bound	Upper Bound
Time, 24h	Time, 48h	17.8230 [*]	5.13446	.003	5.1365	30.5094
	Time, 72h	3.5267	5.13446	1.000	-9.1598	16.2131
Time, 48h	Time, 24h	-17.8230 [*]	5.13446	.003	-30.5094	-5.1365
	Time, 72h	-14.2963 [*]	5.13446	.022	-26.9828	-1.6098
Time, 72h	Time, 24h	-3.5267	5.13446	1.000	-16.2131	9.1598
	Time, 48h	14.2963	5.13446	.022	1.6098	26.9828

Based on observed means.

The error term is Mean Square(Error) = 355.896.

Post-hoc for combination treatment of T98G.

^{*.} The mean difference is significant at the .05 level.

Multiple	Comparisons

		Mean			95% Confiden	ce Interval
I) Concentration	(J) Concentration	Difference (I-J)	Std. Error	Sig.	Lower Bound U	Jpper Boun
Control	20uM CP-91149	12.7600	10.84544	1.000	-28.1732	53.693
	50uM CP-91149	43.9100	10.84544	.027	2.9768	84.843
	50uM TMZ	12.8933	10.84544	1.000	-28.0399	53.826
	100uM TMZ 20uM CP-91149 + 50uM	2.7800 13.6767	10.84544	1.000	-38.1532 -27.2566	43.713 54.609
	TMZ 20uM CP-91149 + 100uM	3.0467	10.84544	1.000	-27.2566	43.979
	TMZ 50uM CP-91149 + 50uM	36.6000	10.84544	.122	-4.3332	77.533
	TMZ 50uM CP-91149 + 100uM	34.8167	10.84544	.175	-6.1166	75.749
20uM CP-91149	TMZ Control	-12.7600	10.84544	1.000	-53.6932	28.173
	50uM CP-91149	31.1500	10.84544	.365	-9.7832	72.083
	50uM TMZ	.1333	10.84544	1.000	-40.7999	41.066
	100uM TMZ	-9.9800	10.84544	1.000	-50.9132	30.953
	20uM CP-91149 + 50uM TMZ	.9167	10.84544	1.000	-40.0166	41.849
	20uM CP-91149 + 100uM TMZ	-9.7133	10.84544	1.000	-50.6466	31.219
	50uM CP-91149 + 50uM TMZ	23.8400	10.84544	1.000	-17.0932	64.773
	50uM CP-91149 + 100uM TMZ	22.0567	10.84544	1.000	-18.8766	62.989
50uM CP-91149	Control		10.84544	.027	-84.8432	-2.976
	20uM CP-91149	-31.1500	10.84544	.365	-72.0832	9.783
	50uM TMZ 100uM TMZ	-31.0167 -41.1300	10.84544	.375	-71.9499 -82.0632	9.916
	20uM CP-91149 + 50uM TMZ	-30.2333	10.84544	.438	-71.1666	10.699
	20uM CP-91149 + 100uM TMZ	-40.8633	10.84544	.051	-81.7966	.069
	50uM CP-91149 + 50uM TMZ	-7.3100	10.84544	1.000	-48.2432	33.623
	50uM CP-91149 + 100uM TMZ	-9.0933	10.84544	1.000	-50.0266	31.839
50uM TMZ	Control	-12.8933	10.84544	1.000	-53.8266	28.039
	20uM CP-91149	1333	10.84544	1.000	-41.0666	40.799
	50uM CP-91149	31.0167	10.84544	.375	-9.9166	71.949
	100uM TMZ 20uM CP-91149 + 50uM	-10.1133 .7833	10.84544	1.000	-51.0466 -40.1499	30.819
	TMZ 20uM CP-91149 + 100uM	-9.8467	10.84544	1.000	-50.7799	31.086
	TMZ 50uM CP-91149 + 50uM	23.7067	10.84544	1.000	-17.2266	64.639
	TMZ 50uM CP-91149 + 100uM	21.9233	10.84544	1.000	-19.0099	62.856
100uM TMZ	TMZ Control	-2.7800	10.84544	1.000	-43.7132	38.153
	20uM CP-91149	9.9800	10.84544	1.000	-30.9532	50.913
	50uM CP-91149	41.1300°	10.84544	.048	.1968	82.063
	50uM TMZ	10.1133	10.84544	1.000	-30.8199	51.046
	20uM CP-91149 + 50uM TMZ	10.8967	10.84544	1.000	-30.0366	51.829
	20uM CP-91149 + 100uM TMZ	.2667	10.84544	1.000	-40.6666	41.199
	50uM CP-91149 + 50uM TMZ 50uM CP-91149 + 100uM	33.8200 32.0367	10.84544	.214	-7.1132 -8.8966	74.753
	TMZ					
20uM CP-91149 + 50uM TMZ	Control		10.84544	1.000	-54.6099	27.256
I M.Z.	20uM CP-91149		10.84544	1.000	-41.8499	40.016
	50uM CP-91149 50uM TMZ		10.84544	1.000	-10.6999 -41.7166	71.166
	100uM TMZ		10.84544	1.000	-51.8299	30.036
	20uM CP-91149 + 100uM TMZ		10.84544	1.000	-51.5632	30.30
	50uM CP-91149 + 50uM TMZ	22.9233	10.84544	1.000	-18.0099	63.856
	50uM CP-91149 + 100uM TMZ	21.1400	10.84544	1.000	-19.7932	62.073
20uM CP-91149 + 100uM TMZ	Control	-3.0467	10.84544	1.000	-43.9799	37.886
	20uM CP-91149 50uM CP-91149	9.7133	10.84544	1.000	-31.2199 0699	50.646 81.796
	50uM CP-91149	9.8467		1.000	-31.0866	50.779
	100uM TMZ 20uM CP-91149 + 50uM	2667	10.84544	1.000	-41.1999 -30.3032	40.666
	TMZ 50uM CP-91149 + 50uM		10.84544	.226	-7.3799	74.486
	TMZ 50uM CP-91149 + 100uM		10.84544		-9.1632	72.70
50uM CP-91149 + 50uM	TMZ Control	.26 6000	10.84544	.122	-77.5332	4.333
TMZ	20uM CP-91149	-23.8400	10.84544	1.000	-64.7732	17.093
	50uM CP-91149	7.3100	10.84544	1.000	-33.6232	48.243
	50uM TMZ	-23.7067	10.84544	1.000	-64.6399	17.226
	100uM TMZ	-33.8200	10.84544	.214	-74.7532	7.113
	20uM CP-91149 + 50uM TMZ		10.84544	1.000	-63.8566	18.009
	20uM CP-91149 + 100uM TMZ 50uM CP-91149 + 100uM		10.84544	1.000	-74.4866 -42.7166	7.379
50uM CP-91149 + 100uM	TMZ Control		10.84544		-75.7499	6,116
TMZ	20uM CP-91149		10.84544			18.876
	50uM CP-91149		10.84544			50.026
	50uM TMZ	-21.9233	10.84544	1.000	-62.8566	19.009
	100uM TMZ 20uM CP-91149 + 50uM		10.84544	.306 1.000	-72.9699 -62.0732	8.896 19.793
	TMZ 20uM CP-91149 + 100uM TMZ	-31.7700	10.84544	.323	-72.7032	9.163
	50uM CP-91149 + 50uM	1.7833	10.84544	1.000	-39.1499	42.716
	TMZ					

50uM CP-91149 + 50uM
TMZ
Based on observed means.
The error term is Mean Square(Error) = 176.435.
*. The mean difference is significant at the .05 level.

Post-hoc for combination treatment of T98G 24h.

W 0		Mean	OH F	ni.	95% Confider	
(I) Concentration	(J) Concentration	Difference (I-J)	Std. Error	Sig.	Lower Bound	
Control	20uM CP-91149	35.6933	17.61968	1.000	-30.8075	102.194
	50uM CP-91149 50uM TMZ	66.4533 19.4500	17.61968	1.000	0475 -47.0508	132.954
	100uM TMZ	.1000		1.000	-66.4008	66.600
	20uM CP-91149 + 50uM	40.4433	17.61968	1.000	-26.0575	106.944
	TMZ	40.4433		1.000	-20.0575	100.944
	20uM CP-91149 + 100uM TMZ	25.5000	17.61968	1.000	-41.0008	92.00
	50uM CP-91149 + 50uM TMZ	65.5533	17.61968	.056	9475	132.05
	50uM CP-91149 + 100uM TMZ	67.6967	17.61968	.043	1.1959	134.19
20uM CP-91149	Control	-35.6933	17.61968	1.000	-102.1941	30.80
	50uM CP-91149	30.7600	17.61968	1.000	-35.7408	97.26
	50uM TMZ	-16.2433	17.61968	1.000	-82.7441	50.25
	100uM TMZ	-35.5933	17.61968	1.000	-102.0941	30.90
	20uM CP-91149 + 50uM TMZ	4.7500		1.000	-61.7508	71.25
	20uM CP-91149 + 100uM TMZ 50uM CP-91149 + 50uM	-10.1933	17.61968	1.000	-76.6941	56.30
	TMZ 50uM CP-91149 + 100uM	29.8600	11.01000	1.000	-36.6408	96.36
	TMZ	32.0033	17.61968	1.000	-34.4975	
50uM CP-91149	Control	-66.4533	17.61968	.050	-132.9541	.04
	20uM CP-91149 50uM TMZ	-30.7600 -47.0033	17.61968	1.000	-97.2608	35.74 19.49
	100uM TMZ	-66.3533	17.61968	.051	-113.5041 -132.8541	.14
	20uM CP-91149 + 50uM	-06.3533		1.000	-132.8541 -92.5108	40.49
	TMZ					
	20uM CP-91149 + 100uM TMZ 50uM CP-91149 + 50uM	-40.9533 9000	17.61968	1.000	-107.4541 -67.4008	25.54
	TMZ 50uM CP-91149 + 100uM	1.2433	17.61968	1.000	-67.4008 -65.2575	67.74
50uM TMZ	TMZ Control	-19.4500	17.61968	1.000	-85.9508	47.05
DUIM TMZ	20uM CP-91149	16.2433	17.61968	1.000	-50.2575	82.74
	50uM CP-91149	47.0033	17.61968	.565	-19.4975	113.50
	100uM TM7	-19.3500	17.61968	1.000	-85.8508	47.15
	20uM CP-91149 + 50uM TMZ	20.9933	17.61968	1.000	-45.5075	87.49
	20uM CP-91149 + 100uM TMZ	6.0500	17.61968	1.000	-60.4508	72.55
	50uM CP-91149 + 50uM TMZ	46.1033	17.61968	.629	-20.3975	112.60
	50uM CP-91149 + 100uM TMZ	48.2467	17.61968	.486	-18.2541	114.74
100uM TMZ	Control	1000	17.61968	1.000	-66.6008	66.40
	20uM CP-91149	35.5933	17.61968	1.000	-30.9075	102.09
	50uM CP-91149	66.3533	17.61968	.051	1475	132.85
	50uM TMZ	19.3500	17.61968	1.000	-47.1508	85.85
	20uM CP-91149 + 50uM TMZ	40.3433	17.61968	1.000	-26.1575	106.84
	20uM CP-91149 + 100uM TMZ	25.4000	17.61968	1.000	-41.1008	91.90
	50uM CP-91149 + 50uM TMZ	65.4533	17.61968	.057	-1.0475	131.95
	50uM CP-91149 + 100uM TMZ	67.5967	17.61968	.044	1.0959	134.09
20uM CP-91149 + 50uM FMZ	Control 20uM CP-91149	-40.4433 -4.7500	17.61968 17.61968	1.000	-106.9441 -71.2508	26.05
	50uM CP-91149	26.0100	17.61968	1.000	-40.4908	61.75 92.51
	50uM TMZ	-20.9933	17.61968	1.000	-87.4941	45.50
	100uM TMZ	-40.3433	17.61968	1.000	-106.8441	26.15
	20uM CP-91149 + 100uM	-14.9433	17.61968	1.000	-81.4441	51.55
	TMZ					
	50uM CP-91149 + 50uM TMZ	25.1100	17.61968	1.000	-41.3908	91.61
10uM CD 04440	50uM CP-91149 + 100uM TMZ	27.2533	17.61968	1.000	-39.2475	93.75
20uM CP-91149 + 100uM FMZ	Control		17.61968 17.61968	1.000	-92.0008 -56.3075	41.00
10000	20uM CP-91149 50uM CP-91149	10.1933		1.000		76.69
			17.61968	1.000	-25.5475	107.45
	50uM TMZ		17.61968	1.000	-72.5508	60.45
	100uM TMZ 20uM CP-91149 + 50uM	-25.4000 14.9433	17.61968 17.61968	1.000	-91.9008 -51.5575	41.10 81.44
	TMZ 50uM CP-91149 + 50uM		17.61968	1.000	-26.4475	106.55
	TMZ 50uM CP-91149 + 100uM		17.61968	.998	-24.3041	108.69
	TMZ					
50uM CP-91149 + 50uM FMZ	Control		17.61968		-132.0541	.94
	20uM CP-91149		17.61968	1.000	-96.3608	36.64
	50uM CP-91149	.9000	17.61968	1.000	-65.6008	67.40
	50uM TMZ 100uM TMZ	-46.1033 -65.4533	17.61968 17.61968	.629	-112.6041 -131.9541	20.39
	20uM CP-91149 + 50uM	-05.4533		1.000	-131.9541 -91.6108	41.39
	TMZ 20uM CP-91149 + 100uM		17.61968	1.000	-106.5541	26.44
	TMZ 50uM CP-91149 + 100uM		17.61968	1.000	-64.3575	68.64
50uM CP-91149 + 100uM	TMZ	-67.6967*	100000000000000000000000000000000000000	.043		
TMZ + 100uM	Control 200M CR 01140	-67.6967 -32.0033	17.61968		-134.1975	-1.19
	20uM CP-91149		17.61968	1.000	-98.5041	34.49
	50uM CP-91149	-1.2433	17.61968	1.000	-67.7441	65.25
	50uM TMZ 100uM TMZ	-48.2467 -67.5967	17.61968	.486	-114.7475	18.25
	20uM CP-91149 + 50uM				-134.0975 -93.7541	-1.09: 39.24
	TMZ		17.61968	1.000		
	20uM CP-91149 + 100uM TMZ	-42.1967	17.61968	.998	-108.6975	24.30
	50uM CP-91149 + 50uM	70 m 0 m 1 m	17.61968	1.000	-68.6441	64.35

Post-hoc for combination treatment of T98G 48h.

	/ D. C	Mean Difference (I-J)	Std. Error	Sig.	95% Confider Lower Bound	
(I) Concentration Control	(J) Concentration 20uM CP-91149	13.0367	16.84386	1.000	-50.5360	76.609
oonaoi	50uM CP-91149	66.9833	16.84386	.032	3.4107	130.556
	50uM TMZ	-3.9667	16.84386	1.000	-67.5393	59.606
	100uM TMZ	-15.8833	16.84386	1.000	-79.4560	47.689
	20uM CP-91149 + 50uM	1.7833	16.84386	1.000	-61.7893	65.356
	TMZ 20uM CP-91149 + 100uM TMZ	8.7000	16.84386	1.000	-54.8727	72.272
	50uM CP-91149 + 50uM TMZ	55.4100	16.84386	.147	-8.1627	118.982
	50uM CP-91149 + 100uM TMZ	66.1600	16.84386	.036	2.5873	129.732
20uM CP-91149	Control 50uM CP-91149	-13.0367	16.84386 16.84386	1.000	-76.6093 -9.6260	50.536
	50uM CP-91149 50uM TMZ	53.9467 -17.0033	16.84386	.178	-9.6260	117.519 46.569
	100uM TMZ	-28.9200	16.84386	1.000	-92.4927	34.652
	20uM CP-91149 + 50uM TMZ	-11.2533	16.84386	1.000	-74.8260	52.319
	20uM CP-91149 + 100uM TMZ	-4.3367	16.84386	1.000	-67.9093	59.236
	50uM CP-91149 + 50uM TMZ	42.3733	16.84386	.777	-21.1993	105.946
	50uM CP-91149 + 100uM TMZ	53.1233	16.84386	.198	-10.4493	116.696
50uM CP-91149	Control	-66.9833	16.84386	.032	-130.5560	-3.410
	20uM CP-91149	-53.9467	16.84386	.178	-117.5193	9.626
	50uM TMZ	-70.9500	16.84386	.019	-134.5227	-7.377
	100uM TMZ	-82.8667	16.84386	.004	-146.4393	-19.294
	20uM CP-91149 + 50uM TMZ	-65.2000°	16.84386	.040	-128.7727	-1.627
	20uM CP-91149 + 100uM TMZ	-58.2833	16.84386	.101	-121.8560	5.289
	50uM CP-91149 + 50uM TMZ	-11.5733	16.84386	1.000	-75.1460	51.999
	50uM CP-91149 + 100uM TMZ	8233	16.84386	1.000	-64.3960	62.749
50uM TMZ	Control 20uM CP-91149	3.9667 17.0033	16.84386	1.000	-59.6060	67.539 80.576
		70.9500	16.84386 16.84386		-46.5693 7.3773	
	50uM CP-91149 100uM TMZ	70.9500 -11.9167	16.84386	1.000	7.3773 -75.4893	134.522 51.656
	20uM CP-91149 + 50uM TMZ	5.7500	16.84386	1.000	-57.8227	69.322
	20uM CP-91149 + 100uM TMZ	12.6667	16.84386	1.000	-50.9060	76.239
	50uM CP-91149 + 50uM TMZ	59.3767	16.84386	.087	-4.1960	122.949
	50uM CP-91149 + 100uM TMZ	70.1267	16.84386	.021	6.5540	133.699
OOUM TMZ	Control	15.8833	16.84386	1.000	-47.6893	79.456
	20uM CP-91149	28.9200	16.84386	1.000	-34.6527	92.492
	50uM CP-91149	82.8667	16.84386	.004	19.2940	146.439
	20uM CP-91149 + 50uM	11.9167 17.6667	16.84386 16.84386	1.000	-51.6560 -45.9060	75.489 81.239
	TMZ 20uM CP-91149 + 100uM TMZ	24.5833	16.84386	1.000	-38.9893	88.156
	50uM CP-91149 + 50uM TMZ	71.2933	16.84386	.018	7.7207	134.866
	50uM CP-91149 + 100uM TMZ	82.0433	16.84386	.004	18.4707	145.616
20uM CP-91149 + 50uM TMZ	Control 20uM CP-91149	-1.7833	16.84386	1.000	-65.3560 -52.3193	61.789
	20um CP-91149 50um CP-91149	11.2533 65.2000	16.84386 16.84386	1.000	1.6273	74.826
	50uM TMZ	-5.7500	16.84386	1.000	-69.3227	57.822
	100uM TMZ	-5.7500	16.84386	1.000	-81.2393	45.906
	20uM CP-91149 + 100uM TMZ	6.9167	16.84386	1.000	-56.6560	70.489
	50uM CP-91149 + 50uM TMZ	53.6267	16.84386	.185	-9.9460	117.199
	50uM CP-91149 + 100uM TMZ	64.3767	16.84386	.045	.8040	127.949
20uM CP-91149 + 100uM	Control	-8.7000	16.84386	1.000	-72.2727	54.872
ГМZ	20uM CP-91149	4.3367	16.84386	1.000	-59.2360	67.909
	50uM CP-91149	58.2833	16.84386	.101	-5.2893	121.856
	50uM TMZ	-12.6667 -24.5833	16.84386	1.000	-76.2393	50.906
	100uM TMZ 20uM CP-91149 + 50uM	-24.5833 -6.9167	16.84386 16.84386	1.000	-88.1560 -70.4893	38.989 56.656
	TMZ 50uM CP-91149 + 50uM TMZ	46.7100	16.84386	.451	-16.8627	110.282
	50uM CP-91149 + 100uM TMZ	57.4600	16.84386	.112	-6.1127	121.032
50uM CP-91149 + 50uM	Control	-55.4100	16.84386	.147	-118.9827	8.162
rmz	20uM CP-91149		16.84386	.777	-105.9460	21.199
	50uM CP-91149	11.5733	16.84386	1 000	-51.9993	75.146
	50uM TMZ	-59.3767	16.84386	.087	-122.9493	4.196
	100uM TMZ		16.84386	.018	-134.8660	-7.720
	20uM CP-91149 + 50uM TMZ 20uM CP-91149 + 100uM		16.84386	.185	-117.1993	9.946
	20uM CP-91149 + 100uM TMZ 50uM CP-91149 + 100uM	-46.7100 10.7500	16.84386	.451	-110.2827 -52.8227	74.322
50uM CP-91149 + 100uM	TMZ Control					-2.581
TMZ	20uM CP-91149		16.84386			
	50uM CP-91149		16.84386 16.84386	1.000	-116.6960 -62.7493	64.396
	50uM TMZ		16.84386 16.84386	.021	-133.6993	-6.554
	100uM TMZ	-70.1267 -82.0433	16.84386	.004	-145.6160	-18,470
	20uM CP-91149 + 50uM	-64.3767	16.84386	.045	-127.9493	804
	TMZ 20uM CP-91149 + 100uM		16.84386	.112	-121.0327	6.112
	TMZ					
	50uM CP-91149 + 50uM TMZ	-10.7500	16.84386	1.000	-74.3227	52.822

Post-hoc for combination treatment of T98G 72h.

Dependent Variable: Viability

Bonferroni

		Mean			95% Confide	ence Interval
(I) Time	(J) Time	Difference (I-J)	Std. Error	Sig.	Lower Bound	Upper Bound
Time, 24h	Time, 48h	-14.8748 [*]	2.85749	<.001	-21.9352	-7.8144
	Time, 72h	-16.7363 [*]	2.85749	<.001	-23.7967	-9.6759
Time, 48h	Time, 24h	14.8748*	2.85749	<.001	7.8144	21.9352
	Time, 72h	-1.8615	2.85749	1.000	-8.9219	5.1989
Time, 72h	Time, 24h	16.7363 [*]	2.85749	<.001	9.6759	23.7967
	Time, 48h	1.8615	2.85749	1.000	-5.1989	8.9219

Based on observed means.

The error term is Mean Square(Error) = 110.231.

Post-hoc for combination treatment of U87 timepoints.

^{*.} The mean difference is significant at the .05 level.

Debug Debu			Mean	Old Farm	01-	95% Confiden	
SOMA CP-91169 1-7903	(i) Concentration	(J) Concentration 20uM CP-91149	Difference (I-J)	Std. Error 7 30323	Sig.		
	Control						
TMUZ Policy CP-91149 + 100MM -8-8000 7-30222 1.000 -77-1641 17-56		100uM TMZ	-16.5767				10.987
Depart Chest 17.56		20uM CP-91149 + 50uM	-3.9300	7.30323	1.000	-31.4941	23.634
TMUZ SOLIDA CP-91149 + SOLIDA TMZ CONTROL CP-91149 + SOLIDA TMZ CONTROL CP-91149 + SOLIDA TMZ CONTROL CP-91149 + SOLIDA TMZ SOLIDA CP-91149 + SOLIDA SOLIDA CP-91149 + SOLIDA TMZ SOLIDA CP-91149 + SOLIDA SOLIDA CP-91149 + SOLIDA SOLIDA CP-91149 + SOLIDA MZ SOLIDA CP-91149 + SOLIDA SOLIDA CP-91149 + SOLIDA MZ SOLIDA CP-91149 + SOLIDA SO			-9.6000	7.30323	1.000	-37.1641	17.964
TMUZ SOUR CP-91149 - 100 M		TMZ				-29 4041	
TRUZ Combal CP-91149 Soud CP-91149 29.533 7.0022 0.12 5.956 5.571 Soud TGC 29.1497 7.0022 0.02 0.02 1.1206 5.951 Soud TGC 29.1497 7.0022 0.02 0.02 1.1206 5.941 100.04 MVZ 11.5700 7.0022 1.000 -1.5941 31.91 200.04 CP-91149 + 50.04 24.2467 7.0022 1.000 -1.5941 51.76 TMZ 50.04 CP-91149 + 50.04 24.2467 7.0022 1.000 -1.5941 51.76 TMZ 50.04 CP-91149 + 50.04 24.3067 7.0022 1.000 -1.2674 51.76 TMZ 50.04 CP-91149 + 100.04 18.5467 7.0022 0.02 2.1202 57.55 TMZ 50.04 CP-91149 + 100.04 29.6937 7.0022 0.00 2.1202 57.55 TMZ 50.04 CP-91149 + 100.04 29.6937 7.0022 0.00 2.1202 57.55 TMZ 50.04 CP-91149 + 100.04 29.6937 7.0022 1.00 -2.5707 2.35 TMZ 50.04 CP-91149 + 100.04 7.8667 7.0022 1.00 -2.5708 2.54 TMZ 50.04 CP-91149 + 50.04 -2.1207 7.0022 1.00 -2.5708 2.54 TMZ 50.04 CP-91149 + 50.04 -2.1207 7.0022 1.00 -2.2708 2.54 TMZ 50.04 CP-91149 + 100.04 -7.8667 7.0022 1.00 -2.2241 30.90 TMZ 50.04 CP-91149 + 100.04 -7.8667 7.0022 1.00 -2.2241 30.90 TMZ 50.04 CP-91149 + 100.04 -7.8667 7.0022 1.00 -2.2241 30.90 TMZ 50.04 CP-91149 + 100.04 -7.8667 7.0022 1.00 -2.2241 30.90 TMZ 50.04 CP-91149 + 100.04 -7.8667 7.0022 1.00 -2.2241 30.90 TMZ 50.04 CP-91149 + 100.04 -7.8667 7.0022 1.00 -7.2610 1.2261 TMZ 50.04 CP-91149 + 50.04 -7.800 7.0022 1.00 -7.2610 1.2261 TMZ 50.04 CP-91149 + 50.04 -7.800 7.0022 1.00 -7.2610 1.2261 TMZ 50.04 CP-91149 + 50.04 -7.800 7.0022 1.00 -7.2610 1.2261 TMZ 50.04 CP-91149 + 50.04 -7.800 7.0022 1.00 -7.2610 1.2261 TMZ 50.04 CP-91149 + 50.04 -7.800 7.0022 1.00 -7.2610 1.2261 TMZ 50.04 CP-91149 + 50.04 -7.800 7.0022 1.00 -7.2611 1.2261 TMZ 50.04 CP-91149 + 50.04 -7.800 7.0022 1.00 -7.2611 1.2261 TMZ 50.04 CP-91149 + 50.04 -7.800 7.0022 1.00 -7.		TMZ					
Sould CP-91149		TMZ					
	20uM CP-91149						
1900ut TIVZ							
DOUM CP-91149 - 100							
Description		20uM CP-91149 + 50uM					51.780
		20uM CP-91149 + 100uM	18.5467	7.30323	.740	-9.0174	46.110
SOUND CP-91149 100 173937 739323 1000 -25 7708 29.55 2		50uM CP-91149 + 50uM	26.3067	7.30323	.073	-1.2574	53.870
DOUM CP-91149			29.6933	7.30323	.026	2.1292	57.257
2004 CP-91149 2-28-333 7.9022 1000 2-28-774 1201	FOUND OF OUT OF						
SOUNT TIME	500M CF-91149						
100M TMZ							
2004 CP-91149 - 5004 -2.1967 7.3022 1.000 -28.7000 25.42							
TMZ 2004 CP-91149 + 10004 3 3 3 400 7 3 30323 1 000 -22 2 2 4 1 2 8 6 6 6 7 3 0 1 2 7 5 1 1 2 7 5 1 1 1 1 1 1 1 1 1 1 1 1 1 1 1 1 1 1							
TMZ		TMZ					
TMZ		TMZ					
TNAZ		TMZ					
2004 CP-91149 -2.8487 7.3022 1.000 -3.0874 25.07		50uM CP-91149 + 100uM TMZ	3.3400	7.30323	1.000	-24.2241	30.904
SOUND CP-91149 -3.433	50uM TMZ						26.86
100M TMZ							
2004 CP-91149 + 500M							10.28
2004 CP-91149 + 1004M		20uM CP-91149 + 50uM					
SOUNT CP-91149 + 50 UM		20uM CP-91149 + 100uM	-10.3000	7.30323	1.000	-37.8641	17.26
SOUNT CP-91149 + 100 but September Sount CP-91149 + 100 but September		50uM CP-91149 + 50uM	-2.5400	7.30323	1.000	-30.1041	25.02
			.8467	7.30323	1.000	-26.7174	28.411
2004 CP-91149 -1.15700 7.0022 1.000 -38.141 15.99							
Sould CP-91149 + 50uM 147833 7.9022 1.000 -12.700 42.24	100uM TMZ						
SOUNT TIZE							
2004 CP-91149 + 5004 12,4467 7,30223 1,000 -14,9174 40,211 1,000							
2004 CP-91149 + 1004M		20uM CP-91149 + 50uM					
SOUNC CP-91149 + 50 UM		20uM CP-91149 + 100uM	6.9767	7.30323	1.000	-20.5874	34.54
TMZ SOUNT CP-91149 + 100UM Sount CP-91149 + 100UM Sount CP-91149 + 50UM Control 3 9000 7 30023 1 000 -23 6341 31 49			14.7367	7.30323	1.000	-12.8274	42.30
DUM CP-91149 + 50UM Control 3 9300 7 30923 1 000 -23 6341 31 49			18.1233	7.30323		-9.4408	45.68
MZ 2004 CP-91149 -242167 730323 138 -517000 3.34	20uM CP-91149 + 50uM	TMZ					
SOUND CP-91149 2.1967 7.3022 1.000 -26.474 29.65	TMZ						
SOUNT TAX							
100M TMZ							
20ML CP-91149 + 100MM							
SOUNT CP-91149 + 100M							
TMZ SOUM CP-91149 + 100UM S 4767 7 30323 1000 -22 0874 33 04 MZ		111100	2.0900	7 20222	1.000	-25 4741	29.65
TMZ		TMZ				==	
M2		TMZ					
SOUNT CH-91149 7.8097 7.30223 1.00 1.17274 35.77	ZUUM CP-91149 + 100uM FMZ						
SOUNT TILE							
100M TMZ							
2004 CP-91149 + 50uM 5 6700 7 30323 1 000 -21 8941 33 23 25 0							
TMZ SOUM CP-91149 + 100uM 7,7600 7,30223 1,000 19,8041 35,32							
TMZ Sould CP-91149 + 100uM		TMZ					35.32
TMZ		TMZ					
MZ 2004 CP-91149		TMZ					
SOUN CP-91149 D467 730323 1000 -275714 27611	PM7						
SOUNTMZ			-20.3007	7.30323			
100M TMZ					1.000	-25.0241	30.10
2004 CP-91149 + 500M -2.0900 7.30323 1.000 -28.6541 25.47.							12.82
2004 CP-91149 + 10004		20uM CP-91149 + 50uM					25.47
SOUNT CP-91149 + 100M 3 3867 7 39323 1 000 -24 1774 30 951		20uM CP-91149 + 100uM	-7.7600	7.30323	1.000	-35.3241	19.80
MMZ Control 1.5467 7.30222 1.000 -281109 26.01 MZ Control 2.004 CP-91149 -29.6933 7.30233 0.00 -29.1109 26.01 SOUM CP-91149 -29.6933 7.30233 1.000 -30.9041 24.22 SOUM TMZ -8.67 7.30223 1.000 -28.4109 26.11 SOUM CP-91149 - 50.00 -5.4767 7.30223 1.000 -33.0409 22.08 TMZ 2.004 CP-91149 - 100.00 -11.1467 7.30223 1.000 -38.7109 16.41 TMZ 2.004 CP-91149 - 1.004 -11.1467 7.30223 1.000 -38.7109 16.41 Control Control -2.004		50uM CP-91149 + 100uM	3.3867	7.30323	1.000	-24.1774	30.950
MZ 2004 CP-91149 -296933 7 30323 006 -57:274 -2:12! 5044 CP-91149 -3.9400 7 30323 1000 -30.9941 4 2-50.954	50uM CP-91149 + 100uM		-1.5467	7.30323	1.000	-29.1108	26.017
500M CP-91149 -33400 7 30323 1000 -309041 24 22	ΓMZ	20uM CP-91149	-29.6933	7.30323		-57.2574	-2.12
500M TMZ		50uM CP-91149				-30.9041	24.224
100M TMZ -181233 7.30223 8.84 4.68674 9.441 20M CP-91149 + 50M -5.4767 7.30323 1.000 -33.0408 22.081 TMZ 20M CP-91149 + 100M -11.1467 7.30323 1.000 -38.7108 16.412		50uM TMZ	0.467	7 20222		-28.4108	26.717
TMZ 20UM CP-91149 + 100UM -11.1467 7.30323 1.000 -38.7108 16.41: TMZ		100uM TMZ	-18.1233		.834		9.44
20uM CP-91149 + 100uM -11.1467 7.30323 1.000 -38.7108 16.41		20uM CP-91149 + 50uM		7.30323	1.000	-33.0408	22.08
		20uM CP-91149 + 100uM	-11.1467	7.30323	1.000	-38.7108	16.417
TMZ			2 2007	7 30323	1 000	-30 9508	24 17

Post-hoc for combination treatment of U87 72h treatment.

Appendix 9

Statistical analysis of cell cycle analysis data.

Multiple Comparisons

Dependent Variable: Population

Bonferroni

		Mean			95% Confidence Interval	
(I) Phase	(J) Phase	Difference (I-J)	Std. Error	Sig.	Lower Bound	Upper Bound
Phase, G1	Phase, S	54.8725 [*]	2.33697	<.001	48.3001	61.4449
	Phase, G2	45.1358 [*]	2.33697	<.001	38.5635	51.7082
	Phase, Sub G1	65.9283 [*]	2.33697	<.001	59.3560	72.5007
Phase, S	Phase, G1	-54.8725 [*]	2.33697	<.001	-61.4449	-48.3001
	Phase, G2	-9.7367 [*]	2.33697	.001	-16.3090	-3.1643
	Phase, Sub G1	11.0558	2.33697	<.001	4.4835	17.6282
Phase, G2	Phase, G1	-45.1358 [*]	2.33697	<.001	-51.7082	-38.5635
	Phase, S	9.7367 [*]	2.33697	.001	3.1643	16.3090
	Phase, Sub G1	20.7925 [*]	2.33697	<.001	14.2201	27.3649
Phase, Sub G1	Phase, G1	-65.9283 [*]	2.33697	<.001	-72.5007	-59.3560
	Phase, S	-11.0558 [*]	2.33697	<.001	-17.6282	-4.4835
	Phase, G2	-20.7925 [*]	2.33697	<.001	-27.3649	-14.2201

Based on observed means.

The error term is Mean Square(Error) = 32.769.

Post-hoc for flow cytometry results on U251.

^{*.} The mean difference is significant at the .05 level.

Dependent Variable: Population

Bonferroni

		Mean			95% Confidence Interval	
(I) Phase	(J) Phase	Difference (I-J)	Std. Error	Sig.	Lower Bound	Upper Bound
Phase, G1	Phase, S	63.3875 [*]	1.32025	<.001	59.6745	67.1005
	Phase, G2	71.2517*	1.32025	<.001	67.5387	74.9647
	Phase, Sub G1	75.0008 [*]	1.32025	<.001	71.2878	78.7138
Phase, S	Phase, G1	-63.3875 [*]	1.32025	<.001	-67.1005	-59.6745
	Phase, G2	7.8642 [*]	1.32025	<.001	4.1512	11.5772
	Phase, Sub G1	11.6133 [*]	1.32025	<.001	7.9003	15.3263
Phase, G2	Phase, G1	-71.2517 [*]	1.32025	<.001	-74.9647	-67.5387
	Phase, S	-7.8642 [*]	1.32025	<.001	-11.5772	-4.1512
	Phase, Sub G1	3.7492 [*]	1.32025	.047	.0362	7.4622
Phase, Sub G1	Phase, G1	-75.0008 [*]	1.32025	<.001	-78.7138	-71.2878
	Phase, S	-11.6133 [*]	1.32025	<.001	-15.3263	-7.9003
	Phase, G2	-3.7492 [*]	1.32025	.047	-7.4622	0362

Based on observed means.

The error term is Mean Square(Error) = 10.458.

Post-hoc for cell cycle analysis results on T98G between cell cycle phases.

^{*.} The mean difference is significant at the .05 level.

Dependent Variable: Population

Bonferroni

		Mean			95% Confidence Interval	
(I) Phase	(J) Phase	Difference (I-J)	Std. Error	Sig.	Lower Bound	Upper Bound
Phase, G1	Phase, S	48.4508 [*]	2.63304	<.001	41.0458	55.8558
	Phase, G2	25.4967 [*]	2.63304	<.001	18.0917	32.9017
	Phase, Sub G1	57.1025 [*]	2.63304	<.001	49.6975	64.5075
Phase, S	Phase, G1	-48.4508 [*]	2.63304	<.001	-55.8558	-41.0458
	Phase, G2	-22.9542	2.63304	<.001	-30.3592	-15.5492
	Phase, Sub G1	8.6517	2.63304	.015	1.2467	16.0567
Phase, G2	Phase, G1	-25.4967 [*]	2.63304	<.001	-32.9017	-18.0917
	Phase, S	22.9542	2.63304	<.001	15.5492	30.3592
	Phase, Sub G1	31.6058	2.63304	<.001	24.2008	39.0108
Phase, Sub G1	Phase, G1	-57.1025 [*]	2.63304	<.001	-64.5075	-49.6975
	Phase, S	-8.6517 [*]	2.63304	.015	-16.0567	-1.2467
	Phase, G2	-31.6058 [*]	2.63304	<.001	-39.0108	-24.2008

Based on observed means.

The error term is Mean Square(Error) = 41.597.

Post-hoc for cell cycle analysis results on U87 between cell cycle phases.

Multiple Comparisons

Dependent Variable: Population

Bonferroni

Domenton						
		Mean			95% Confidence Interval	
(I) Concentration	(J) Concentration	Difference (I-J)	Std. Error	Sig.	Lower Bound	Upper Bound
Control	10uM	5.1000 [*]	1.45000	.047	.0556	10.1444
	50uM	2.8833	1.45000	.492	-2.1610	7.9277
	100uM	3.0100	1.45000	.429	-2.0344	8.0544
10uM	Control	-5.1000 [*]	1.45000	.047	-10.1444	0556
	50uM	-2.2167	1.45000	.989	-7.2610	2.8277
	100uM	-2.0900	1.45000	1.000	-7.1344	2.9544
50uM	Control	-2.8833	1.45000	.492	-7.9277	2.1610
	10uM	2.2167	1.45000	.989	-2.8277	7.2610
	100uM	.1267	1.45000	1.000	-4.9177	5.1710
100uM	Control	-3.0100	1.45000	.429	-8.0544	2.0344
	10uM	2.0900	1.45000	1.000	-2.9544	7.1344
	50uM	1267	1.45000	1.000	-5.1710	4.9177

Based on observed means.

The error term is Mean Square(Error) = 3.154.

Post-hoc test between treatment concentrations from cell cycle analysis in S phase on U87 cells.

^{*.} The mean difference is significant at the .05 level.

^{*.} The mean difference is significant at the .05 level.